Using grain size analysis to understand transverse versus axial sediment supply to a rift: Example from the Sperchios rift, Greece

Master's thesis in Petroleum Geology

Ole Sannes Riiser

Department of Earth Science

Faculty of Mathematics and Natural Sciences

University of Bergen

June 2016

Abstract

In order to better understand the interaction between different controlling variables in fluvial systems in a rift basin, and the differences between transverse and axial drainage in the same setting, I present the results of numerical modelling in which downstream grain size trends along the fluvial systems in the Sperchios rift basin in Central Greece are analysed. The model is used to explore the relationship between (1) the spatial distribution of subsidence, (2) sediment supply and (3) downstream grain size fining trends in such systems. The transverse systems drain from the footwall, across the border faults, and feed coarse alluvial fans that prograde into the centre of the rift whereas the axial system supplies sediment to a fine grained birds foot delta in the Maliakos Gulf. The model used has been developed in recent years by Fedele and Paola (2007) and Duller et al. (2010). I first demonstrate how the grain size data from the Sperchios rift is obtained and quantified, and then present the modelling results based on the obtained grain size data, where the effects of – and interaction between – the controlling variables is explored. Furthermore, I demonstrate how the amplitude and spatial distribution of subsidence impacts grain size fining trends and the distribution of deposition and bypassing. I also show how the sediment supplied to the system impacts the grain size fining trends and distribution of deposition and bypassing. For the fluvial systems in the Sperchios rift, I then compare the transverse systems with the axial system. This study indicates that the model developed by Fedele and Paola (2007) and Duller et al. (2010), despite some weaknesses and necessary assumptions, provides a greater understanding of the interaction between the controlling variables impacting fluvial deposition in rifts.

Acknowledgements

First of all, I would like to thank my supervisor Rob Gawthorpe (Department of Earth Science) for arranging such an interesting project, and for his interest in my opinions and my background and his encouragement of my application when I first spoke to him about the project in 2014. I am also very grateful for the funding of the field work in Greece which was provided by the MultiRift project. A special thanks also goes to Sofia Pechlivanidou for all the invaluable help with ideas and modelling, and assistance in the fieldwork in Greece, both relating to geology and relating to the Greek language. I now know the usual politeness phrases, I can read Greek (understanding what I read is a different story) as well as knowing how to order coffee and pastries! The other two field assistants, Christos Pennos and Charikleia Gkarlaouni also deserve a special thanks. It was an absolute pleasure doing field work with you all. I would also like to extend my gratitude to Charikleia's parents for their kindness and hospitality, making sure I was well fed with both lunch and dinner during the days in field.

Furthermore, I would like to thank the University of Bergen for the desk at the study room – Hjørnerommet (the corner room). Big thanks also go to the lovely group of co-students there for laughs, talks and friendly reminders of how they miss me when I have been absent. I would also like to thank my family and boyfriend for support and encouragement throughout this year of working with the thesis.

The biggest thanks belongs to my supervisor, Patience Cowie (Department of Earth Science), who has been incredibly supportive, open minded, inspirational, and wholeheartedly interested in making sure I am comfortable with the thesis and with the work. You have an excellent ability to make the student feel confident and his or her opinions appreciated. The feedback you have given me during the work has been very valuable, professional and highly appreciated. I am very grateful for all your help, and it has been a great pleasure having you as my supervisor.

Innhold

Abstract ..... **i**

Acknowledgements ..... **iii**

1.0 Introduction **1**

1.1 Theory 1

1.2 Objectives 3

1.3 Geologic setting 4

1.3.1 Tectonic setting 6

1.3.2 Topography and geomorphology 9

1.3.3 Lithology 12

1.3.4 Drainage 13

1.4 Modelling based on grain size analysis 16

2.0 Methodology **21**

2.1 Grain size pictures 21

2.2 Modelling 25

2.3 ArcGIS 25

2.4 Accessory work 27

2.4.1 Naming 27

2.4.2 TruePulse laser measurements 27

2.4.3 Schmidt hammer measurements 27

2.4.2 ArcGIS 28

3.0 Results **29**

3.1 Observations 30

3.1.1 Inahos 30

3.1.2 Xerias 32

3.1.3 Lefkada 33

3.1.4 Vitoli 34

3.1.5 Fossilized fan 35

3.2 Grain size analysis result 40

3.2.1 Inahos 40

3.2.2 Xerias 41

3.2.3 Sperchios 43

3.2.4 Lefkada 45

3.2.5 Vitoli 47
3.3 Modelling 50
3.3.1 Modelling procedure 50
3.3.2 Xerias 56
3.3.3 Inahos 59
3.3.4 Sperchios 61
4.0 Discussion 64
4.1 Fan volumes 64
4.2 Validity of the modelling results 66
4.2.1 Inahos 66
4.2.2 Xerias 67
4.2.3 Age of the fans and related volumes 69
4.3 Comparison of drainages 70
4.3.1 Comparison of the transverse drainages 70
4.3.2 Comparison of transverse drainages and axial drainage 71
4.4 Uncertainties 73
4.4.1 Fault subsidence rates 73
4.4.2 Fan volume calculation 73
4.4.3 Limitations in the grain size measuring method 73
Conclusions 76
References 78
APPENDIX A – SLOPE LASER MEASUREMENTS 81
APPENDIX B – SCHMIDT HAMMER MEASUREMENTS 83

1.0 Introduction

1.1 Theory

Landscape response to tectonic and climatic forcing is recorded by the stratigraphy preserved in sedimentary basins (Allen, 2008). Sedimentary basins and their recorded grain size variations comprise a time-integrated archive of the changes in depositional environments through time (Whittaker et al., 2011). As Whittaker et al. (2011) explains, this record can therefore be used to gain important information on tectonic and climatic boundary conditions at the time of deposition. As demonstrated by Duller et al. (2010) and Whittaker et al. (2010) it is necessary to quantify how grain size and other field observables record the changes in these external boundary conditions if one wishes to read the stratigraphic archive of landscape response to tectonic and climatic forcing.

In sedimentary systems, downstream fining is a result of the selective removal of the least mobile grains from a mixed grain-size population. The most common explanations for downstream fining are (1) abrasion, where large particles are broken down into smaller sizes by fracturing, and (2) selective deposition where finer grains are preferentially transported downstream (Fedele and Paola, 2007). Selective deposition is thought to be the dominant factor causing downstream fining in most aggrading fluvial systems, indicated by observations of fining rates with a strong positive correlation with deposition lengths. The fact that observed fining rates in natural streams often are orders of magnitude higher than those that can be attributed to abrasion alone also strengthens this assumption (Fedele and Paola, 2007).

According to the theory of selective deposition there are three important controlling variables that also influence the locus and calibre of sediment preserved within stratigraphy: (1) The range of sizes in the sediment supply (sometimes described as the probability density function of grain size in the input sediment supply), (2) the volumetric magnitude of sediment supply to the basin, and (3) the spatial distribution of tectonic subsidence (Fedele and Paola, 2007, Duller et al., 2010, Whittaker et al., 2011). These three factors are dependent on the climatic and tectonic boundary conditions affecting the sediment routing system (Whittaker et al., 2011).

To study the three aforementioned variables in detail it is necessary to have a field area with some known constrains on sediment supply, the sediment volumes and subsidence distribution. Such an area can be found in central Greece, in a sedimentary basin known as the Sperchios Basin.

1.2 Objectives

The Sperchios basin is, with its active tectonics, fluvial systems, and other geomorphologic phenomena, a perfect locality for studying the interaction between tectonics and geomorphologic processes. This is also well documented in previous papers (incl. Eliet and Gawthorpe, 1995, Goldsworthy and Jackson, 2000, Apostolopoulos, 2005, D'Alessandro et al., 2014, Whittaker and Walker, 2015). In this thesis, I have studied a selection of channels and fan structures in the Sperchios basin – the Inahos fan, the Xerias fan, a fossilized fan, and the axial Sperchios River (figure 1.14). The main objectives during the study of these fans and rivers was:

- Using a grain size sampling method to gather data about spatial trends in grain size distribution for two transverse systems and one axial system, specifically:
    - Downstream variations in the fourth percentile grain size (D_{84}) and the median grain size (D_{50}).
- Implementing a self-similarity based model of grain size fining to the obtained data with the goal of:
    - Exploring the relationship between grain size fining rate, initial sediment volumes supplied to the system and spatial distribution of tectonic subsidence along the system.
    - Analysing results and discussing their validity.
    - Comparing my own results to results derived from a study of the axial river in the same field area performed by Pechlivanidou et al. (2016, manuscript in preparation).

The mechanics of the self-similarity based model will be described in the next chapter, and the grain size sampling technique I applied will be described further in the methodology chapter.

Figure 1.1: Map showing my field area marked in red.

1.3 Geologic setting

The field locality studied in this thesis is located in the central region of Greece, approximately 150 kilometres northwest of Athens (figure 1.1). The area, called the Sperchios Basin, is a sedimentary basin stretching 100 kilometres long and 30 kilometres wide (figure 1.2), and is an ideal locality for studying how tectonics influence geomorphology, as the fault activity and extensional regime in the area are well documented (Eliet and Gawthorpe, 1995, Goldsworthy and Jackson, 2000, Apostolopoulos, 2005, Kilias et al., 2008, Whittaker and Walker, 2015,). In the following paragraphs I will describe the Sperchios Basin in more detail, focusing on the tectonics, lithology, geomorphology and drainage patterns.

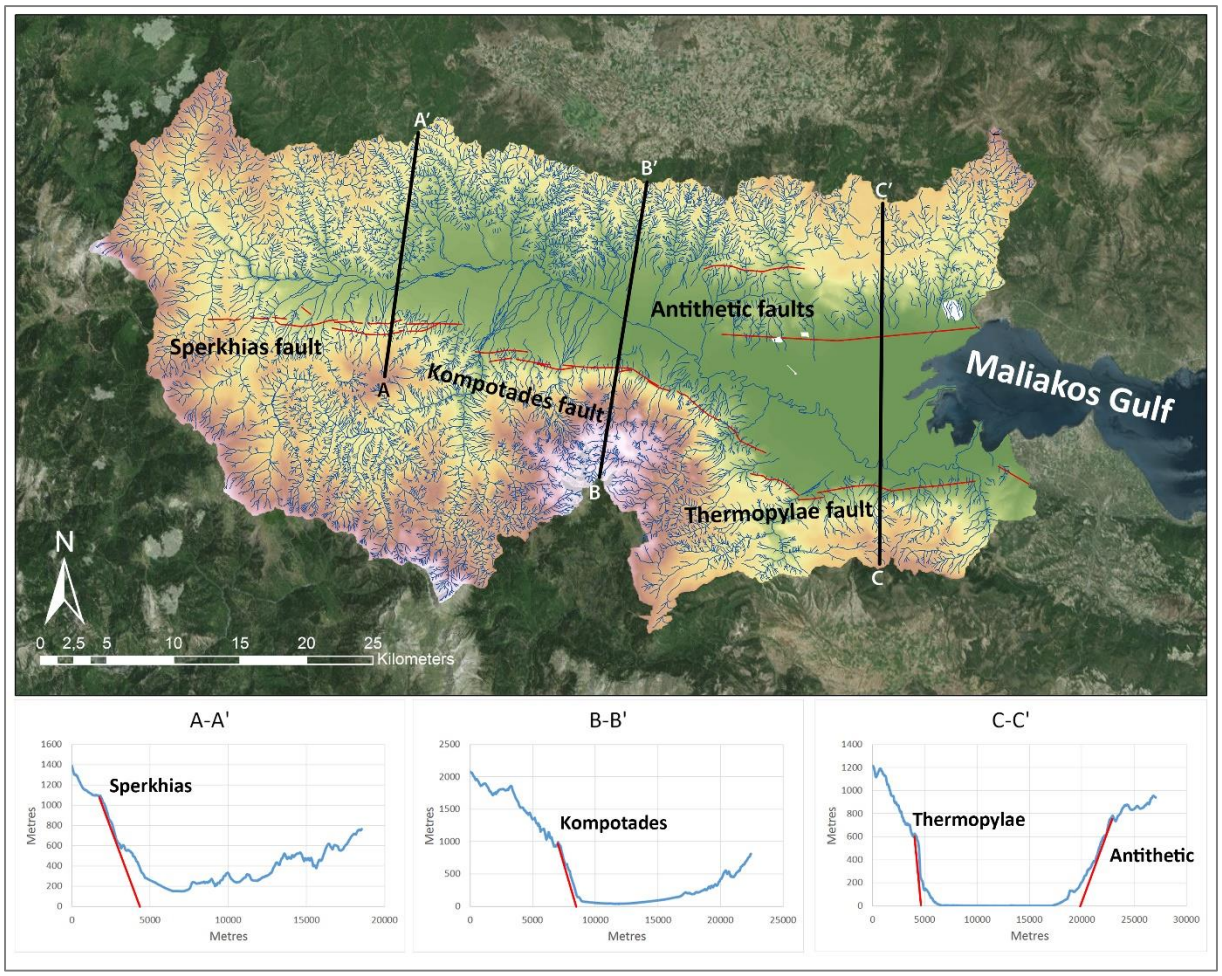

Figure 1.2: An overview of the Sperchios basin, with three cross section profiles. The three cross sections show how the basin narrows from east to west.

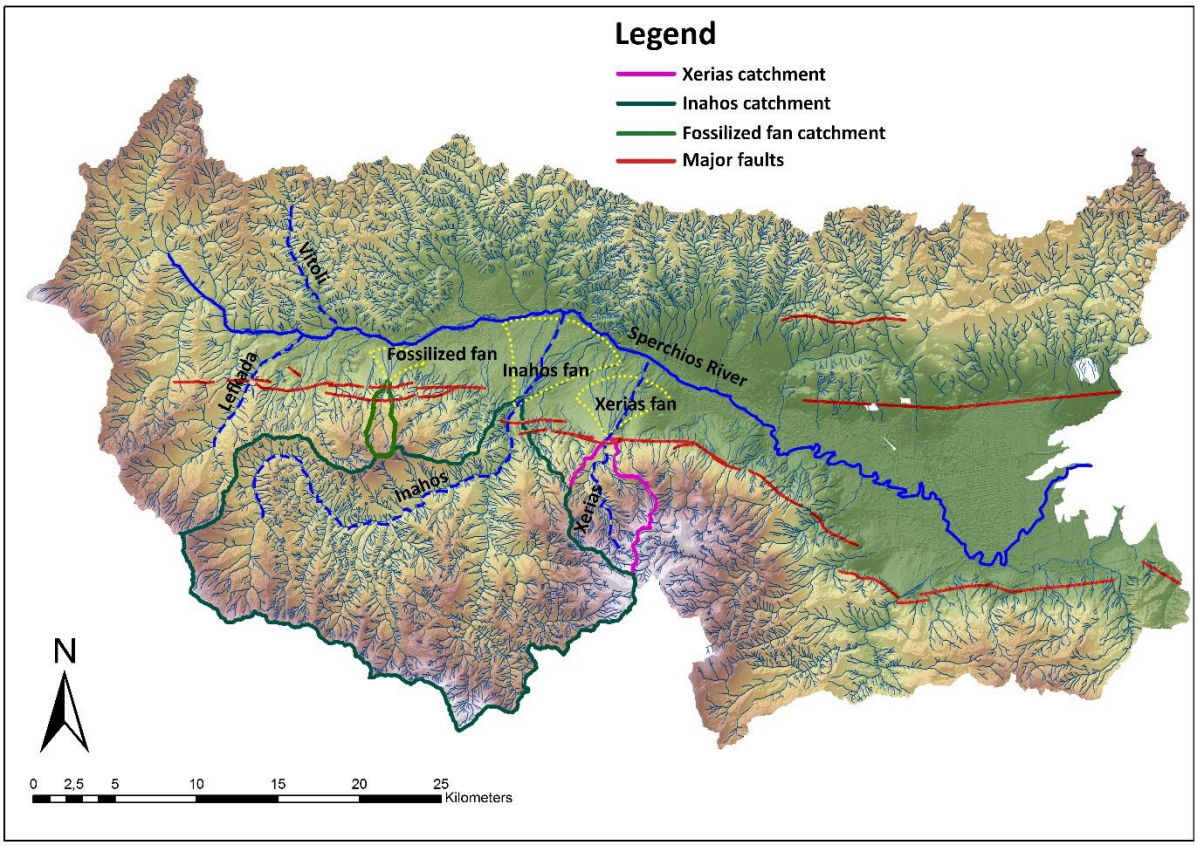

Figure 1.3: A map showing the names of the different fans, rivers and catchments I have studied.

1.3.1 Tectonic setting

Central Greece is dominated by an ENE-WSW-trending extensional fault system, with a north-south extension direction as a consequence (Eliet and Gawthorpe, 1995, Goldsworthy and Jackson, 2000). The N-S extension is prominent throughout the whole Aegean region. This extensional fault system accommodates the westward motion of Turkey (Anatolia) relative to Eurasia, and northeast verging subduction of the African plate under the Eurasian plate along the Hellenic Trench. (Kilias et al., 2008, Whittaker and Walker, 2015).

The most active system is in and around the Gulf of Corinth, but also extends northwards albeit with a slower extension rate (Goldsworthy and Jackson, 2000). This extensional setting results in a series of asymmetric half grabens throughout central Greece (Eliet and Gawthorpe, 1995). The extension has been going on since the early Pliocene, around 5 Ma (Leeder and Jackson, 1993), is thought to have been active

through Pleistocene, and is still active at a rate of approximately 10-20 mm a^{-1} for the region as a whole (Eliet and Gawthorpe, 1995). Although the extension rate is significantly lower further north, at approximately 1-3 mm a^{-1} in the Northern Gulf of Evia and the Sperchios basin, central Greece as a whole is one of the most rapidly extending regions on the continents today (Whittaker and Walker, 2015).

Studies has shown that there is a discrepancy between the roughly N-S slip vectors on normal faults in Central Greece and the overall SW movement of the region as a whole. This suggests that there must be a significant clockwise rotation along the vertical axis in the fault blocks in Central Greece (Goldsworthy and Jackson, 2000, Goldsworthy et al., 2002). As proven through GPS measurements made by Goldsworthy et al. (2002), the whole of the Central Aegean Sea and South East Peloponnese is moving as a single coherent block. Goldsworthy et al. (2002) continues by presenting a simplified model that can explain and reproduce the tectonics of the Aegean and Central Greece. It shows how the extensional graben systems are connected to strike slip faults in the Aegean Sea, and explains why the graben systems north of the Gulf of Corinth seem to die out in the west whereas the Gulf of Corinth itself sees an increase in extension to the west (figure 1.4).

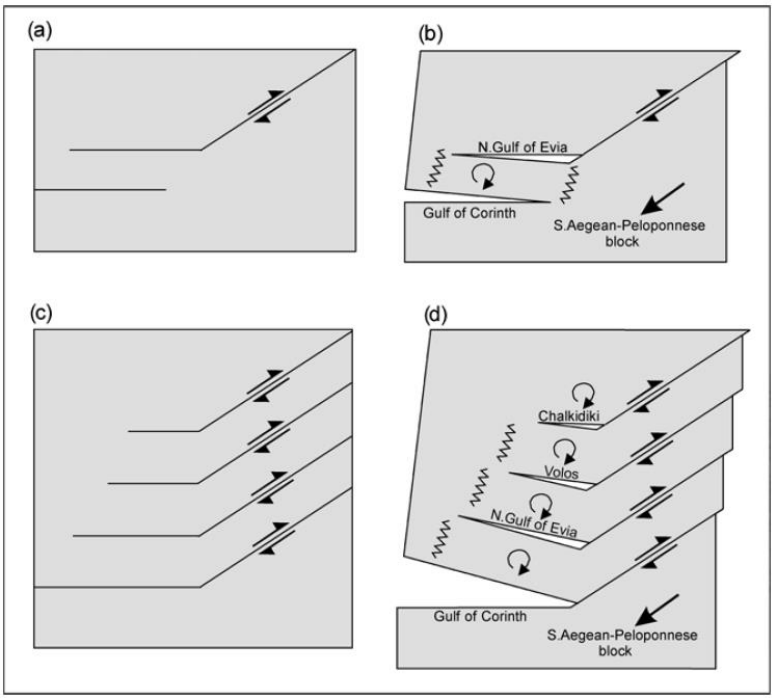

Figure 1.4: (a) and (b) illustrates strike slip faulting that ends in a normal fault system that dies out in the west – here with the Gulf of Evia as an example, with consequent clockwise rotation of the fault blocks to the south. (c) and (d) illustrates how the extension in the Gulf of Corinth increases to the west with the addition of further strike-slip and normal fault blocks to the north. (Goldsworthy et al., 2002)

The Sperchios basin is located at the end of the Gulf of Evia (figure 1.2). The basin is an asymmetric half graben approximately 100 km long and 30 km wide, narrowing from east to west (figure 1.2). As with most of the sedimentary basins of central Greece, it is bounded to the south by major NW-SE striking normal fault segments, typically 20-30 km long (Eliet and Gawthorpe, 1995) and displaying evidence of linkage since they became active (Cowie et al., 2008, Whittaker and Walker, 2015). The north, hanging wall side of the basin sees minor antithetic faulting. The most important fault segments along the south margin of the basin are the Sperkhias fault and the Kompotades fault – which together comprise what is known as the Sperchios Fault System (SFS), and the Thermopylae fault, which is part of the Coastal Fault System (CFS) (fig 1.2). According to Whittaker and Walker (2015), linkage within the SFS is thought to have occurred about 1.6 Ma, based on the presence of knickpoints in the long profiles of the rivers crossing the fault sections in the SFS. However, the validity of this assumption is questionable as my field observations in the area suggest that the knickpoints identified in Whittaker and Walker (2015) might be the result of dams and lithological boundaries. Analysis in the Whittaker and Walker (2015) study was based on a DEM of low resolution without any field data collection. This will be discussed later in the thesis. Along with linkage within the SFS itself, it is also thought to interact with the CFS to the east (Apostolopoulos, 2005).

The faults in the basin are not well defined at their tips, but they are very clear towards the centres where they produce large topographic relief, and they are thought to extend to crustal depths of 10-15 kilometres (Whittaker and Walker, 2015). The relief along the basin-bounding normal faults extends to more than 2000 metres. According to Eliet and Gawthorpe (1995), seismic data from the Maliakos Gulf suggest subsidence rates exceeding 1.8 mm a^{-1} along the border fault zone. However, Whittaker and Walker (2015) point out the weakness of this estimate due to the limited extent of the seismic data used by Eliet and Gawthorpe (1995), and suggest a lower long-term rate of 1.1 mm a^{-1} in the Maliakos Gulf based on the estimated total throw of ~4 km and the assumption that displacement had commenced by 3.6 Ma as suggested by the sedimentary basin fill.

At present, there are both fluvio-deltaic and alluvial fan depositional systems in the basin that are active today. The topography of the basin is a typical example of an asymmetric half graben, with more than 2.5 km of sediment preserved at its centre,

deposited during the Plio-Pleistocene and Holocene. The alluvial fan depositional systems form as a result of several catchments draining into the basin, from the hanging wall as well as the footwall. (Eliet and Gawthorpe, 1995)

Eliet and Gawthorpe (1995) provides a very solid and detailed description of the geology of the Sperchios basin, and a summary of this will be presented in the following paragraphs, with some additions and findings from other contributors as well.

1.3.2 Topography and geomorphology

The active faults along the southern margin of the basin (fig. 1.2) strongly affect the geomorphology of the basin (figure 1.5). The border fault zone in the eastern part of the basin shows consistent elevations above 900 metres, with limestone escarpments dominating the topography. Topographic lows at 20 km intervals break the continuity of the footwall escarpment, and these lows represent the linkage/transfer zones between the previously mentioned fault segments. At the western end of the basin, escarpments are less steep and not as high as in the eastern end. In contrast to the steep escarpments of the footwall, the hanging wall dip-slope along the northern margin of the basin is dominated by a 600 metre ridge climbing to 1400 metres in the Othrys range to the east. The sedimentary basin comprises a wide alluvial/delta plain passing eastwards into the Maliakos Gulf.

Topography and slope gradients vary systematically along the length of the basin, on both footwall and hanging-wall slopes. Across intra-basinal transfer zones, elevations are low on both footwall and hanging-wall sides of the basin (<500 metres). However, topography reaches maximum elevations of almost 2000 metres within the central portion of the fault segments.

Deposition along the hanging-wall side of the basin is dominated by generally large, low gradient alluvial fans, with areas of >10 km^2, which often coalesce to form a broad hanging wall alluvial fan bajada. In contrast, the footwall side is – with a few exceptions – characterised by small alluvial fans, often <2 km^2 (figure 1.5).

The faults in the Sperchios Basin expose varying lithologies (figure 1.6), and this affects the characteristics of the different fault segments. The Kompotades and Thermopylae fault segments run through limestone, and display topographical characteristics typical of faults running through this kind of lithology. The fault planes appear relatively

undissected, with the exception of a few steep canyons crossing the faults, some exposed fault surfaces, and a drainage pattern that is more tightly controlled by the fault segmentation (Goldsworthy and Jackson, 2000). The Sperkhias fault segment is very different in terms of geomorphology, and one immediately notices the absence of a steep, undissected fault plane/footwall ridge. This is because the streams here incise much more easily into the footwall block because of the higher erodibility of flysch, where landsliding is a more dominant process which causes the surface expression of active faulting to be subdued (Goldsworthy et al., 2002). This causes the footwall ridge to look more dissected. It also causes the locations where streams cross the fault to be less related to the fault continuity (Goldsworthy and Jackson, 2000). The already mentioned knickpoints in the streams crossing the Sperkhias fault, as documented by Whittaker and Walker (2015), is also a typical characteristic of faults formed in schist or other easily erodible lithologies, when the knickpoints formed at the scarp migrates upstream with time (Goldsworthy and Jackson, 2000, Cowie et al., 2006). Again, the actual presence of these knickpoints is doubtful and will be discussed later.

The Sperchios River itself flows from west to east axially along the basin (fig. 1.3). Both subsidence along the border fault and transverse alluvial fan systems influence the position of the river, where the latter in some areas divert the Sperchios River away from the footwall scarp. The river discharges into the Maliakos Gulf in the east of the study area, where it has constructed a series of bird's foot delta lobes.

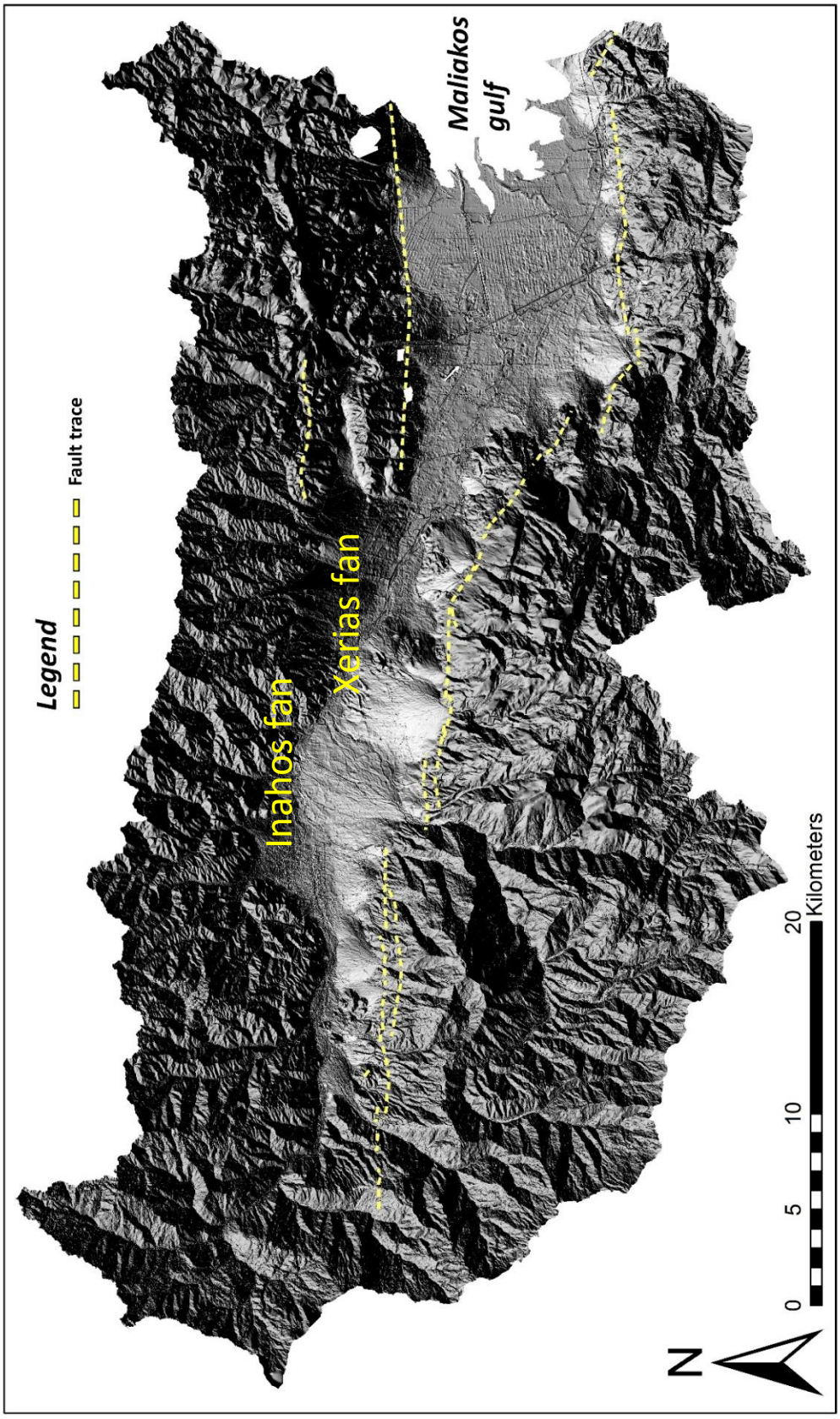

Figure 1.5: A vertically exaggerated (40x) hillshade map showing the topography of the Sperchios basin. Here projected to emphasize the alluvial fans deposited by systems draining across the faults, from the footwall to the hanging wall.

1.3.3 Lithology

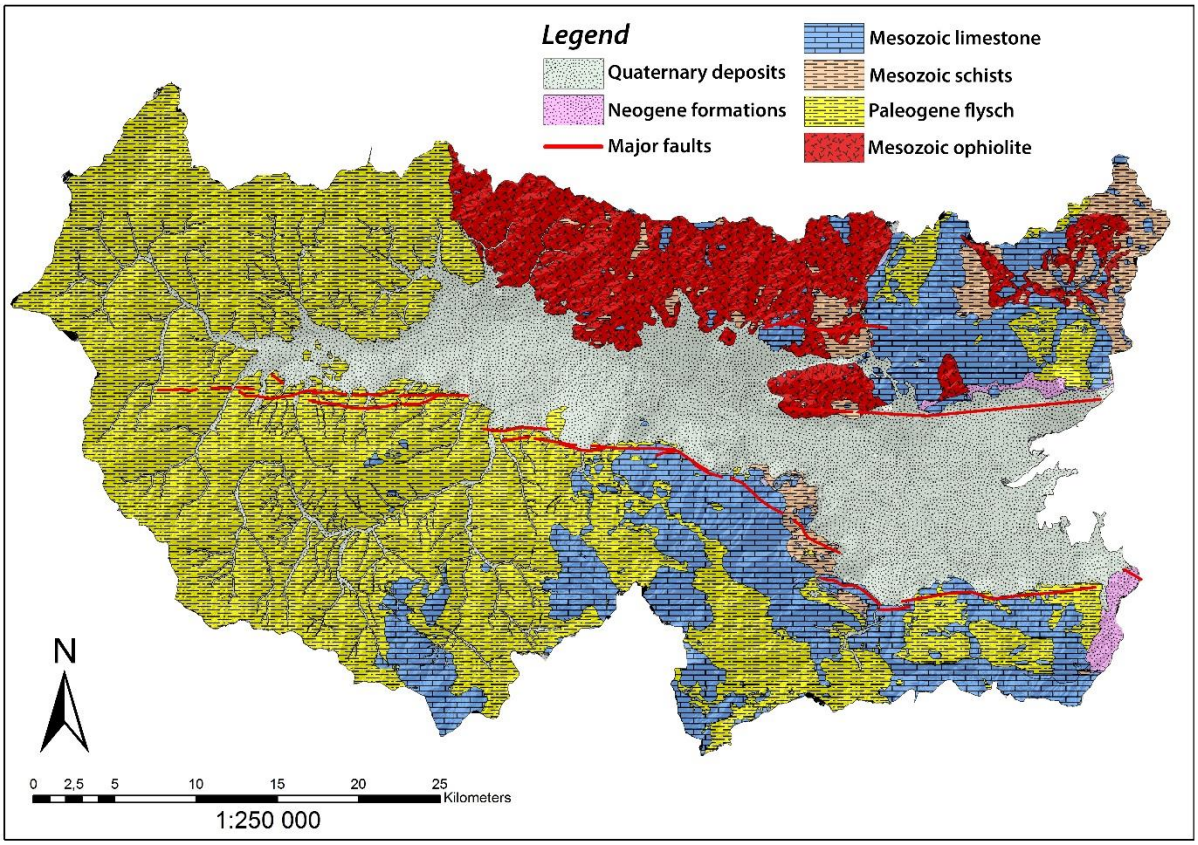

Figure 1.6: Lithological map of the Sperchios Basin.

Figure 1.7: An outcrop showing nicely folded flysch, with both anticlines and synclines (or antiforms and synforms).

In the Sperchios basin, the exposed bedrock can be sub-divided into three major zones: in the west a pre-rift clastic zone composed of flysch (figure 1.7), in the north an ophiolite and limestone dominated zone with some flint as well, and in the south upland a zone dominated by limestone escarpments and unconsolidated Neogene basin sediments (figure 1.6). The footwall scarp topography is clearly influenced by the composition of the bedrock; the limestone dominated Kompotades segment has significantly higher maximum elevations than the flysch dominated Sperkhias segment. The limestones in the area date from the Jurassic to Triassic periods whereas the flysch is of Cretaceous age (Apostolopoulos, 2005, D'Alessandro et al., 2014).

1.3.4 Drainage

Tectonic relief and gradients produced by normal faulting strongly influence the drainage networks feeding into the Sperchios basin. The drainage catchments in the Sperchios basin can be classified into four different domains based by their characteristics regarding size, area, length and tectonic or lithological substrate.

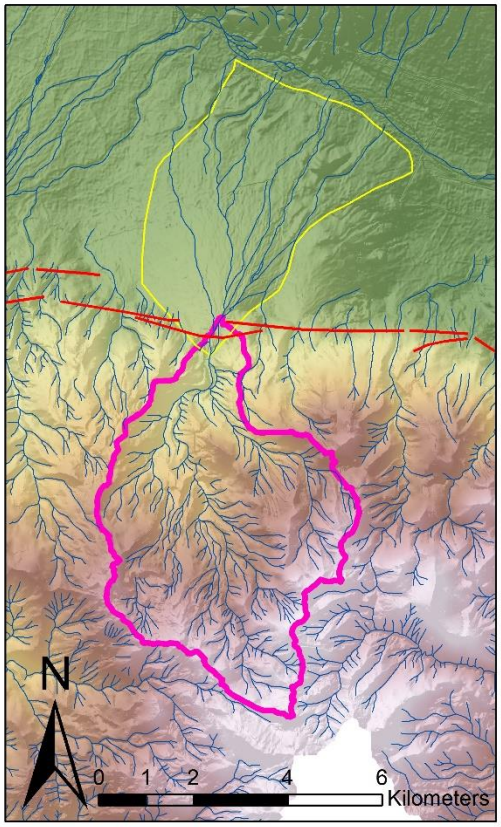

Figure 1.8: Map showing the extent of the Xerias catchment and fan.

The *footwall drainage domain* comprises catchments developed along the footwall scarp of fault segments, and are recognized by their small size (mean area of 6.25 km2), steepness and shortness. The rate of erosion within the catchment is controlled by bedrock lithology as well as uplift rate, and these together influence the ultimate size of the footwall drainage catchment. Catchments along all the three major fault segments on the south margin of the basin, the Sperkhias, Kompotades and Thermopylae segments (figure 1.2), show comparable characteristics that fit well into the footwall drainage domain classification. However, there is a variation in the mean catchment area due to lithological variations. The catchments along the Sperkhias segment are slightly bigger than for the two other segments as it is dominated by pre-rift clastic deposits, whereas the catchments along the two other fault segments are

dominated by harder Mesozoic limestone. The Xerias catchment (figure 1.8) is a typical example of a footwall drainage domain, as it drains right across the Kompotades fault segment. An interesting observation regarding this catchment is that the size of the catchment and the size of its fan do not correspond well; the size of the fan would imply a much larger catchment. Another fan coming out of a footwall drainage domain at the centre of the Sperchios Fault Segment displays an even greater discrepancy between catchment area and fan area. The reasons for these discrepancies will be further discussed later.

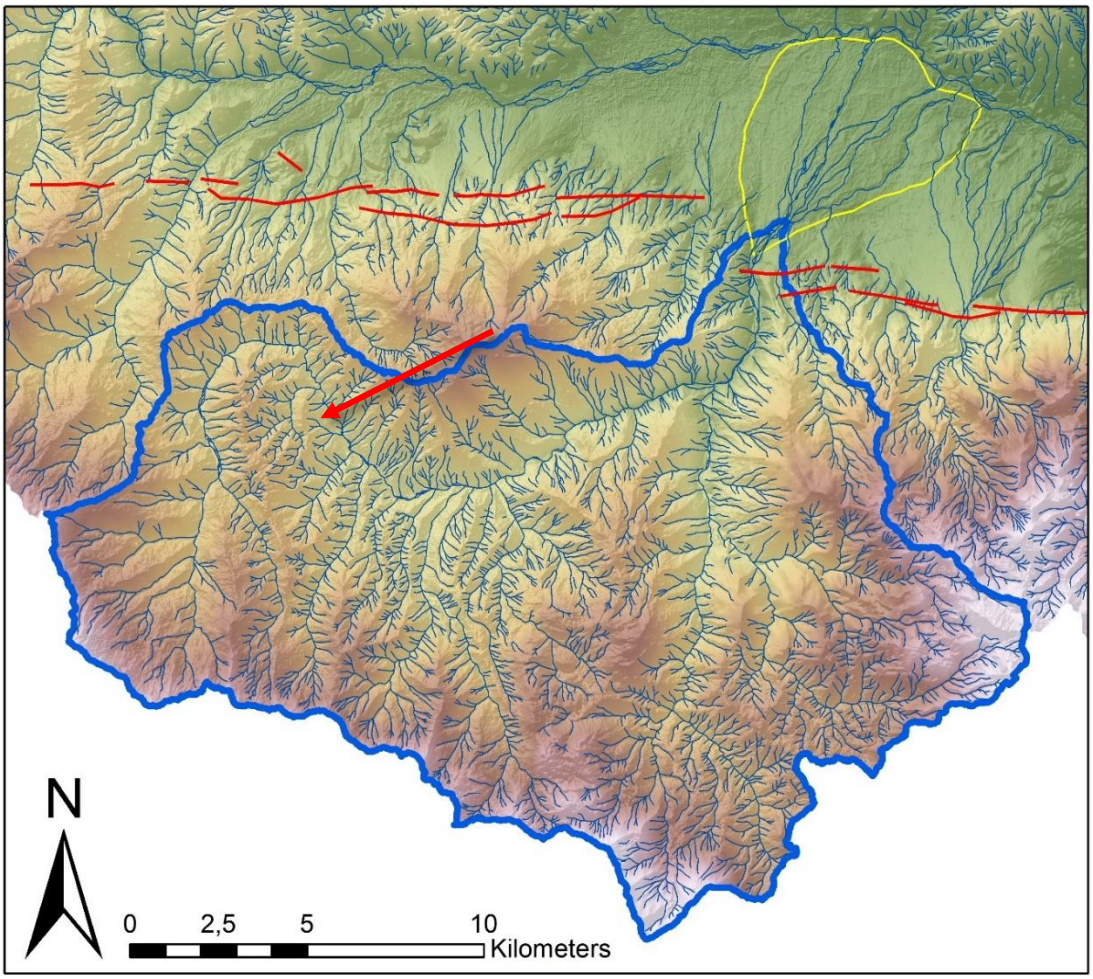

Figure 1.9: Map showing the extent of the Inahos catchment and fan. The red arrow marks the position of trellis drainage.

Another drainage domain present in the basin is the *transfer zone drainage domain*, which compared to footwall catchments has a lower gradient, much larger drainage area and can extend for several tens of kilometres into the footwall. The mean size of the transfer zone catchments along the Sperchios border fault zone is 87.5 km^2. As for the

footwall drainage domain, bedrock lithology is also important in controlling catchment area in transfer zones. In the transfer zone between the Kompotades and Sperkhias fault segments, a large catchment drains into the Sperchios basin. This catchment, called Inahos (figure 1.3 and 1.9) (also referred to as Vistriza, Bistritsa in other studies), has an area of 300 km^2 and drains pre-rift clastic deposits. There are other examples of transfer zone catchments in the transfer zone between the Kompotades and Thermopylae segments, and although these are smaller (<60 km2), they are considerably larger than those draining the footwall of the adjacent fault segments. Present in the Inahos is also a good example of trellis drainage (figure 1.9), which is an indicator of possible river capture events having occurred here. The development of trellis networks is a result of blocks of sediment being backtilted at faulting due to extension (Leeder et al., 1991, Seger and Alexander, 1993, Cowie et al., 2006), and the implication of the trellis drainage in this catchment will be discussed later.

A third drainage domain present in the basin is the hanging-wall drainage domain. This domain is characterised by catchments developed on the hanging-wall dip slope of the rift, larger than their footwall counterparts (mean area of 10.9 km2) and with a large variation in catchment area and forms. This variation reflects along-strike variations in bedrock lithology, hanging-wall dip and position of antithetic fault segments. The hanging wall catchments in the Sperchios basin are well ordered and with catchments an order of magnitude larger than their adjacent catchments occurring approximately every 12 km along the hanging wall.

The final drainage domain present in my study area is the axial drainage domain, which in the Sperchios basin comprises the catchment at the western end of the basin that supplies sediment to the Sperchios River. The area of this catchment is 228 km2, making it smaller than the Inahos catchment, the largest of the transfer zone catchments. The Hellenide thrust sheets to the west of the basin restricts westward extension of the Sperchios drainage networks.

For further details, see Eliet and Gawthorpe (1995), Goldsworthy and Jackson (2000), Goldsworthy et al. (2002), Apostolopoulos (2005), Cowie et al. (2006), D'Alessandro et al. (2014), Whittaker and Walker (2015). A schematic overview of the focus area for this thesis is illustrated in figure 1.10.

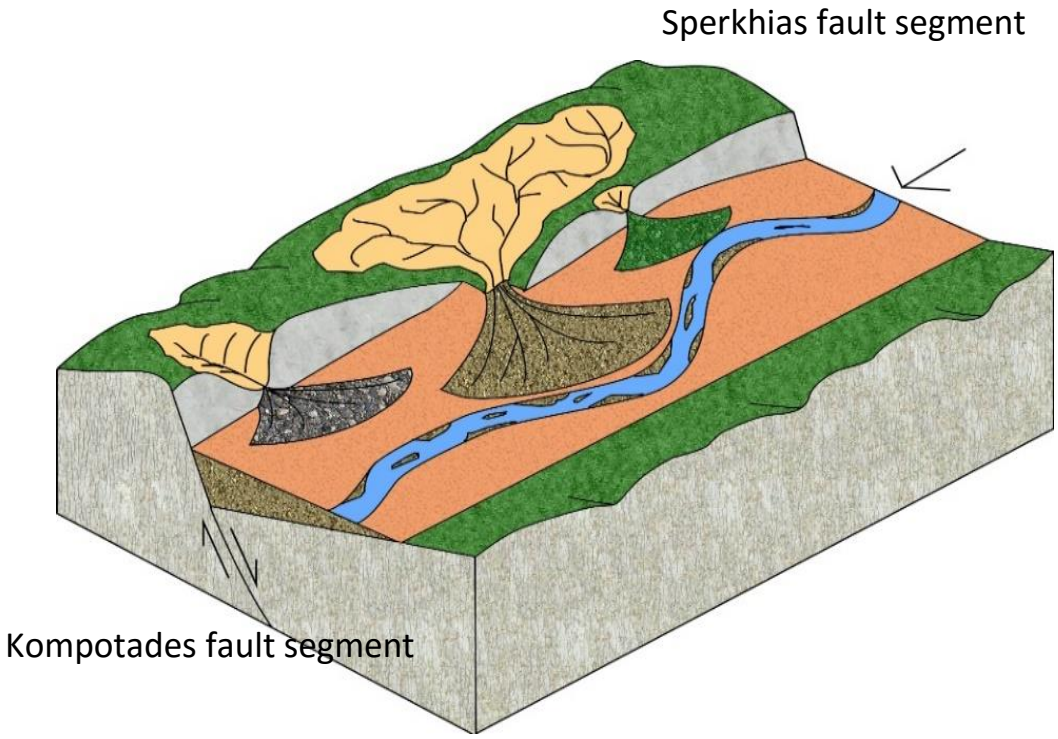

Figure 1.10: Schematic figure of a section of the Sperchios basin with the two fans I have focused on in the modelling (left), the fossilized fan (right) and the axial system flowing parallel to the fault. Here seen from north-east.

1.4 Modelling based on grain size analysis

As stated previously, one of the goals in this project is to explore the relationship between grain size fining rate, initial volumes of sediment supply and spatial distribution of tectonic subsidence for the Sperchios basin. There are several approaches that allow for modelling downstream grain size sorting from parameters measurable in the sedimentary record, but most of them are developed for application to modern rivers, based on variables that are not very easily measurable in the sedimentary record (Duller et al., 2010). Such variables include catchment hydraulic geometries, sediment transport relationships and time-dependent distribution of channel discharges (Duller et al., 2010, Whittaker et al., 2011). Furthermore, the models are often so complex that the simplicity of the grain segregation process is obscured (Fedele and Paola, 2007). Fedele and Paola (2007) present a different approach to modelling downstream sediment sorting with a reformulated model that is based on the assumption that grain size distributions are self-similar. If a physical phenomenon or property is to be called self-similar, it should appear to be temporally or spatially invariant, meaning it looks the same at each point (Duller et al., 2010). In the case of grain size distribution along a river, it means that the relative distribution of grain sizes should be similar at each point

along the system. In this thesis, detailed field measurements of downstream variations in grain size, made using the Wolman point count (Wolman, 1954), are presented for several sedimentary systems in the Sperchios basin. For three of the systems, the grain size trends are coupled with spatial variations in tectonic subsidence and sediment supply, using a self-similarity grain-size model that has been developed by (Fedele and Paola, 2007) and further explored by Duller et al. (2010) and Parsons et al. (2012).

The formulation presented by Fedele and Paola (2007) allows exploration of the impact of controlling variables on fining profiles, without having to model details of hydraulics and sediment transport, and it involves a minimum number of physically based parameters. The concept of self-similarity is dependent on the probability density of the input grain size supply to the system and the similarity variable ξ:

$$\xi = \frac{D - \overline{D}_{(x*)}}{\sigma_{(x*)}}$$

where D is a given sediment size, and $\overline{D}_{(x*)}$ and $\sigma_{(x*)}$ are the mean and standard deviation of the mixture at a normalized longitudinal location x_* ($x_* = x/L$) along a depositional system of total length L. The controlling variables that are explored in this model are, as mentioned above, (1) the sediment input into the system, where an increase in initial volume causes a decrease in the rate of downstream fining in a fluvial system, (2) the amplitude and wavelength of tectonic subsidence where high amplitude/short wavelength systems increase the rate of downstream fining, and (3) the variance in grain sizes supplied to the system, where an increase in grain size spread in the sediment supply increases the rate of downstream fining (Duller et al., 2010).

According to Duller et al. (2010) there are a few requirements and assumptions that are either implicit or explicit in this grain size fining model. The system must be depositional along its entire length if the down-system fining is to take place, and deposits must be the products of streamflow processes and not debris flow processes. This is necessary to make sure that selective transportation of individual particles can be inferred unambiguously. Furthermore, the model has a few limitations as the self-similar solutions are only valid for unimodal grain size distributions, the mechanical breakdown of particles, also known as abrasion, is unaccounted for, no lateral input of sediment is allowed other than that at the upstream boundary, and predictions are limited to two-

dimensional distributions of grain size; the model does not replicate a full three-dimensional lateral variation of grain size, and nor does it describe facies partitioning of grain sized down-system.

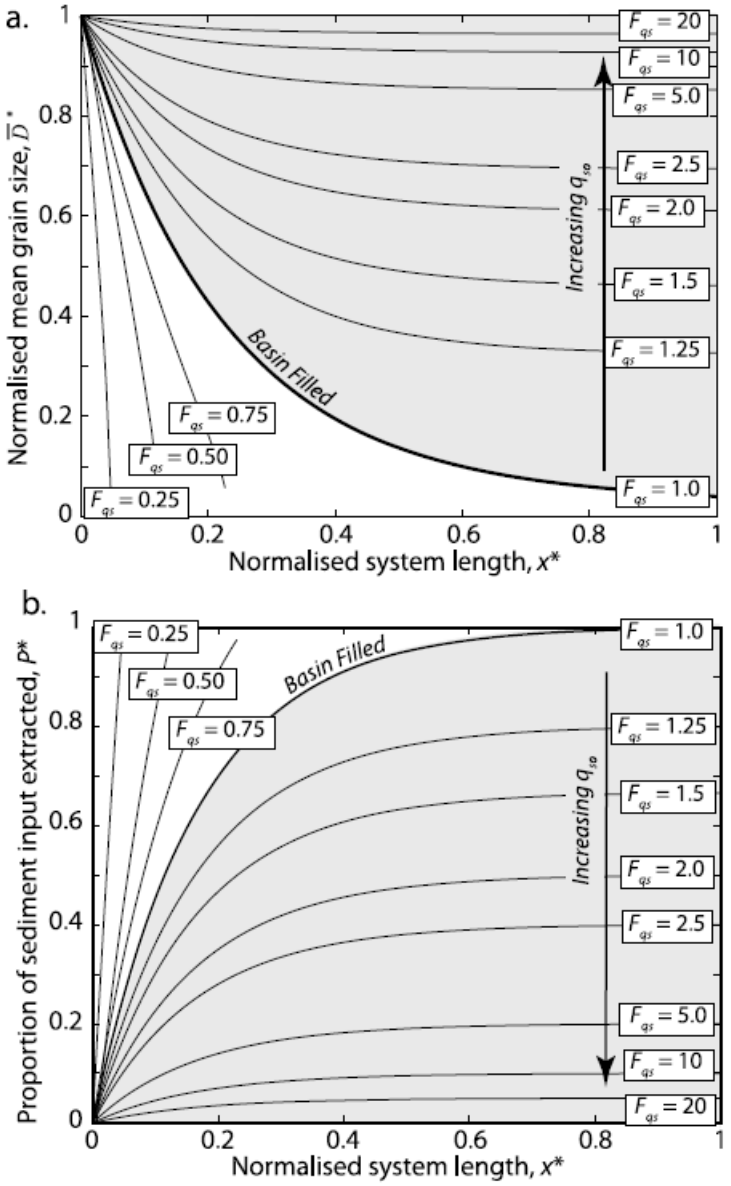

Figure 1.11: Model sensitivity results illustrating the impact of varying initial sediment discharge on grain size fining trend and sediment extraction in a generic scenario. (Duller et al., 2010)

Before applying the model to field data, a sensitivity analysis can be used to show how the variations in different controlling parameters impact the spatial trend of grain sizes for generic scenarios. Such an analysis has been performed by Duller et al. (2010), and the results can be seen in figure 1.11 and 1.12. Figure 1.11 presents the results of the

sensitivity analysis made by varying the initial sediment discharge, and how this impacts downstream fining and sediment extraction. Initial sediment discharge, q_{so}, is here represented as F_{qs} which represents the fraction of the perfect filling case, i.e. a perfectly filled system = $F_{qs} = 1$. As is evident from the analysis, increasing the initial sediment discharge makes the downstream fining slow down significantly in addition to a general increase in overall grain size. We also see that an increase in initial sediment discharge decreases the amount of sediment extracted from the fan, as increasing sediment discharge increases the degree to which the fan is overfilled.

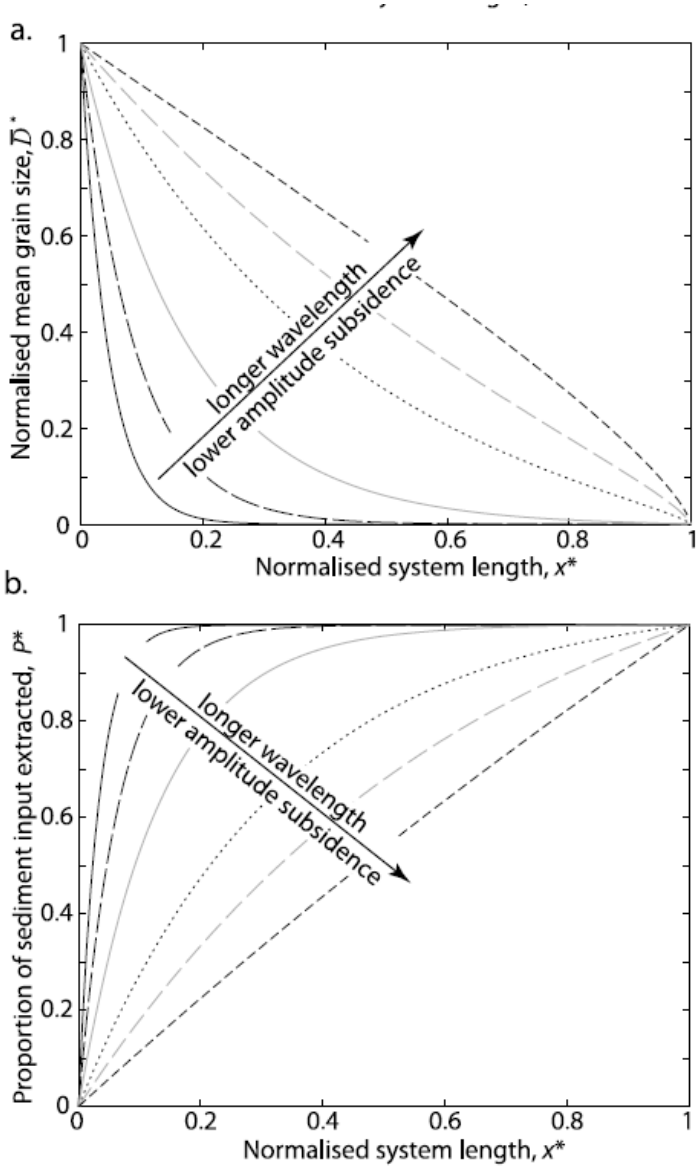

Figure 1.12: Model sensitivity results illustrating the impact of varying amplitude and wavelength of subsidence on grain size fining trends and sediment extraction. (Duller et al., 2010)

Figure 1.12 displays the results of a sensitivity analysis where spatial distribution/wavelength and amplitude of subsidence has been varied, and how this impacts grain size fining and sediment extraction. Although wavelength and amplitude varies, the subsidence decreases downstream in all examples. What is evident from this analysis is that decreasing amplitude and increasing wavelength of subsidence causes the downstream fining to approach a linear distribution. We also see the same trend regarding sediment extraction; lower amplitude, longer wavelength subsidence causes the sediment extraction to be more linear, i.e. the extraction is more evenly spread throughout the system, whereas high amplitude, short wavelength subsidence causes a very abrupt fining trend which flattens out early.

2.0 Methodology

2.1 Grain size pictures

Figure 2.1: A typical example of how a grain size photo looks like.

A two-week field trip in the Sperchios region in Greece was undertaken to acquire the field data needed for this thesis, from the 26th of September to the 10th of October 2015. During the field trip, Schmidt hammer measurements, sieving, laser measurements and grain size photos were the field methods I used, of which the latter was the most important method. The Schmidt hammer measurements were applied for measuring and comparing (hardness) of limestones and flysch in the area. Sieving was applied to measure the proportion of fines in the sediments of the channel bars in the Sperchios axial river. The true pulse laser scanner was used to measure width, depth and most importantly inclination of the channels. The grain size photos were, as mentioned above, by far the most important method and the one I used most of the time. The purpose of taking grainsize photos is to characterise the grain size distribution in a fluvial system. Understanding the dynamics of the sediment routing system in my field area required quantification of grain size distribution along the fluvial systems I have focused on. To do so, I measured the grain sizes in the coarse fraction (>1 mm) of the

sediments using a technique involving scaled grain size photos of active gravel bars based on a method called the Wolman point count (Wolman, 1954). I calculated the downstream variations of the median grain size (D_{50}) and the 84th percentile size (D_{84}).

The tools I used when taking the grainsize photos were a digital single lens reflex camera and a scale bar measuring 15 cm, in addition to a GPS to keep track of, and geographically organize, my measurements. When taking the photos, I found a suitable channel bar and took three to four photos in a suitable spread on the bar, thus making sure I would get a reasonable representation of the grain sizes present at the bar in question. These three to four photos from one single bar are treated as one point. The photos were taken perpendicular to the ground, and in every photo the scale bar was included (figure 2.1).

Extracting useful information from the grainsize photos required thorough post-processing in the form of careful length measurement of 100 grains from each photo in a photo editing software, in my case Adobe Photoshop CS6 Extended. The measurements were done on the grains' intermediate axis. The selection of 100 grains on each photo was done by overlaying the images with a grid measuring 11x11 squares, which gives lines that intersect at 100 points with a regular interval within the grid. I measured the grains that are located at these intersections by using the measurement tool in Adobe Photoshop (figure 2.2). As not all intersections in all the photos would lie directly on top of a grain, it was not possible to reach a total of 100 measurements on every photo. Grains smaller than 1 mm were also difficult to see and/or measure, so these were excluded from the measurements. Since I took three to four photos from every channel bar I was interested in, I have at least 250-270 measurements from each point, with a maximum of 400 measurements in the locations where there were no difficulties measuring grains in the photos. Every measurement was saved in a table, which was then exported as a .txt-document and copied over to excel for further post-processing and modelling purposes.

In total, the grains measured amount to 14425, from 49 locations in the Sperchios basin (figure 2.3).

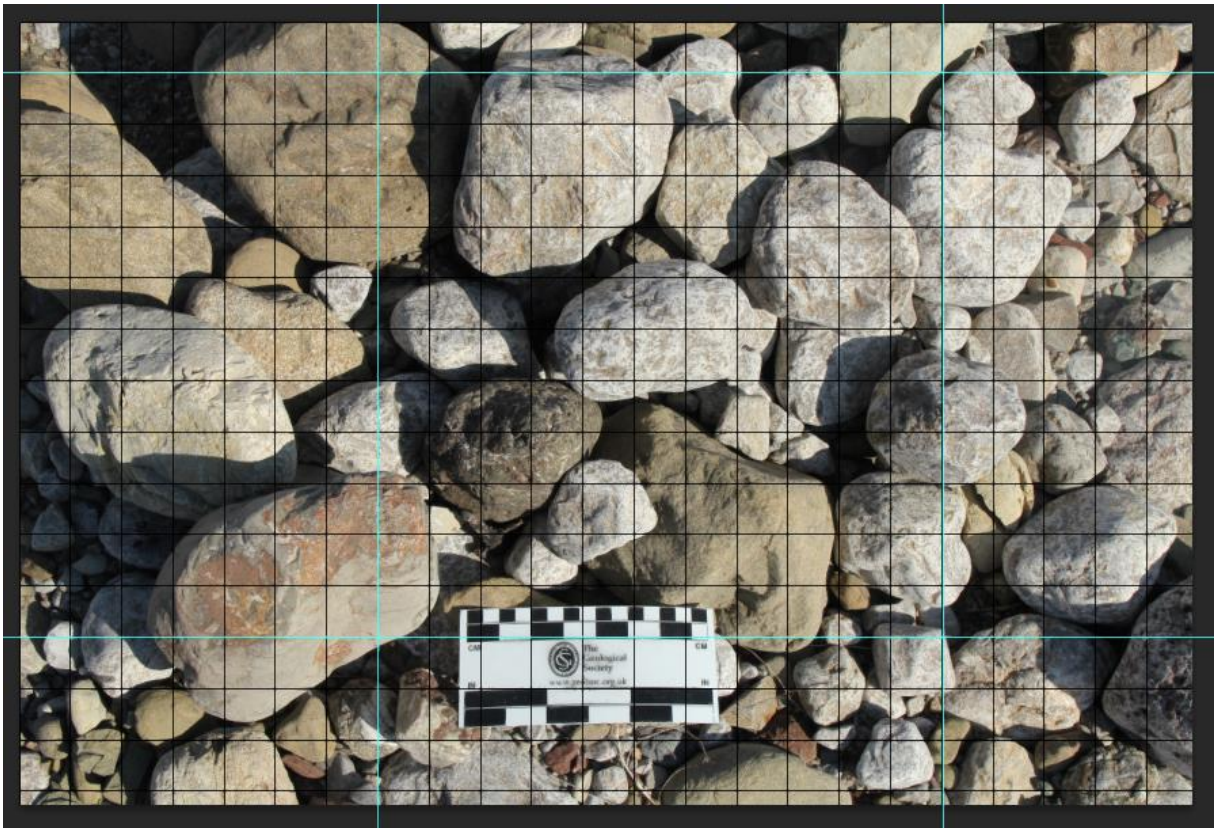

Figure 2.2: A screenshot of a typical grain size photo with the grid (black) and guidelines (cyan) for grain size measuring. The grains outside of the guide lines are not measured.

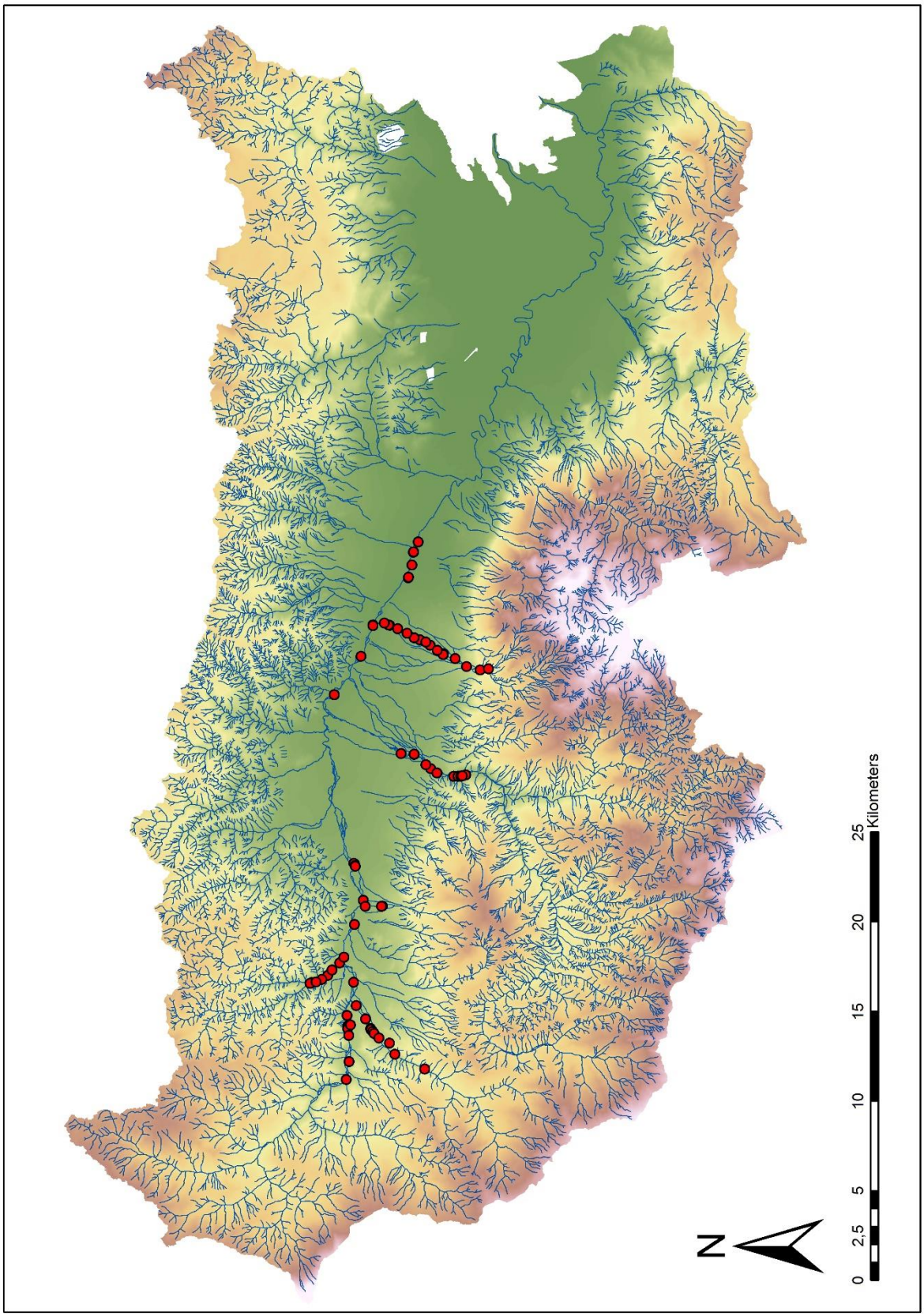

Figure 2.3: This map shows all the waypoints at which I have taken grainsize pictures. Each waypoint represents three to four localities where a photo has been taken.

2.2 Modelling

The modelling itself is performed in excel, where the main controlling factors can be altered to explore how variations in these factors impact the projected downstream fining rate and sediment volumes. The modelling can be done both in 2D – not taking channel width into account – or in 3D – taking channel width into account. My modelling is done in 3D, which means that I have also included an estimate of the channel width along the systems I do my modelling on, or in this case fan width. The measurements are not manual measurements done in field, but calculated based on a linear increase in width from the apex to the base. The calculated widths have been quality checked by doing manual measurements in the 5m DEM in ArcGIS and measuring on satellite imagery from Google Earth. To make sure my model would behave properly and according to the theories presented above, I ran a sensitivity analysis on my own data to see that variations in the different controlling factors would impact the spatial distribution of fining trends the same way as it should in theory, as demonstrated in chapter 1.2. The results of this analysis will be presented later in the thesis.

2.3 ArcGIS

GIS (Geographical Information Systems) was an important tool during the work with this thesis. Many of the figures in this thesis, along with the long profile of the fans at Xerias and Inahos, are made with the use of a GIS software, in my case ArcGIS. I obtained a 5 metre DEM raster dataset from the Sperchios basin and close surroundings. Although a DEM does not depict the actual geomorphology with 100 % accuracy, the 5m DEM I obtained is very detailed due to its high resolution and is thus of high quality. A 5 metre DEM means that every pixel is 5x5 metres in size, which means that features smaller than 5x5 metres will not be detected. Each pixel can be attributed a unique value, in this case elevation. However, most geomorphological features are far bigger than 5x5 metres, which is why this DEM is more than good enough for its purpose in this thesis.

The most important tasks I had to do in ArcMap was to extract stream networks and catchment boundaries for use in the figures in this paper. However, I also used other tools in ArcMap to visualize different properties of the geology and geomorphology in the area. This will be described later. The process of extracting stream networks and

catchment boundaries consisted of several steps which will be described in the following paragraph.

By using the hydrology toolbox in ArcGIS, I made sure the hydrological surface of the DEM was consistent by using a tool called “Fill”, which makes sure any sinks in the DEM are neutralized so that water flow calculation is not disturbed by artefacts, for example cells with no values. After doing that, I was able to calculate the direction in which water flows in all pixels in the DEM, the accumulation of water flow in each pixel of the DEM, and from there define the drainage network itself as a raster dataset. To define the stream network effectively, I had to define a lower boundary so that I could rule out minor streams that are not interesting. I defined a threshold of 5000, meaning that only cells that have more than 5000 pixels draining into them was kept. This threshold corresponds to catchments with a drainage area ≥ 0.125 km^2. Other cells was given a null value. The drainage network in the raster was defined according to the Strahler method of stream ordering, which classifies streams according to how many tributaries they have. First order streams have no tributaries, and the order increases downstream when two streams of the same order join (Strahler, 1957). The drainage raster was then converted to a vector dataset, so that streams are represented by continuous vectors (lines) rather than pixels (raster). With the combination of a raster dataset in the hydrologically defined DEM and a vector dataset in the drainage network, I was able to define the watersheds within the Sperchios basin as well as the main watershed delimiting the basin itself. The watersheds were defined by defining pour points which calculates the drainage flowing into that single pixel. This calculation is done on the basis of the flow accumulation raster generated earlier in the process. So, to calculate the area of each of the catchments I was interested in, I had to define a pour point at the end of the stream coming from that catchment. By combining all the watersheds into one raster and converting it to a polygon, I was able to clip the DEM so that the areas not draining into the Sperchios basin at all were cut out. By then, I had a dataset that included all the necessary information regarding the Sperchios basin when it comes to drainage, and also excluding all areas that are not interesting due to the fact that they do not drain into the basin.

2.4 Accessory work

2.4.1 Naming

The names used on the catchments, fans and streams discussed in this thesis have been varying throughout my work on this project, due to some uncertainty of the actual names of the features, different names in different maps, papers, studies etc. However, I have landed on the names presented below, which are the correct names according to Greek topographic maps (Sofia Pechlivanidou, pers. com.). The fossilized fan has not been given any name, as it is uncertain if the stream flowing across it has a name. The large catchment seen in figure 1.9 has been named Inahos (greek: Inaχos), named after the river that has been depositing the fan, which is referred to the Inahos fan. This is often referred to as Vistriza (or even Bistritsa) in other studies. The catchment crossing the Kompotades fault (fig. 1.8) is referred to as Xerias (greek: Ξerias) in this thesis, named after the river that deposits the fan, which is thus referred to as the Xerias fan.

2.4.2 TruePulse laser measurements

A handheld laser measuring device was used at certain points along the different fans and rivers to measure the slope along the active channels. The reason for doing this was to be able to compare the DEM measurements with laser measurements in the field to make sure the slopes derived from the DEM are actually reasonable. The slope measurements obtained from the laser measurements can be seen in appendix A.

2.4.3 Schmidt hammer measurements

To measure the rock strength of the flysch and limestones in the Sperchios basin, a Schmidt hammer was used at a selection of localities where these lithologies were nicely exposed in outcrops. The rock strength classifications obtained from the Schmidt hammer measurements can be seen in appendix B.

2.4.2 ArcGIS

In addition to defining stream networks and extracting catchment boundaries, I used ArcMap to produce several other figures. A hillshade map was created to visualize the geomorphology of the basin and highlight the fan structures in the basin. The DEM was, together with the drainage network vectors and imported GPS waypoints used to create a map showing the localities at which I made grain size readings etc. ArcMap was also used to produce the lithological map in this thesis. The cross section charts from the basin were also made in ArcMap, by dragging lines across the DEM where elevations along the line are plotted in a diagram.

3.0 Results

In this chapter, results from field work and modelling will be presented in the following order

- Observations and characterisations of the fans and streams studied
- Discussion relating to the fossilized fan and its implications for the geologic development of the basin
- Results of the grain size analysis for two fans – Inahos and Xerias – and the Sperchios axial system (with data from both Pechlivanidou et al. (2016, manuscript in preparation) and myself)
- Modelling results for Inahos and Xerias
- A sensitivity analysis for my model

The presentation of these results will hopefully give the reader a good understanding of the characteristics of the two fans and how they differentiate from the axial system, along with an understanding of other interesting geomorphological phenomena, and will thus form a basis for the discussion in chapter 4.

3.1 Observations

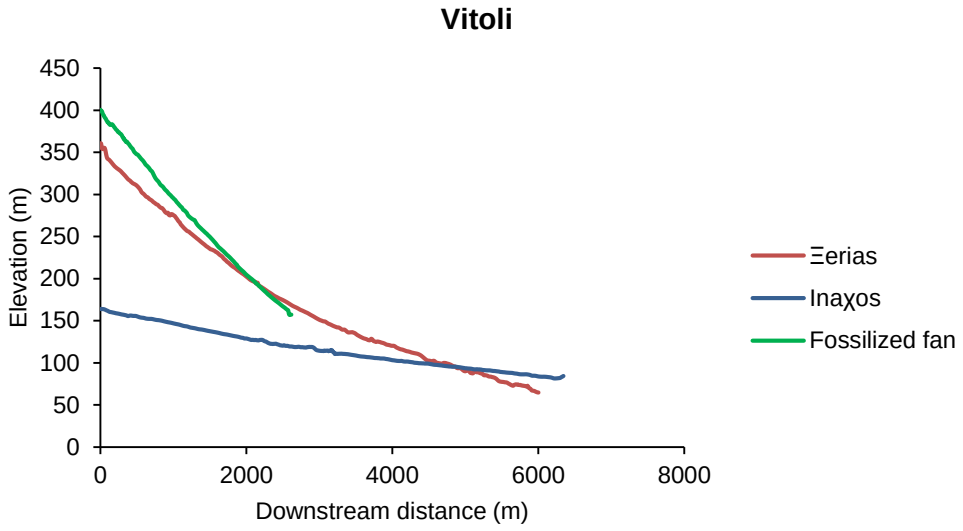

Figure 3.1: Graph showing the slopes of the different fans I have studied.

3.1.1 Inahos

Impressions

The fan prograding out of the Inahos catchment (figures 1.3, 1.5, 1.9) does at first glance seem very large compared to the other fans in the basin, with an approximate area of 26 km^2. It stretches all the way from the fault and down to the Sperchios river, where it seems to have displaced the latter. Most of the fan surface area is covered with agricultural land, except for the active channel and the areas in its close proximity. Prone to flooding during the melting season and severe weather events, they are probably less attractive for agricultural use. The active channel seems to have been canalised in the lower parts of the fan.

Slope

Evident from both slope measurements made on the DEM in ArcGIS (figure 3.1) and from measurements done in the field with a laser (appendix A), the Inahos fan has a gentle slope of around 0.74°, more gentle than most of the other fans in the area. At its toe, along the active channel, the elevation is 84 metres above sea level, whereas at its apex, elevation is 164 metres above sea level.

Clast lithology, rounding, depositional fabric

The lithology of the clasts in the Inahos fan reflects the lithology of its catchment (figure 1.6) and is dominated by sandstone and siltstone (flysch), but there are also minor

elements of chert. In terms of rounding we see mostly sub-angular, sub-rounded and rounded grains. They have a low degree of sphericity, with many grains displaying a prominent disc-shape often parallel with the internal stratification of each individual clast. There are also rod- and blade-shaped clasts. In areas with nicely exposed stratigraphy, one can see clear evidence of typical AB-plane imbrication where the clasts long axis is transverse to the flow direction and intermediate axis is parallel to the flow direction. The low degree of sphericity in the grains enhances imbrication.

Human activity

The Inahos fan is to a certain degree affected by human activity. As mentioned earlier, a large portion of its surface area is covered in agricultural land. Along the river bank efforts have been made to constrain the extent of the channel and reduce risk of flooding by creating artificial river embankments forming a canal at the lower reaches of the fan. These embankments are made up of piles of stacked netting cages filled with gravel and cobbles, presumably extracted from the channel bed or fan surface. We also observed this in action in the downstream part of the Inahos fan where channel bed material was extracted and transported out of the channel by large lorries. These embankments are very prominent along the active channel of the Inahos fan, and might cause disturbance in the grainsize distribution pattern along the channel as they constrain the area where sediment can be deposited.

Figure 3.2: An example of how the man made netting cages forming the artificial embankments looks like. Here from the lower parts of the Inahos fan.

3.1.2 Xerias

Impressions

The fan prograding out of the Xerias catchment (figure 1.3, 1.5 and 1.8) is somewhat smaller than the Inahos fan (fig. 1.3, 1.9), with an area of approximately 18 km^2. It stretches from the fault scarp in the south, at its apex, 6 km northwards into the basin where it has its toe. The Xerias fan surface is partially untouched, and has two very distinct halves that have different appearances and characteristics; a clear fan structure is only visible for the upper 3.5 kilometres of the actual fan, dominated by scrub vegetation, alluvium and smaller inactive channels, whereas the areas north of this clear fan structure is dominated by agricultural land. Most of the agricultural land is on the west side of the active channel. The scrub vegetation on the upper parts of the fan might imply that the fan has been much more active at earlier times. For this reason, together with the discrepancy between the fan size and catchment size, Eliet and Gawthorpe (1995) calls this fan fossilized. However, I will not be calling it that, as I will be describing another fan that is, to a much larger extent, fossilized.

Slope

Compared to the Inahos fan, the Xerias fan is much steeper with a slope of approximately 2.51°, measured from a 5m DEM in ArcGIS (figure 3.1) and also with laser in the field (appendix A). The laser and DEM measurements deviate by almost 1 degree here, but I consider the DEM measurement to be the most exact measurement because of its good quality. The steeper slope is also clearly visible to the eye when simply observing them in the field. At its toe along the active channel, the elevation is 129 metres above sea level, and at its apex, elevation is 360 metres above sea level.

Clast lithology, rounding, depositional fabric

The lithology of the clasts in the Xerias fan is more mixed than in the Inahos fan. We find limestone as the most dominant clast lithology, but there are also sandstone and siltstone (flysch) clasts, as well as chert. Limestone is the most dominant clast lithology due to the lithology of the catchment itself; the Xerias catchment is a limestone dominated catchment (figure 1.6). The clasts are slightly less rounded in the Xerias fan, with more irregular surfaces from angular, sub-angular and sub-rounded clasts. As opposed to the Inahos fan, the clasts in the Xerias fan – especially the limestone clasts –

are much more spherical due to their lack of inner stratification and weakness planes, which makes it more difficult to spot any apparent imbrication.

Human activity

The extent of human activity is much more limited on the Xerias fan compared to the Inahos fan. As previously mentioned there is little agricultural land covering the fan surface area, at least in the upper half of the fan, and there seems to be little or no effort made in constraining the extent and direction of the fans active channel. This might be linked to the fact that the Xerias fan drains a much smaller catchment, thus being less prone to flooding events causing the surrounding areas to be less vulnerable.

3.1.3 Lefkada

Impressions

The Lefkada River is a tributary to the Sperchios River, flowing in from the southwest of the Sperchios basin (figure 1.3). The whole river is approximately 15 kilometres long, and is a braided river. There is no apparent fan structure at its base, and studies of satellite imagery yields no significant findings when it comes to identifying such a structure. However, by creating a hillshade raster of the basin and exaggerating the Z-values 40 times, a clear fan shape can be identified, being about 1500 metres at its widest. It is thus a very small fan compared to many of the other much larger fans in the basin.

Slope

The lower seven kilometres of the Lefkada River where I did my grainsize analysis has a gentle steep of 1.93°, measured from both the DEM (figure 3.1) and laser measurements (appendix A) done in the field. The channel is at 231 metres above sea level at its base where it meets the Sperchios River, and reaches 400 metres above sea level seven kilometres further upstream.

Clast lithology, rounding, depositional fabric

The clast lithology in the Lefkada River is similar to the one found in the Inahos fan, which is reasonable as the lithology in the Lefkada catchment is similar to the Inahos catchment, mostly consisting of flysch (figure 1.6). Unsurprisingly, sandstone and siltstone (flysch) is the dominant lithology among the clasts, but there are also minor elements of chert. In terms of rounding there is also a large degree of similarity to the

Inahos fan, with mostly sub-angular, sub-rounded and rounded grains. They also have a low degree of sphericity, with many grains displaying a prominent disc-shape often parallel with the internal stratification of each individual clast. There are also rod- and blade-shaped clasts.

Human activity

Human activity is likely to make a heavy impact on the Lefkada River, at least in recent times. Large portions of the channel are being dug up because of apparent mass extraction for which the reasons are unknown, with associated makeshift construction site roads made up of riverbed and –bar material. There is also the construction of a large pipeline along the channel, and after consulting one of the workers in the area we were told the plan was to pipe the whole channel. This is likely one of the causes for the mass extraction, but mass extraction also took place further downstream which might suggest that the extracted mass is put to use for other purposes as well.

3.1.4 Vitoli

Impressions

The Vitoli River is a tributary to the Sperchios River, flowing in from the northwest of the Sperchios basin (figure 1.3). The whole river is approximately 11 kilometres long, and is a braided river. There is no apparent fan structure at its base, and studies of satellite imagery and DEM yields no significant findings when it comes to identifying such a structure.

Slope

The lower two and a half kilometres of the Vitoli River where I did my grainsize analysis has a very gentle steep of 1.39°, measured from both the DEM (figure 3.1) and laser measurements done in the field (appendix A). The channel is at 200 metres above sea level at its base where it flows into the Sperchios River, and reaches 257 metres above sea level two and a half kilometres further upstream.

Clast lithology, rounding, depositional fabric

As for the Lefkada River, the clast lithology in the Vitoli River is rather similar to the one found in the Inahos fan, which is reasonable as the lithology in the Vitoli catchment is also similar to the Inahos catchment, mostly consisting of flysch (figure 1.6). Again, sandstone and siltstone (flysch) is consequently the dominant lithology among the

clasts, but there are also minor elements of chert. In terms of rounding there is also a large degree of similarity to the Lefkada River and Inahos fan, with mostly sub-angular, sub-rounded and rounded grains. They also have a low degree of sphericity, with many grains displaying a prominent disc-shape often parallel with the internal stratification of each individual clast. There are also rod- and blade-shaped clasts. In areas with nicely exposed stratigraphy, one can – as in the Lefkada River and Inahos fan – see clear evidence of AB-plane imbrication.

Figure 3.3: AB-plane imbrication in an outcrop at the bank of the Vitoli River. Current from right to left.

Human activity

Human activity is very limited in the Vitoli River. The only man made construction or disturbance I identified in my field work was a small dam/step, about 1.5 metres tall, right upstream from where I took my first grain size photo, approximately 2.2 kilometres upstream from where it flows into the Sperchios River.

3.1.5 Fossilized fan

Another fan that is worth mentioning but will not be a part of my modelling is the fossilized fan located seven kilometres west of the Inahos fan (fig. 1.3).

Impressions

The fan covers an area of approximately 3.6 km^2, is covered in dense scrub vegetation,

and has only a few narrow, active channels. There seems to be a discrepancy in the relationship between the relatively large size of the fan and the very limited extent of its catchment. The dense vegetation cover implies a low degree of fluvial activity at present time which allows for the growth of scrub and forest. This, together with the fact that fan size and catchment extent does not seem to match, is why I have chosen to characterise it as fossilized.

The fan stretches from the Sperkhias fault segment down to the Sperchios River (2.3 km) where the latter incises into the toe of the fan. This gives us a 4-5-metre high outcrop from which we can get a detailed overview of the characteristics of grain sizes and clast lithology, not only of the active channels of the fan, but also deeper in the fan's stratigraphy.

Slope

If we look at the slope of the fossilized fan, we see that it is significantly steeper than comparable fans in the basin (figure 3.1) at 5.4°, based on DEM measurements and laser measurements done in the field (appendix A) . At its toe, the elevation is 150 metres above sea level, whereas at its apex, elevation is 400 metres above sea level.

Clast lithology, rounding, depositional fabric

The lithology of the clasts in the fossilized fan is varied, with limestone, sandstone and siltstone (flysch), and also minor elements of chert and ophiolites. A striking difference between this fossilized fan and the other active fans is found by looking at the degree of clast rounding. The clasts in the stratigraphy of this fan are much more angular, stretching from very angular to sub-angular and sub-rounded. Slickensides can be found on several clasts deeper in the stratigraphy – seen in the outcrop where the Sperchios Rives cuts the toe of the fan – and the sorting is poor. The clasts in the active channels are much less angular, stretching from sub-angular to rounded, and show a greater degree of similarity to the Inahos and Xerias fans. However, in terms of clast lithology there is a great deal of variation here as well, and we can find siltstone and sandstone (flysch), limestone, chert, ophiolites etc.

Figure 3.4: Angular chert pebbles amongst sub-angular to sub-rounded cobbles and pebbles of limestone, sandstone and siltstone.

Human activity

The fossilized fan seems very little affected by human activity. The fan is mostly covered by scrub vegetation, and there seems to be no agricultural use of the fan, and no mass extraction like in some of the other fans/rivers.

Discussion

The fossilized fan is an intriguing and interesting phenomenon in the Sperchios Basin, when considering tectonic geomorphology and the development of the basin itself. Although not directly related to the modelling part of this thesis, it is an important geological phenomenon and can tell us a lot about the development of the basin, catchment development and the age of fault initiation and linkage. It is therefore interesting to discuss the characteristics of the fossilized fan and its catchment and what implications this has on the historic development of the basin.

As stated, the size of the fan does not match the size of its catchment, which might be explained by the catchment having been much larger at the time of deposition. Angular clasts, clasts with slickensides and poor sorting are all typical evidences of a high yield catchment crossing active fault segments with high slip rates (Cowie et al., 2006), and since only one of these three important factors are fulfilled, in this case a catchment

crossing an active fault, it is thought that the fan must have drained from a catchment that is bigger in extent than what it is at present time. It is thought that parts of the present Inahos catchment previously drained into the now fossilized fan (Eliet and Gawthorpe, 1995), which might explain its size, and this also explains why the Inahos catchment has come to be so large compared to other catchments draining into the basin. The presence of trellis networks in the Inahos catchment (figure 1.9) might also act as evidence of river capturing events, and a possible wind gap south of the fossilized fan might be connected to this. The possible wind gap (fig. 3.5) can be an indication of where the former catchment drained into the present day much smaller catchment.

Figure 3.5: The arrow marks the location of a possible wind gap south of the fossilized fan.

The capturing event might have been initiated by footwall back tilting after fault initiation, which – when reaching a certain point and depending on bedrock erodibility – can cause rivers to deviate away from the fault scarp and find other ways to drain into the basin (Leeder et al., 1991, Seger and Alexander, 1993, Cowie et al., 2006). This same theory can be applied to the Xerias fan which sees similar size discrepancies between fan size and catchment size; parts of the catchment what would previously have drained into the Xerias fan is thought to have been captured by the Inahos catchment due to backtilting of the footwall block along the Kompotades fault segment (Eliet and Gawthorpe, 1995).

The presence of limestone, chert and ophiolite in the stratigraphy of the fan also supports the idea that this catchment must have been much bigger when the fan was

deposited, as there are no limestones, cherts or ophiolites present in its present constrained area (figure 1.3, 1.6). However, limestone, chert and ophiolite can be found in what is now part of the Inahos catchment, which strengthens the theory that the Inahos catchment captured large parts of the catchment that previously drained into the now fossilized fan.

Furthermore, it is important to consider the steep slope of the fan (fig. 3.1). Its steepness at 5° might imply a much younger age than the other fans in the basin. If the fan was as old as the Xerias and Inahos fans, we would expect it to have subsided more into the basin. The problem then is that if we consider the age estimate of fault linkage established by Whittaker and Walker (2015), at 1.6 Ma, the fan would either have subsided well into the basin long ago since it has such a low sediment input, or it would have to have built up incredibly fast with huge amounts of sediment in recent time which is not possible due to the small size of its catchment. However, as I have established, the age estimate presented by Whittaker and Walker (2015) is based on highly questionable data. The case of the fossilized fan may well prove that the Sperkhias fault segment was activated more recently, i.e. younger than 1.6 Myr, which also rhymes well with the tectonic development of the Sperchios Basin itself with increasingly younger fault segments in the western part of the basin (Goldsworthy et al., 2002). If we consider that the fan morphology reflects the fault activity, this can also indicate that the fault activity in this area is generally low which leads to very little fan deposition overall, and that can explain why the fan seems abandoned/fossilized.

3.2 Grain size analysis result

In the following subchapters, I will present the results from the analysis of the grain size photos taken during the field work, for all the fans and rivers analysed with this method.

3.2.1 Inahos

Distance downstream (m)	D_{50} (mm)	D_{84} (mm)
0,00	62,13	123,16
210,00	72,11	233,05
460,00	49,81	144,60
1740,00	50,33	118,75
2180,00	29,02	83,01
2550,00	41,21	97,93
3500,00	35,53	81,44
3510,00	30,25	64,93
4330,00	29,96	72,15

Table 1: Table showing the results of the grain size analysis for Inahos.

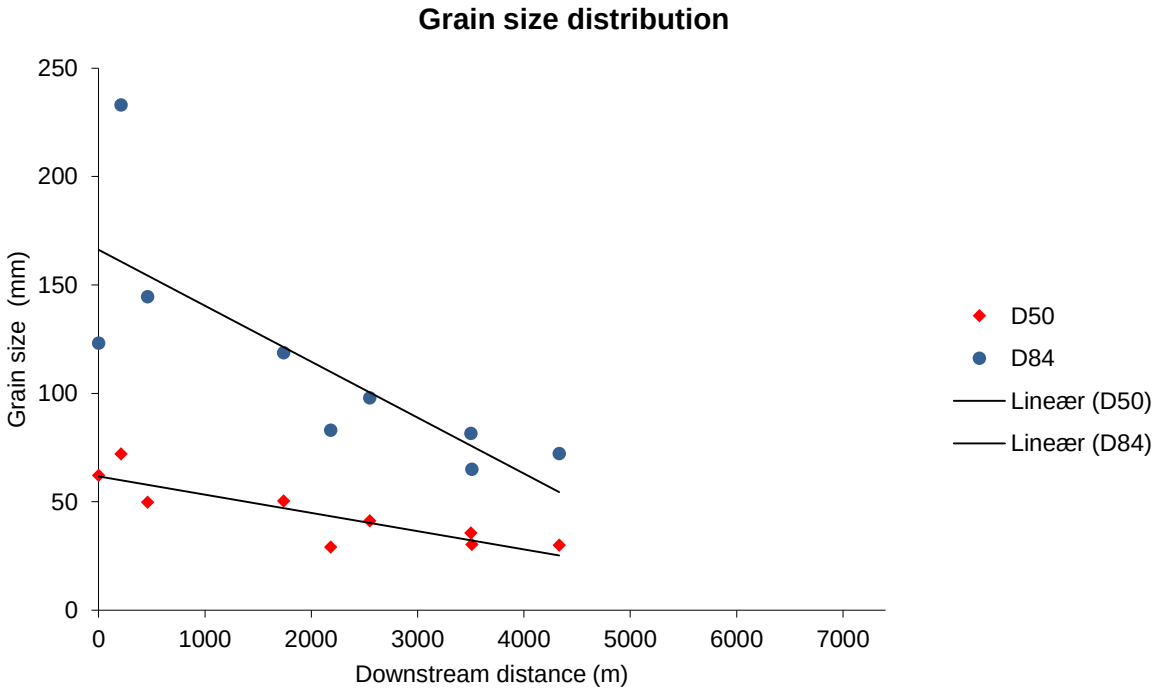

Figure 3.6: Graph showing the grain size distribution (D_{50} and D_{84}) for Inahos. The linear trend lines are displayed for comparison between D_{84} and D_{50} fining trends only. They do not reflect modelled grain size trends.

I measured the grainsize at a total of nine different points along the Inahos river/fan, over a total length of 4.33 km (figure 2.3). The measurement was conducted on 30 photos taken from those nine waypoints, and the amount of grains measured is 2572. The results of the measurements can be seen in table 1. As is visible from table 1 and

figure 3.6, the grainsize trend is fining downstream for both D_{50} and D_{84}, and the fining trend is steeper for D_{84} than for D_{50}. The self-similarity plot also shows that the grain size distribution at all measured points along the river displays a significant degree of self-similarity, with only a few outliers (figure 3.7).

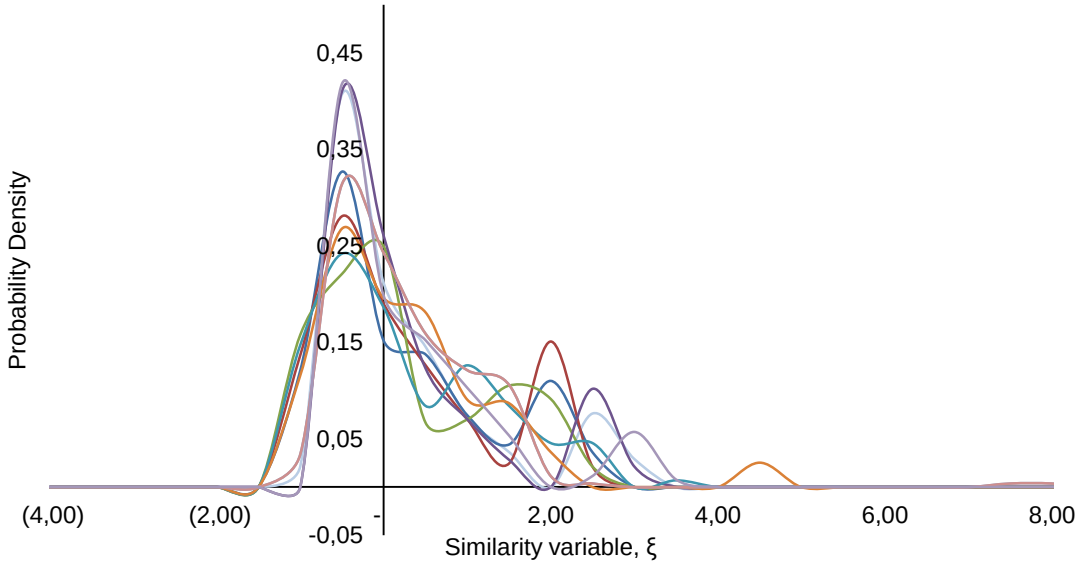

Figure 3.7: Figure sowing the self-similarity curves for Inahos.

3.2.2 Xerias

Distance downstream (m)	D_{50} (mm)	D_{84} (mm)
0	81,64	270,40
850	85,10	155,50
1660	58,72	172,20
2420	43,96	124,95
2830	39,94	115,59
3380	42,17	88,21
3690	40,32	115,86
4070	37,27	77,19
4420	28,07	124,75
4920	28,83	68,72
5570	25,63	59,56
6140	28,16	66,59
6410	26,59	65,94

Table 2: Table showing the results of the grain size analysis for Xerias.

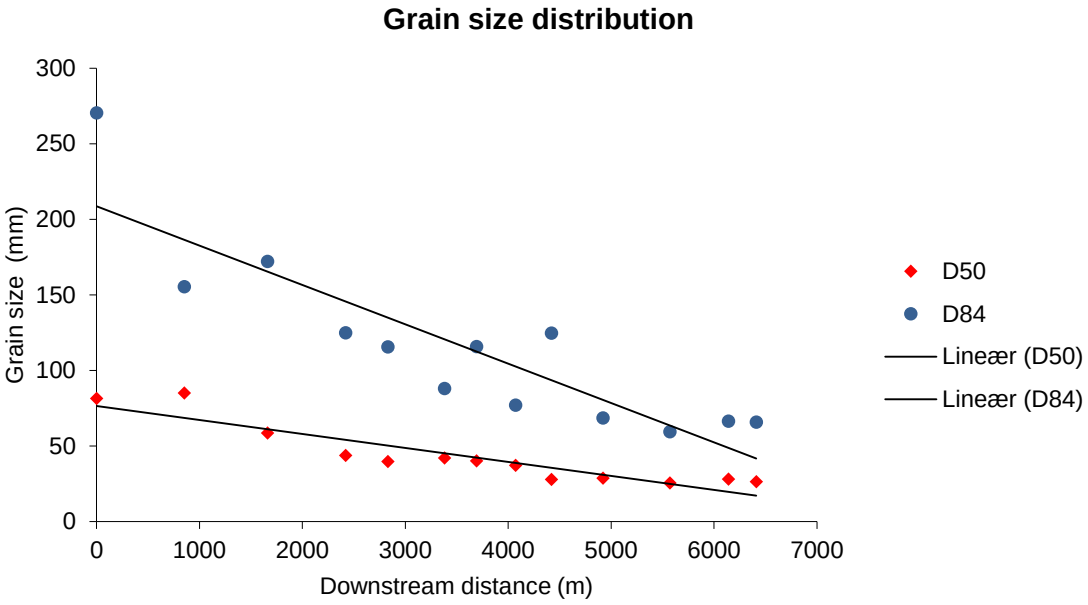

Figure 3.8: Graph showing the grain size distribution (D_{50} and D_{84}) for Xerias. The linear trend lines are displayed for comparison between D_{84} and D_{50} fining trends only. They do not reflect modelled grain size trends.

I measured the grainsize at a total of 14 different points along the Xerias river/fan (figure 2.3), covering a total length of 6.88 km. The measurement was conducted on 50 photos taken from those 14 waypoints, and the amount of grains measured is 4418. The results of the measurement can be seen in table 2. As visible from table 2 and figure 3.8, the grainsize trend is fining downstream for both D_{50} and D_{84}, and the fining trend is steeper for D_{84} than for D_{50}. The self-similarity plot also shows that the grain size distribution at all measured points along the river displays a significant degree of self-similarity, with only a few outliers (figure 3.9).

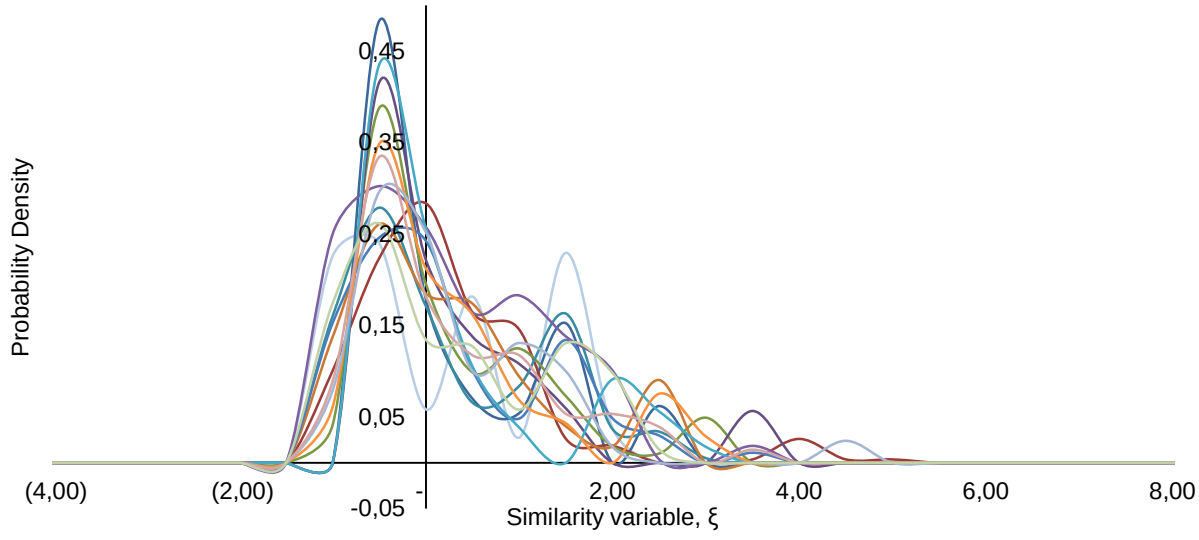

Figure 3.9: Figure showing the self-similarity curves for Xerias.

3.2.3 Sperchios

Distance downstream (m)	D_{50} (mm)	D_{84} (mm)
0	55,15	126,25
3147	65,33	99,47
6692	57,28	113,41
8612	40,63	87,27
11780	40,29	100,41
12957	42,54	113,73
13047	63,47	138,88
15468	22,99	49,66
19507	32,51	66,07
24318	37,06	73,31
27428	58,86	91,61
27773	33,09	63,10
31225	54,68	94,26
33618	36,11	79,03
34217	28,03	59,98
38495	32,14	67,11
43801	26,46	41,35
46805	22,46	31,16
50282	12,35	20,82
52980	11,11	14,05

Table 3: Table showing the results of the grain size analysis for Sperchios. Parts of the data is borrowed from Pechlivanidou et al. (2016, manuscript in preparation).

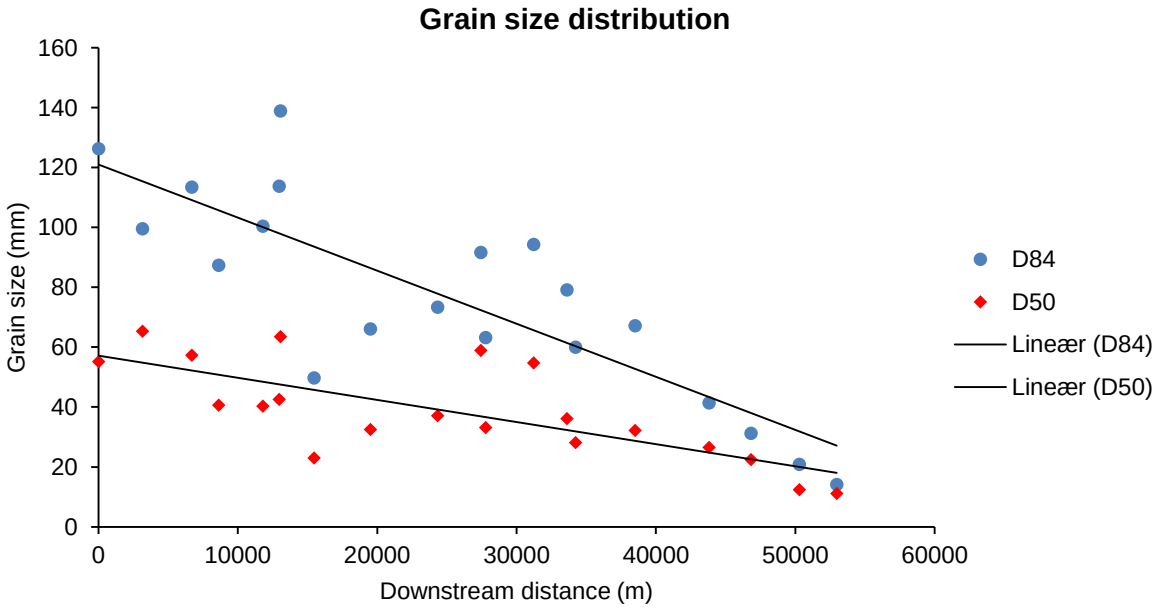

Figure 3.10: Graph showing the grain size distribution (D_{50} and D_{84}) for Sperchios. The linear trend lines are displayed for comparison between D_{84} and D_{50} fining trends only. They do not reflect modelled grain size trends.

I conducted grain size analysis at a total of 7 points along the Sperchios River (figure 2.3). As Pechlivanidou et al. (2016, manuscript in preparation) already has done extensive analysis at several points, my analyses were done in areas where Pechlivanidou's coverage was sparse. We exchanged data and made sure our measuring methods yielded approximately similar results before we continued using it for modelling purposes. A total of 32 pictures were analysed by me, with a total amount of 3202 grains measured. The results of the measurement can be seen in table 3. As visible from the table and figure 3.10, the grainsize trend is fining downstream for both D_{50} and D_{84}, and again the fining trend is steeper for D_{84} than for D_{50}. As is seen from the self-similarity plot, the grain size distribution at all measured points along the Sperchios River also shows a significant degree of self-similarity (figure 3.11).

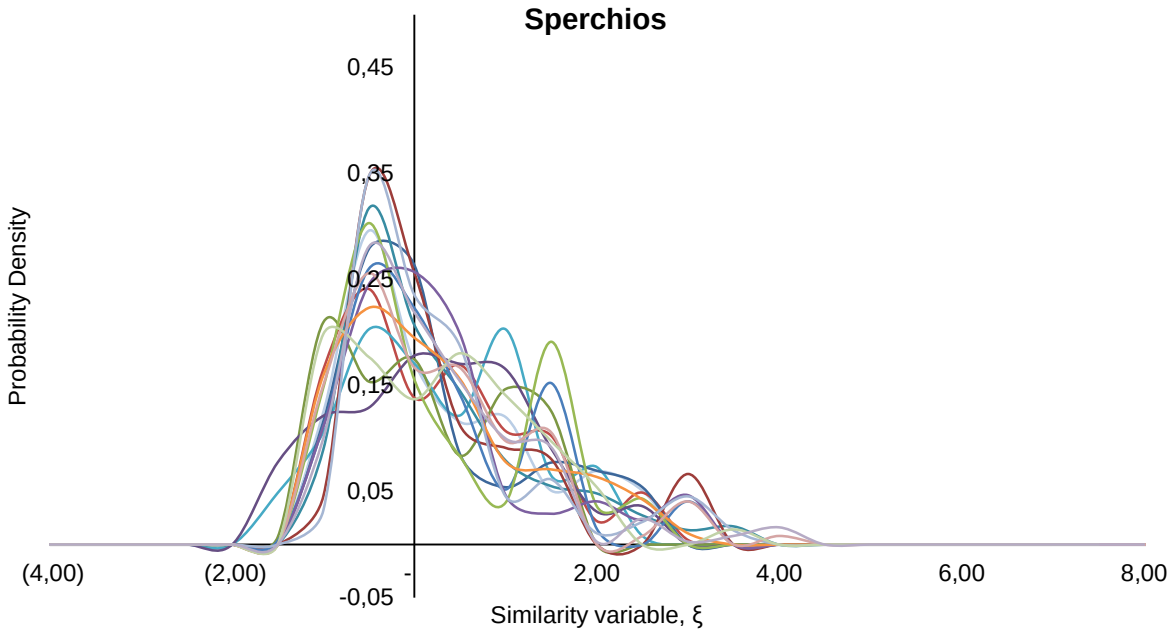

Figure 3.11: Figure showing the self-similarity curves for Sperchios.

3.2.4 Lefkada

I conducted grain size analysis of the other systems as well, namely the Lefkada and Vitoli Rivers (figure 1.3). In the case of Lefkada, I was interested in trying to figure out if it would be possible to identify any fault related influence to the grain size distribution, since it is unclear if the channel crosses the western end of the Sperkhias fault, or if the fault tip is located east of the channel. However, the quality of the data and the results of the analysis is questionable as the Lefkada River is, as previously mentioned, highly influenced by human activity. Running the model on such uncertain source data would yield highly questionable results, which is why it is not included in the modelling study.

Distance downstream(km)	D_{50} (mm)	D_{84} (mm)
0,00	48,59	137,38
2,20	19,54	65,53
3,34	36,53	79,71
3,74	39,26	76,72
3,88	32,81	73,71
4,09	51,64	102,25
4,79	24,72	60,75
5,81	39,53	74,19

Table 4: Table showing the results of the grain size analysis for Lefkada.

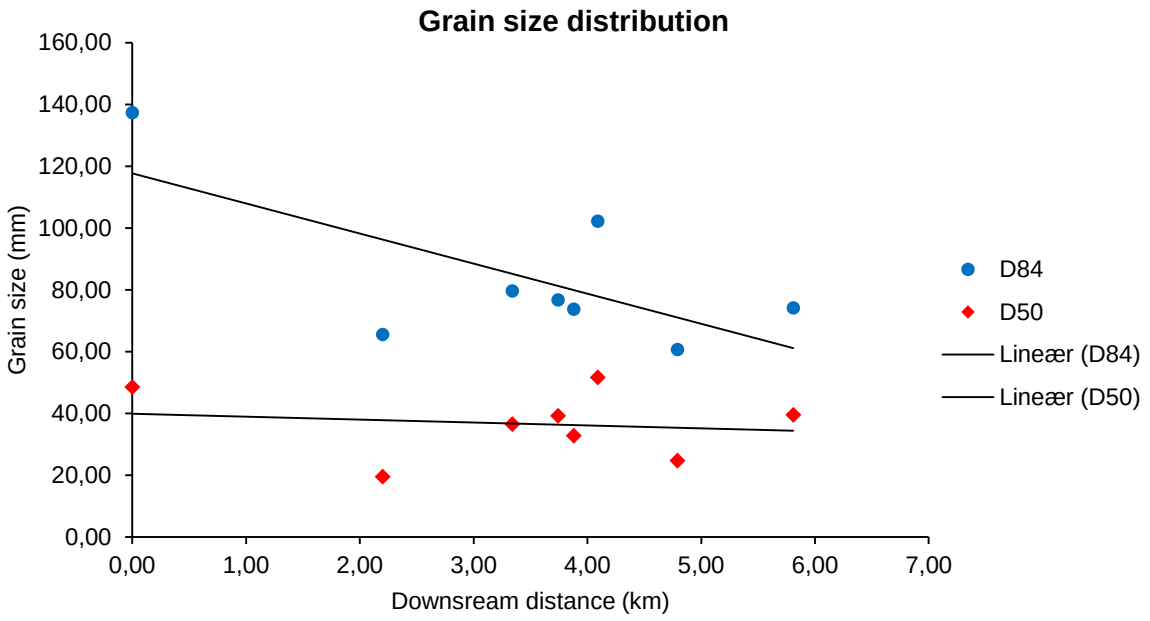

Figure 3.12: Graph showing the grain size distribution (D_{50} and D_{84}) for Lefkada. The linear trend lines are displayed for comparison between D_{84} and D_{50} fining trends only. They do not reflect modelled grain size trends.

I conducted grain size analysis at a total of eight points along the Lefkada river (figure 2.3), analysing 26 pictures amounting to 2389 grains. The distribution of grain sizes is shows in table 4. As we see from table 4 and figure 3.12, there is hard to see a trend in the D_{50} distribution – it seems fairly constant – whereas there might be a downstream fining trend seen in the D_{84} distribution. This might be attributed to abrasion of large clasts whereas small clasts have reached some sort of threshold, or it might be just noise in the data. The lack of any clear trends might also suggest that there is little mass extraction due to the low degree of accommodation creation, as this is at the very end of the basin where subsidence is low and the proximity to the axial system is very close. There is a very subtle fan structure at the end of the river, but it is much smaller than the other fan structures I have studied. It is also unclear where the fault segment runs, or if it crosses the Lefkada River at all, which increases the uncertainty regarding this system. From the self-similarity plot, we can see that the grain size distribution at all measured points along the river displays a significant degree of self-similarity (figure 3.13).

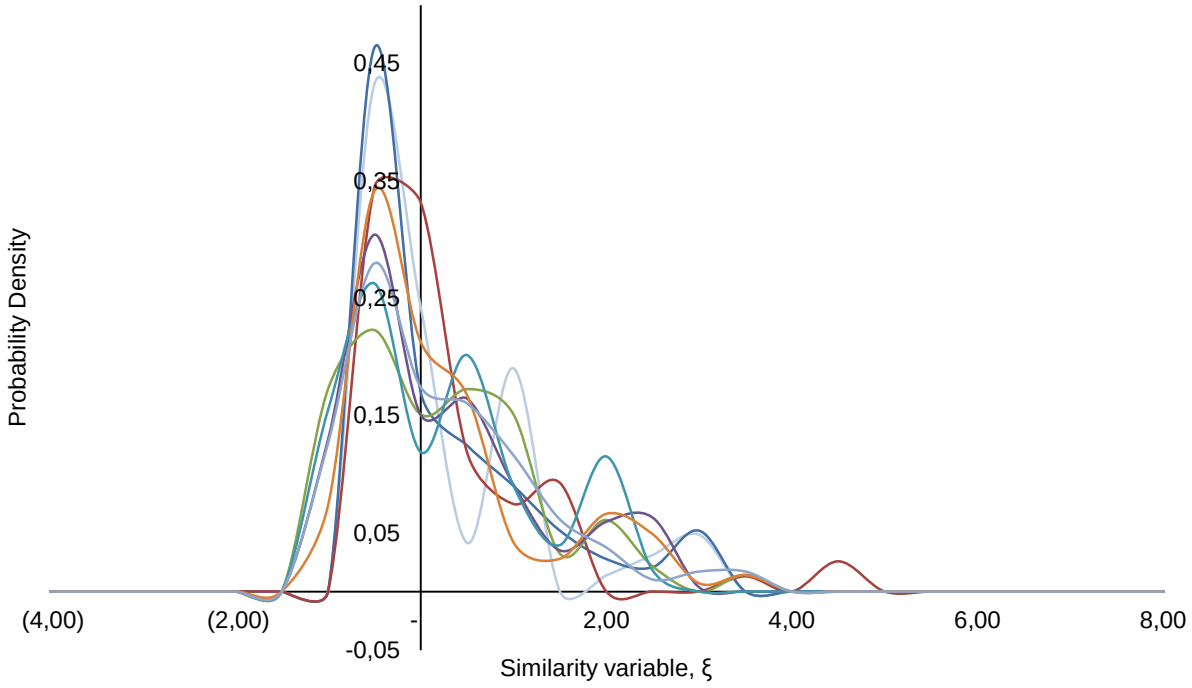

Figure 3.13: Figure showing the self-similarity curves for Lefkada.

3.2.5 Vitoli

The Vitoli River (figure 1.3) was interesting to study because it drains the hanging wall segment of the basin, and was initially planned to be included to compare it with the systems that drain across the fault. The aim was to characterise a system that is unperturbed by tectonics. However, in the case of Vitoli, I did not include it in the modelling study since it does not deposit a clear fan structure. Furthermore, I was only able to collect data over a distance of two kilometres.

Distance downstream (km)	D_{50} (mm)	D_{84} (mm)
0,00	56,09	131,48
0,11	53,69	190,72
0,36	50,64	137,30
0,75	58,10	109,61
1,18	41,98	69,56
1,60	29,33	71,09
2,21	31,31	59,31

Table 5: Table showing the results of the grain size analysis for Vitoli.

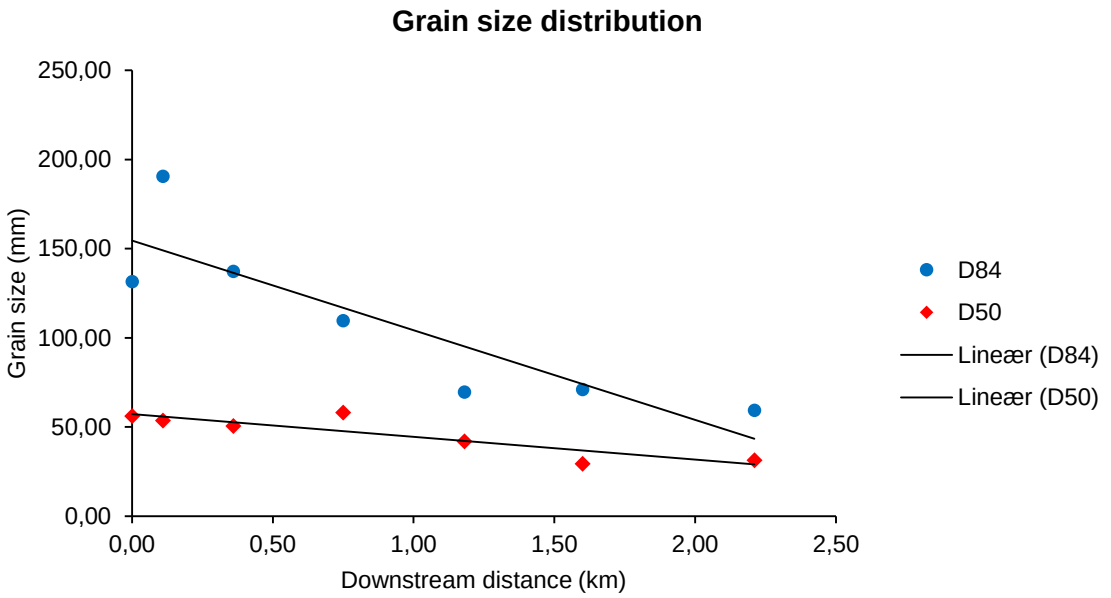

Figure 3.14: Graph showing the grain size distribution (D_{50} and D_{84}) for Vitoli. The linear trend lines are displayed for comparison between D_{84} and D_{50} fining trends only. They do not reflect modelled grain size trends.

Analysis was performed on 22 pictures taken from seven waypoints along the river (figure 2.3). The total amount of grains measured is 1844. As we see from table 5 and the grain size distribution plot (figure 3.14), the fining trend for both D_{50} and D_{84} is much more evident here, steeper for D_{84} than D_{50} here as well, and the data itself seems much less noisy. From the self-similarity plot (figure 3.15), we can see that the distribution of grain sizes displays a clear self-similarity for the entire system length. Since this river does not produce any fan structure, it is tempting to think that the grain size fining is simply due to abrasion, without any mass extraction/deposition involved. That would imply a very strong abrasion effect, as we see a quite rapid decrease in grain size over just 2.2 kilometres. However, even though there is no fan structure here, the river is braided in the lower parts of the valley it drains through, which is thought to be due to deposition as the base level has been lifted by deposition from the axial system. The lack of any fan structure can be linked to the fact that there is no fault in this area, so that the river is in a steady state. The reason for the generally large amount of large grains can possibly be attributed to the interbedded nature of the flysch, where disintegration of the soft siltstone beds will cause large blocks of sandstone to break free and consequently feed the system with large cobbles of sandstone.

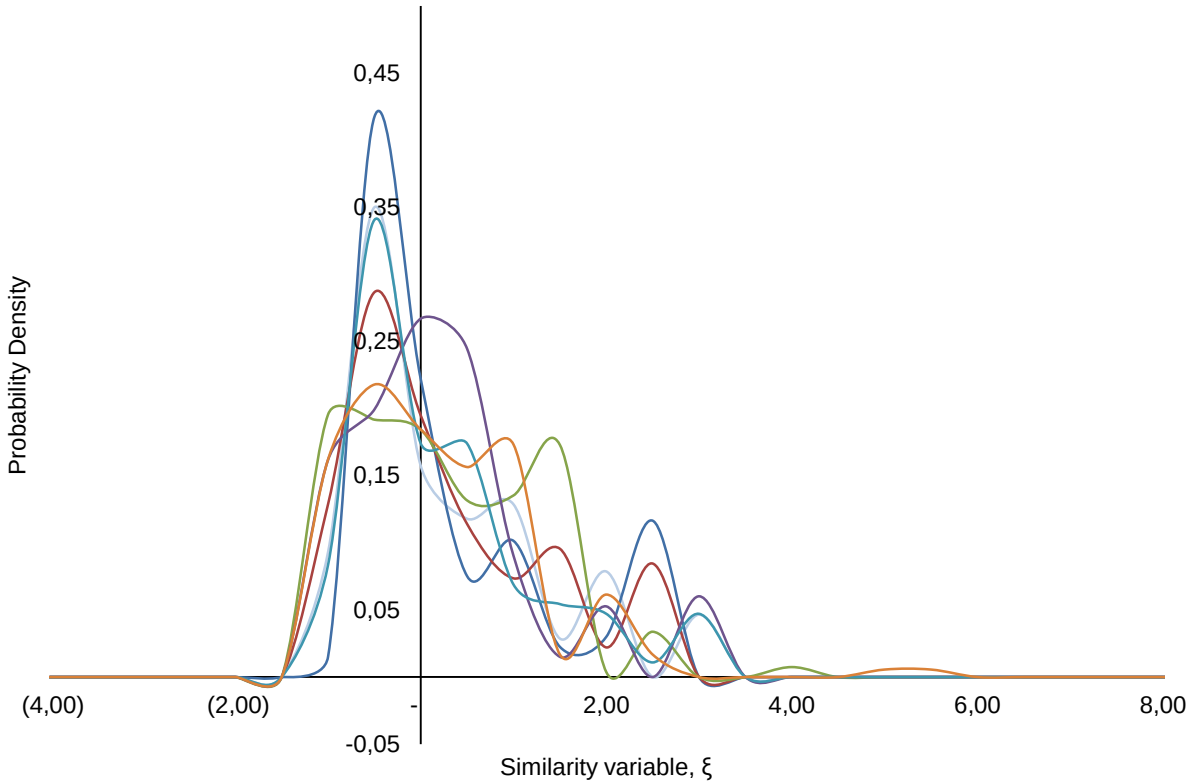

Figure 3.15: Figure showing the self-similarity curves for Vitoli.

3.3 Modelling

3.3.1 Modelling procedure

Below I will present the modelling procedure with examples from Xerias, with figures displaying how projected grain size distribution is affected by changes in the spatial distribution and amplitude of subsidence, and changes in the initial sediment volume discharge into the system. The same procedure was used for modelling on the Inahos fan. I experimented with both an exponential decrease in subsidence and a linear decrease as a function of distance from the fault, and concluded that the exponential decrease was the most reasonable solution for this location. One can argue that the subsidence at the point of the axial system should be the same as it is in the model presented in Pechlivanidou et al. (2016, manuscript in preparation) for the axial system (figure 3.27), but this is not the case in my model. However, the accommodation space created by the axial subsidence is thought to already be filled up by sediment from the axial system itself. Therefore, the relative subsidence "felt" by the sediment discharge coming from the two transverse catchments in my focus area will be close to zero where it intersects the axial system.

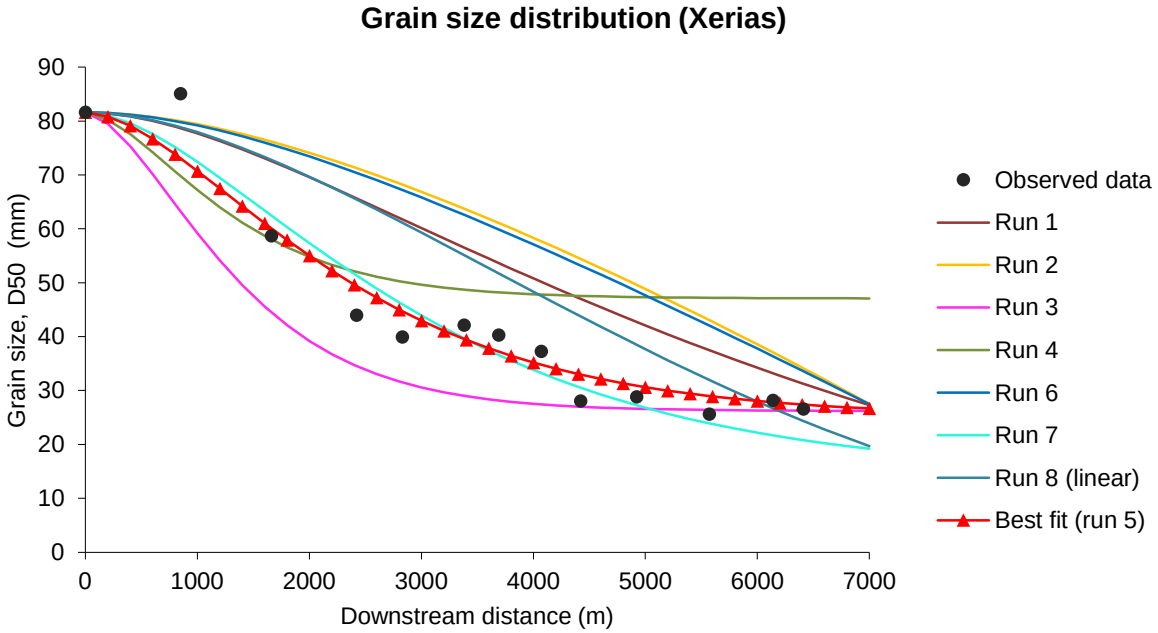

Figure 3.16: Graph showing the results of the model sensitivity analysis on grain size distributions with eight different model runs (see table 6).

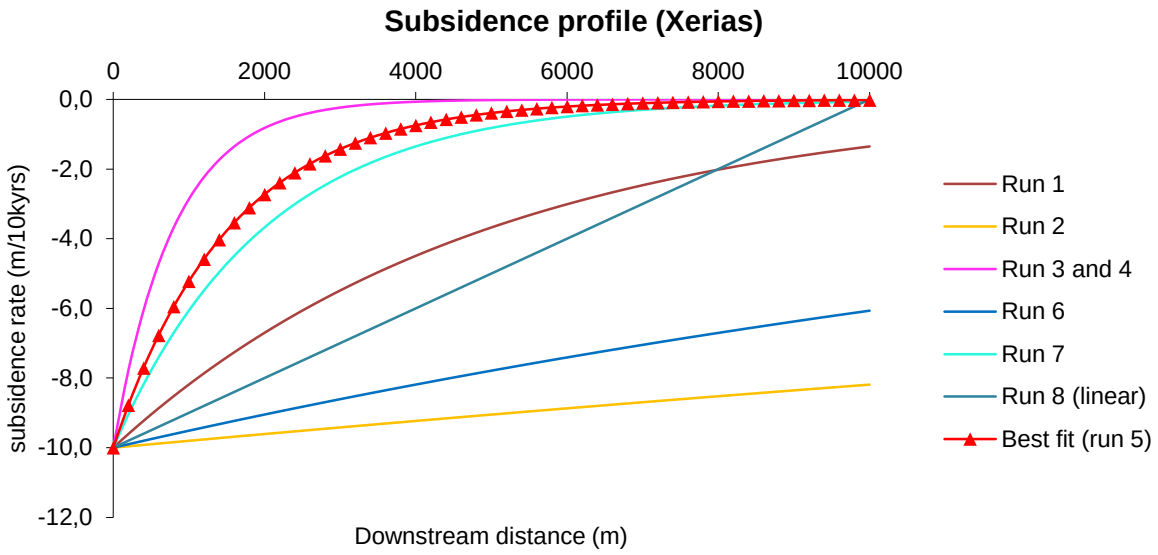

Figure 3.17: Graph showing the different subsidence profiles used for the different model runs.

Run	Equation ($y=a\times e^{b}$)	Fraction (F_{qs})	Sediment supply (m^3 pr. yr.)
Run 1	$y = -10 \times e^{-0,2}$	1,9	$1,33\times10^4$
Run 2	$y = -10 \times e^{-0,02}$	1,9	$2,65\times10^4$
Run 3	$y = -10 \times e^{-1,25}$	1,9	$1,28\times10^3$
Run 4	$y = -10 \times e^{-1,25}$	2,9	$1,96\times10^3$
Run 5	$y = -10 \times e^{-0,65}$	1,9	$3,67\times10^3$
Run 6	$y = -10 \times e^{-0,05}$	1,9	$2,35\times10^4$
Run 7	$y = -10 \times e^{-0,5}$	1,7	$4,74\times10^3$
Run 8	$y = 0.001x - 10$	1,7	$1,50\times10^4$
Run 9	$y = -12 \times e^{-0,65}$	1,9	$5,69\times10^3$

Table 6: Table showing the different values for subsidence and sediment discharge used for the different model runs, and the different volumes of sediment supply resulting from the changes in variables. The fraction variable here is the same as the F_{qs} variable described in chapter 1.2 and below, and governs the degree of filling in the depositional system.

Figure 3.16 and 3.17 and table 6 present the results of the sensitivity analysis I made on the downstream fining model. During the analysis, I have varied the values governing spatial distribution of subsidence, and the initial sediment discharge into the system. The equation used for spatial distribution and amplitude of subsidence is given as:

$$y = a \times e^{b}$$

where a is the initial subsidence (i.e. amplitude), and b is the spatial distribution of subsidence (i.e. wavelength). This is also sometimes referred to as the *fining* parameter. During the sensitivity analysis where I focused on variations in the spatial distribution of

subsidence, I made eight runs with different values. Amplitude at the fault was kept constant in all runs. As is evident from figures 3.16 and 3.17, we can see that its curvature, i.e. the rate of downstream fining, is very sensitive to the spatial distribution of subsidence. With a short wavelength subsidence, such as in runs 3 and 4, the fining rate is very high initially, but is distinctly flattening out after approximately one third of the total system length. With a long wavelength subsidence, such as in runs 2 and 6, the fining rate is slow at first, but increases quite steadily after 500-600 metres into the system. We also see a significant difference between run 3 and 4, and this comes from the change in the fraction value. The *fraction value* (F_{qs}) is a dimensionless parameter based on the ratio of initial sediment discharge, q_{so}, to accommodation creation, and represents the fraction of the perfect filling case (Duller et al., 2010). As will be demonstrated the analysis, it governs to what extent the depositional system is filled, under-filled or over-filled. Cases of under-filled systems will not be explored in this analysis as my model is based on the principle that all fans are over-filled. Therefore, F_{qs}=1 indicates a perfectly filled depositional system and F_{qs}>1 indicates an overfilled depositional system.

By looking at runs 3 and 4, we can see what happens to grain size distribution when we alter the fraction value, keeping the spatial distribution of subsidence constant. What we see is that when F_{qs} is very high (at 2.9), more of the fine material is bypassing the fan. All grains larger than 47 millimetres is bypassed into the axial river. With a lower F_{qs} value and lower sediment discharge, sediment calibre of the bypassing fraction decreases because more sediment is being deposited in the fan itself.

As previously mentioned, the b-value governs the spatial distribution of the subsidence, where high values give short wavelength subsidence, meaning that the subsidence rapidly decreases with increasing distance from the fault, whereas low values gives long wavelength subsidence, meaning that the subsidence still decreases with increasing distance from the fault, but at a much slower rate. The geological interpretation of these runs is therefore that in the case of a rapid decrease in subsidence, most of the coarse material is deposited very close to the fault while only the finer grains are transported further downstream. On the other hand, in the case of a slow and steady decrease in subsidence, much more of the coarse material is being transported further into the

system, together with fines, which leads to a more even distribution and a slower and more steady decrease in grain size with increasing distance from the fault.

Run 8 (figure 3.16, 3.17) shows how it would look in the case of a linear decrease in subsidence, and as evident from figure 3.16, the grain size distribution is similar to the results seen with high wavelength exponential subsidence, although the decrease in grain size occurs slightly earlier in the down-system length.

It is also interesting to consider the impacts of how initial sediment discharge and the spatial distribution of subsidence impacts sediment bypassing. As already established, the fan in question is overfilled, so we are interested in seeing to what extent bypassing is influenced by variations in the aforementioned controlling factors.

Figure 3.18 displays four runs where F_{qs} is kept constant but with a varying degree of subsidence wavelength. A constant F_{qs} value means that in all cases, the proportion of the sediment input that is bypassing into the axial river is the same. For short wavelength subsidence we see that deposition is increasing in the initial 3000-4000 metres of the fan, whereas it then slows down (flattens out) towards the end of the system. For longer wavelength subsidence, we see that the distribution of deposition is quite different; deposition is low at first and then increases slowly and steadily for the entire system length, without the distinct flattening-out signature that we see for short wavelength subsidence. Figure 3.19 displays four runs where subsidence wavelength is kept constant but where F_{qs} is altered. For high F_{qs} values, we see that a higher amount of sediment is bypassing (65% bypassing for the highest F_{qs}), whereas the amount of sediment bypassing decreases with decreasing F_{qs}. I have also included a run with an F_{qs} that is below 1 to demonstrate what effect it has; creating an underfilled system, i.e. the fan is decoupled from the axial river.

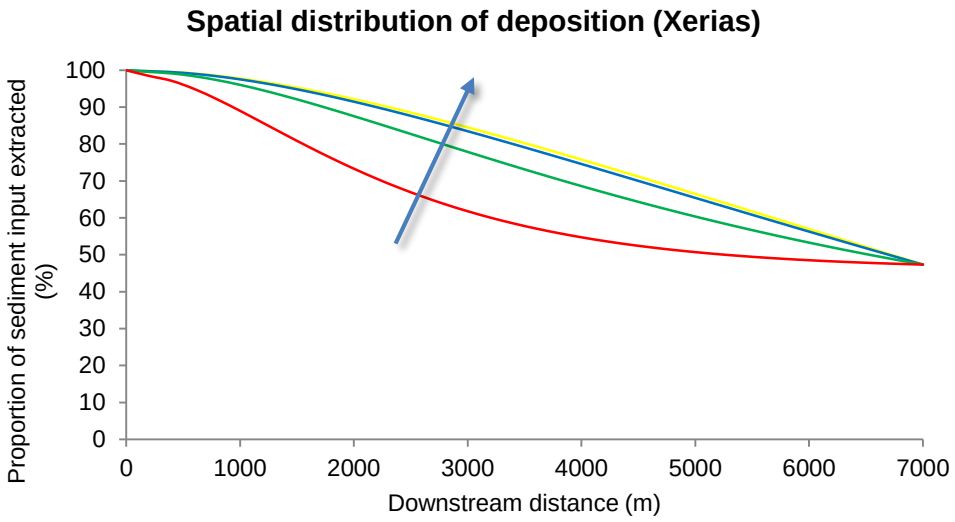

Figure 3.18: Graph showing how the spatial distribution of deposition is affected by variations in spatial distribution of subsidence (wavelength). Subsidence wavelength increases in the direction of the arrow. As F_{qs} is constant, approximately 50% of the sediment input is bypassing into the axial river in all cases.

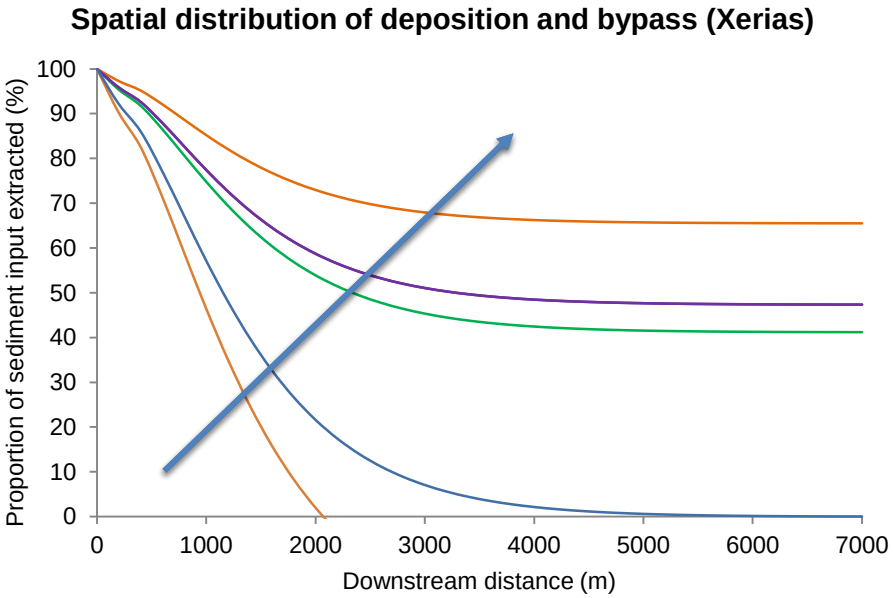

Figure 3.19: Graph showing how the spatial distribution of deposition and bypass is affected by increasing F_{qs} (increases in the direction of the arrow). Here we also see how it affects sediment bypass.

Based on the above analysis, the grain size distribution is most sensitive to changes in subsidence rate, both with regards to spatial distribution and the amplitude of subsidence.

When it comes to sediment volumes, we can see from figure 3.16 that a 53% increase in the F_{qs} value with a constant subsidence equation as in run 3 vs. 4 cause a 53% increase in sediment volumes (table 6). This increase comes because the fraction value determines the degree of filling of the depositional system, as explained above. When all the other variables are kept constant, an increase in sediment volume is necessary to increase the degree of filling. If we look at the fining parameter (b), or subsidence wavelength, we can see that if we decrease the b-value by 48%, giving a longer subsidence wavelength as in run 3 vs. 5 (figure 3.16, table 6), we see a 193% increase in sediment volumes (table 6). This is also reasonable, as the fining parameter determines the spatial distribution of subsidence. A decrease of this parameter means an increase in subsidence wavelength, which leads to more accommodation space created with consequently higher sediment volumes. The last thing worth considering is the impact of changes in subsidence rates to the sediment volumes. If we compare runs 5 and 9 (figure 3.16, table 6), we see that a 20% increase in subsidence causes a 55% increase in sediment volumes (table 6). This is because an increase in subsidence generates more accommodation space which will accommodate larger sediment volumes.

Based on the above analysis, it is evident that subsidence amplitude and wavelength are the variables to which the modelled sediment volumes are most sensitive. The results of these test runs were used to determine which values for the different parameters best fit the observed data, i.e. the obtained data from the grain size photos. The runs that best fit the observed data will be presented for each of the fans in the following paragraphs and will form the basis for further discussion of the model itself and the validity of the results.

3.3.2 Xerias

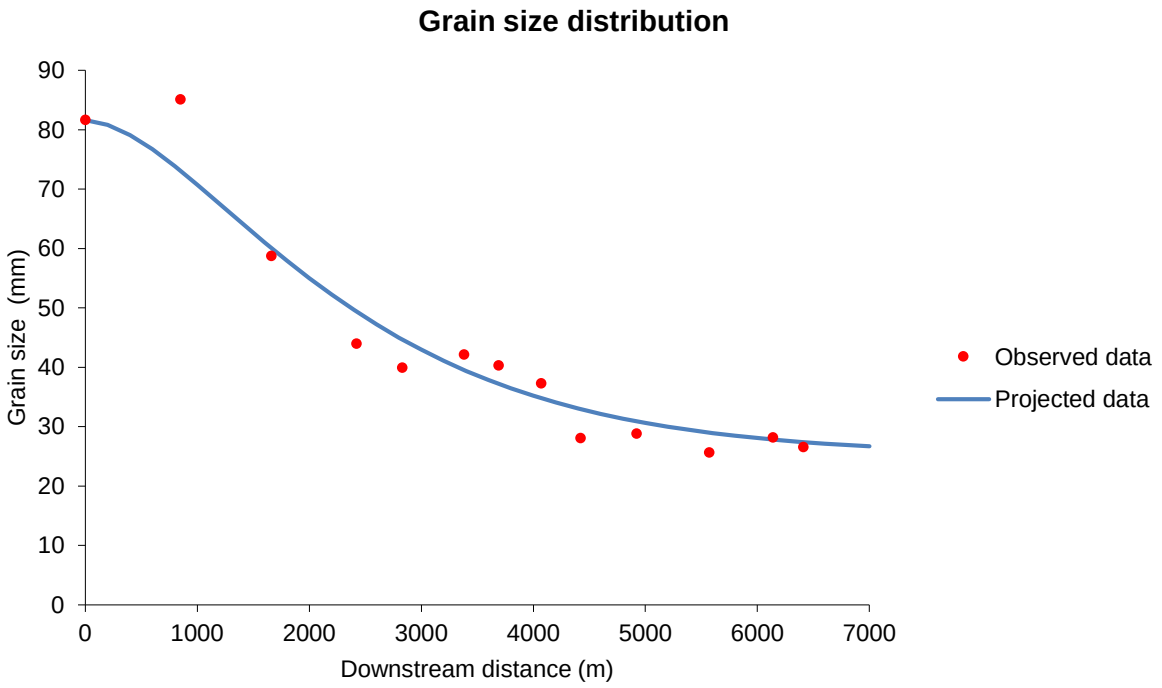

Figure 3.20: Graph showing the observed grain size fining trend, and the grain size trend predicted by the model with the variables that best fit the observed data.

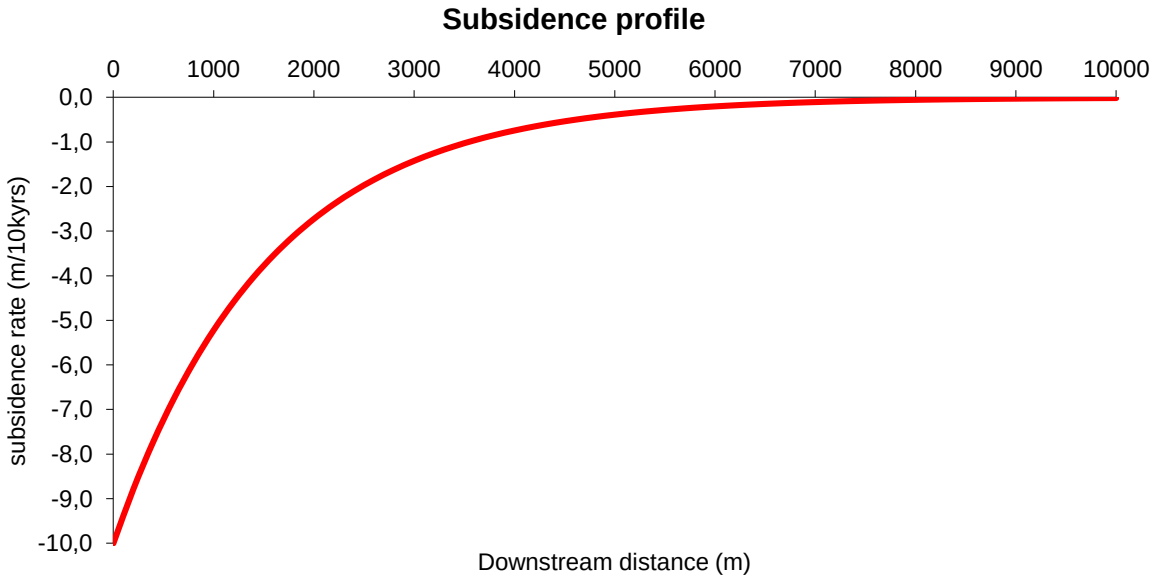

Figure 3.21: Graph showing the subsidence profile for Xerias that best fits the observed data.

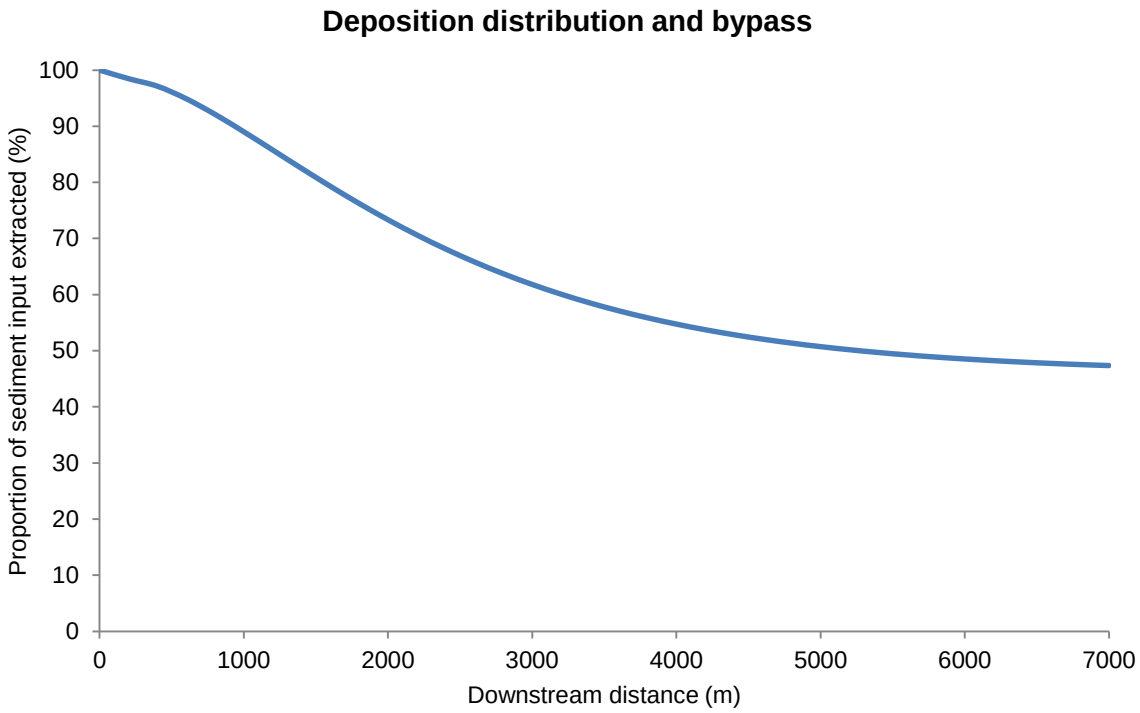

Figure 3.22: Graph showing the relationship between bypassing and deposition along the Xerias fan, according to the variables that best fit the observations made in the field.

Subsidence parameters here $y = a \times e^{b}$	
coefficient, a	-1
fining parameter, b	-0,65
Fraction (F_{qs})	1,9

Table 7: Table showing the subsidence equation for Xerias, i.e. the variables governing the spatial distribution and amplitude of subsidence.

Total sediment flux (m^3 pr. yr)	Gravel fraction (m^3 pr. yr)	Percentage
5,00E+04	$3{,}67 \times 10^3$	7,33

Table 8: Table showing the volume of gravel input in the Xerias fan. Total sediment flux numbers come from a stream power model based on erosion rates and catchment volume (Pechlivanidou, pers. com.), and are only used here to calculate the relative amount of gravel in percentage.

In the tables and graphs above, the final result of the modelling of the Xerias system is displayed. Table 7 shows the subsidence variables, whereas table 8 shows the total sediment volume delivered to the fan, and how big the gravel fraction is. In Xerias, approximately 7.3% of the total sediment flux is gravel. The graphs presented show modelling results for the grain size analysis (figure 3.20), as well as subsidence distribution (figure 3.21) and distribution of deposition and bypass (figure 3.22). We can see that the curve from the projected data fits well with the observed data (figure 3.20).

The initial subsidence is 1 millimetre per year, with a “fining parameter” of -0.65. The fraction value is 1.9, meaning that the fan is overfilled. The decrease in grain size is abrupt in the first 3 kilometres of the system down-length, whereas it decreases for the last 4 kilometres. From an initial grain size (D_{50}) of approximately 81 mm, it decreases to approximately 27 mm at the tip of the fan. From the subsidence profile graph, we can see that subsidence approximates 0 at the tip of the fan. As explained earlier, this is due to the fact that the western catchment draining into the axial Sperchios River supplies enough sediment to fill the valley, so that the accommodation space for the transverse systems is relatively limited in the central part of the valley. Therefore, even though the actual subsidence is higher than 0, the subsidence “felt” by the transverse system is approximately 0 at the toe of the fan as there is no accommodation space left for these systems to dump their sediment. As previously mentioned, the last graph shows how much of the gravel is bypassed at each point along the system length, out of the total amount feeding into the system. The amount bypassed decreases a bit rapidly at first, before it starts to flatten out after about 3 kilometres. This tells us that the amount of gravel deposited decreases with a higher rate in the first 3 kilometres than in the last 4 kilometres. At the end of the fan, approximately 53% of the total gravel input has been deposited in the fan, whereas the remaining 47% is bypassing.

3.3.3 Inahos

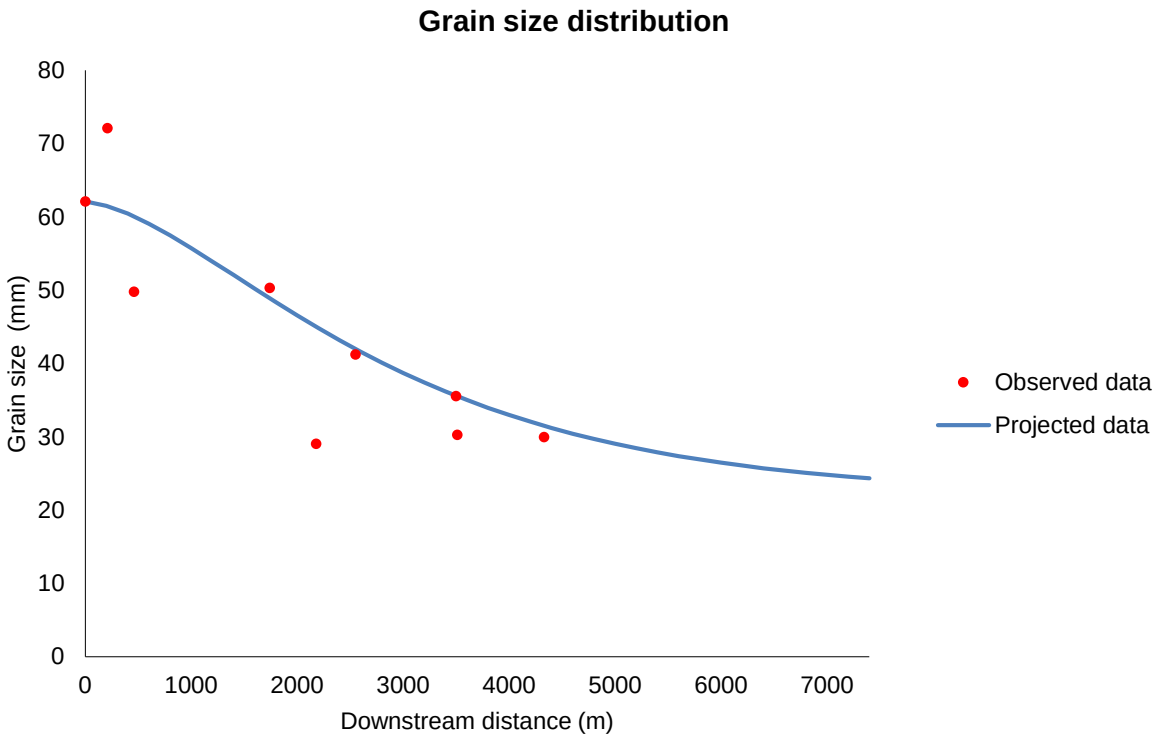

Figure 3.23: Graph showing the observed grain size fining trend for the Inahos fan, and the grain size trend predicted by the model with the variables that best fit the observed data.

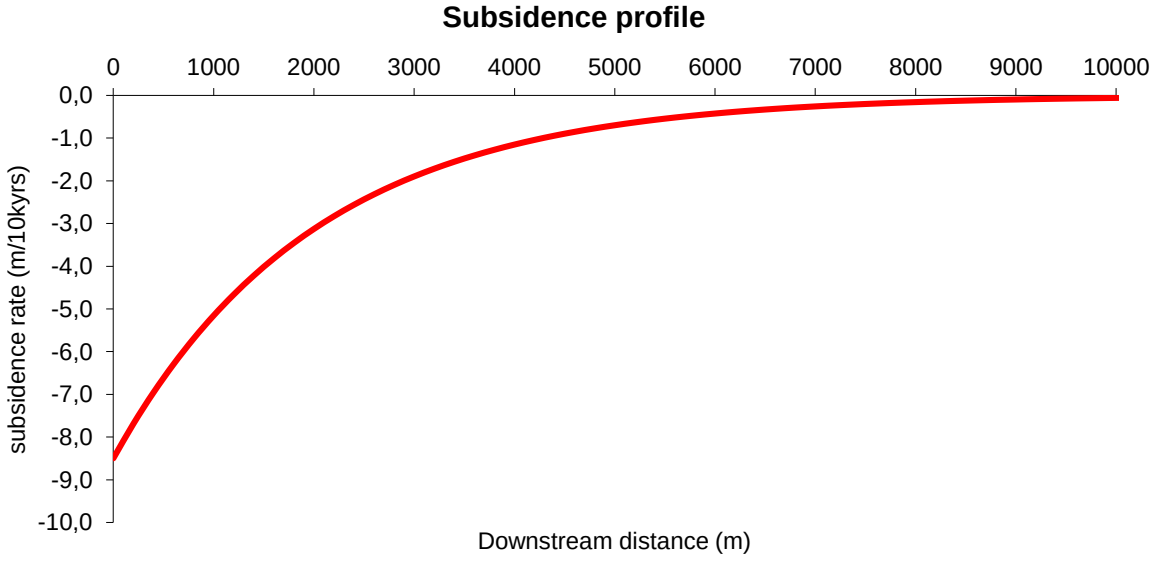

Figure 3.24: Graph showing the subsidence profile for Inahos that best fits the observed data.

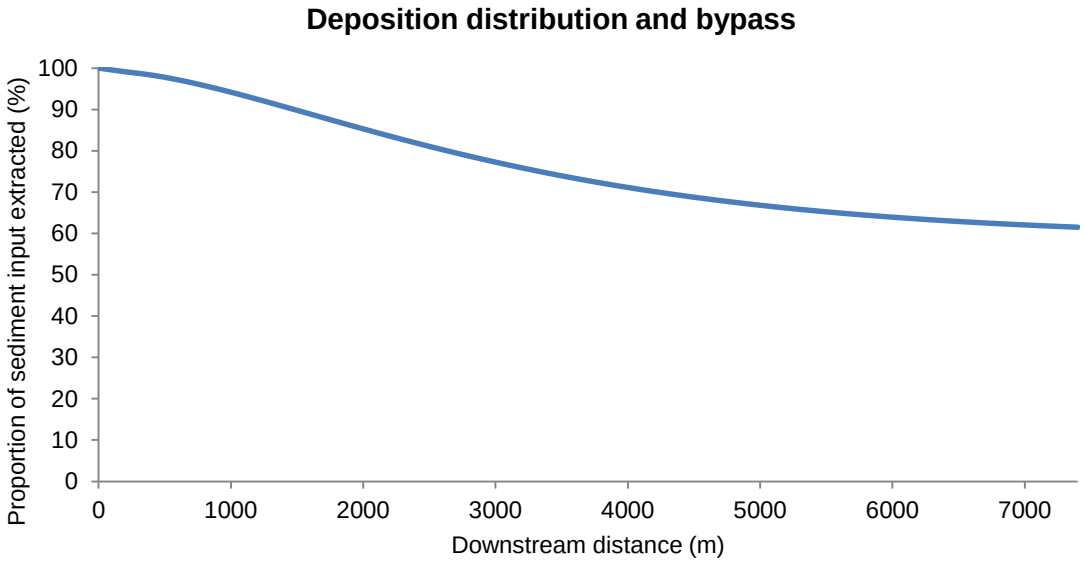

Figure 3.25: Graph showing the relationship between bypassing and deposition along the Inahos fan, according to the variables that best fit the observations made in the field.

Subsidence parameters here $y = a \times e^{b}$	
coefficient, a	-0,85
fining parameter, b	-0,5
Fraction (F_{qs})	2,6

Table 9: Table showing the subsidence equation for Inahos, i.e. the variables governing the spatial distribution and amplitude of subsidence.

Total sediment flux (m^3 pr. yr)	Gravel fraction (m^3 pr. yr)	Percentage
4,30E+05	$9{,}35 \times 10^3$	2,17

Table 10: Table showing the volume of gravel input in the Inahos fan. Total sediment flux numbers come from a stream power model based on erosion rates and catchment volume (Pechlivanidou, pers. com.), and are only used here to calculate the relative amount of gravel in percentage.

In the tables and graphs above, the final result of the modelling of the Inahos system is displayed. Table 9 shows the subsidence variables, whereas table 10 shows the total sediment volume delivered to the fan, and how big the gravel fraction is. In Inahos, approximately 2.2% of the total sediment flux is gravel. The graphs presented show modelling results for the grain size distribution analysis (figure 3.23), as well as subsidence distribution (figure 3.24) and distribution of deposition and bypass (figure 3.25). We can see that the curve from the projected data fits rather well with the observed data. The initial subsidence is 1 millimetre per year, with a fining parameter of -0.5. That means that the decrease in subsidence is more abrupt here than in the Xerias

system. The fraction value is 2.6, meaning that the fan is overfilled to a much larger extent than the Xerias fan. The decrease in grain size is abrupt in the first 2 kilometres of the system down-length, whereas it decreases for the last 5.4 kilometres. From an initial grain size (D_{50}) of approximately 62 mm, it decreases to approximately 28 mm at the tip of the fan. Thus the grainsize at the toe of the fan is similar to what we see in Xerias, but the initial grainsize is much smaller. From the subsidence profile graph, we can see that subsidence approximates 0 at the tip of the fan. This is due to the same reasons as for Xerias – the subsidence "felt" by the transverse system is approximately 0 at the toe of the fan as there is no accommodation space left for these systems to dump their sediment. As previously mentioned, the last graph shows how much of the gravel is bypassing at each point along the system length, out of the total amount feeding into the system. The amount of sediment bypass decreases faster in the first 2.5 kilometres than in the last 4.9 kilometres, although the decrease is slow. This tells us that the amount of gravel deposited decreases with a higher rate in the first 2.5 kilometres than in the last 4.9 kilometres. At the end of the fan, approximately 40% of the total gravel input has been deposited in the fan, whereas the remaining 60% is being bypassed.

3.3.4 Sperchios

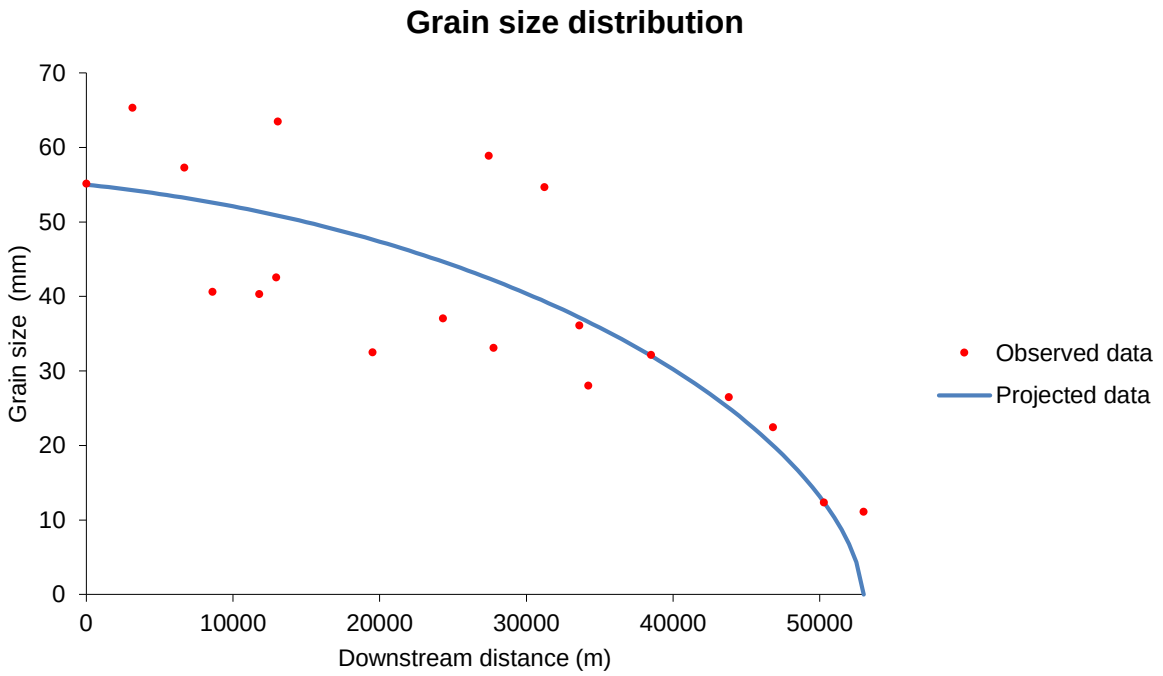

Figure 3.26: Graph showing the observed grain size fining trend, and the grain size trend predicted by the model with the variables that best fit the observed data.

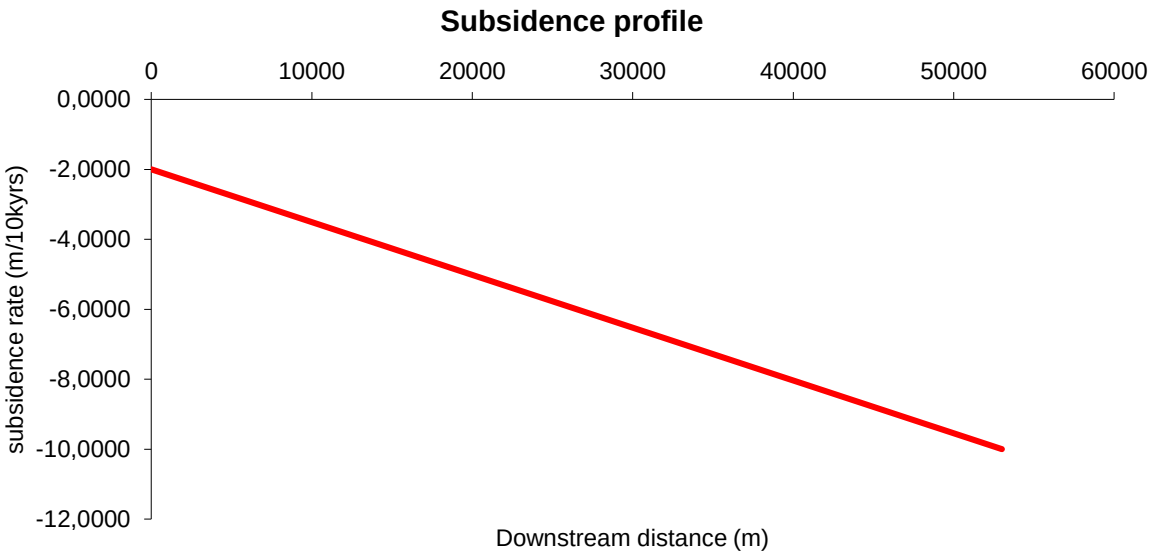

Figure 3.27: Graph showing the subsidence profile for Sperchios that best fits the observed data.

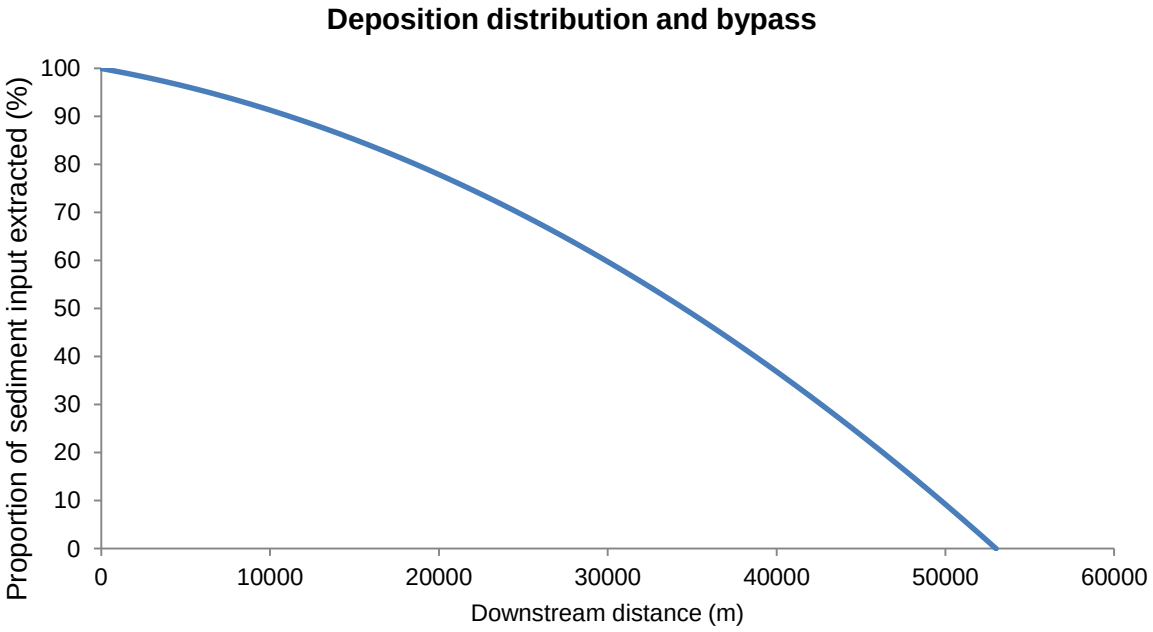

Figure 3.28: Graph showing the relationship between bypassing and deposition along the Sperchios River, according to the variables that best fit the observations made in the field.

In the graphs above, the final result of the modelling of the Sperchios system is displayed. The graphs presented show modelling results for the grain size analysis (figure 3.26), as well as subsidence distribution (figure 3.27) and sediment bypass (figure 3.28). The initial subsidence is 2 millimetres per year, with a linear increase downstream to about 10 millimetres at the eastern end of the basin. The fraction value (F_{qs}) is 1, meaning that the basin is perfectly filled; the amount of sediment discharged is

filling up the basin without any bypassing. The decrease in grain size is quite slow and steady in the first 30-40 kilometres of the system down-length, whereas it decreases much more rapidly for the last 10 kilometres. From an initial grain size (D_{50}) of approximately 55 mm, it decreases to 0 at the end. We can also see two spikes in grain size at approximately 13 and 30 kilometres downstream.

As previously mentioned, the last graph (figure 3.28) shows how much of the gravel that is bypassing at each point along the system length, out of the total amount feeding into the system. The amount of sediment bypassing decreases slowly and steadily for the entire down-system length, and at the end the amount of bypass is zero. This tells us that the amount of gravel sediment discharged is, as established earlier in this paragraph, just enough to fill the basin without anything bypassing.

An interesting aspect to notice here is the way the grain size fining trend curve is different from the trends in the transverse systems. There, we see a sudden and quite abrupt increase in fining at first, which then starts to flatten out towards the end of the system. Here, we see the opposite; a rather flat trend with a gentle decrease in grain size at first with an abrupt fining towards the end. Again, this is a characteristic of a linear subsidence distribution, as demonstrated in the sensitivity analysis.

4.0 Discussion

4.1 Fan volumes

One of the variables that is quantified in the modelling results (chapter 3.3) is the sediment volume delivered to the fan. To be able to discuss and validate these volumes, it is necessary to quantify the volumetric extent of the fans. To calculate the volume of the fans, the 5m DEM was used as a basis. I assume that the fan structures identified on the DEM have been formed during the Holocene, because they reflect the most recent fan development. The fans look relatively young and are still active, which is why I have made this assumption.

The shape of the fans was outlined after visual evaluation with the help of the DEM and hillshade maps, and then made into polygons (figure 1.8 and 1.9, p. 13 and 14). These polygons were then used to construct a flat surface, with the elevation value set to the lowest point at the toe of the fan, approximately 60 metres above sea level for Inahos and 54 metres above sea level for Xerias. Using the "cut fill" tool in ArcGIS, the elevation of the arbitrary surface was subtracted from the present topography in the fans (figure 4.1), and this calculation gave the total volumes of the fan as 1.0×10^9 m^3 for Inahos and 1.6×10^9 m^3 for Xerias.

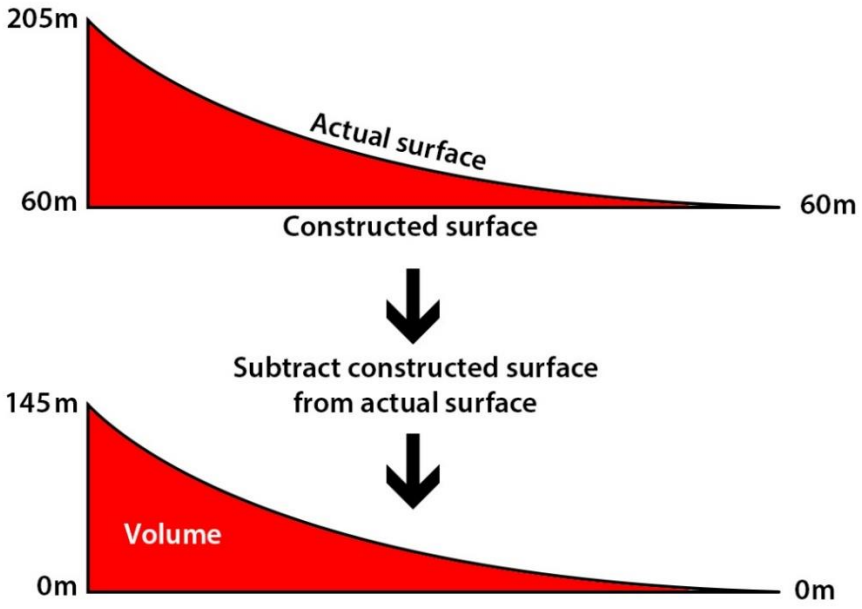

Figure 4.1: This figure illustrates how the total volume of the fans were estimated.

This method is a way of trying to calculate a maximum estimate of the total volume of the fan. However, to calculate a minimum estimate of the volume of the most recent deposits, more likely to be just from the Holocene, a different approach was applied. Here, a copy of the fan surface was made, which was then lowered by 7.5 metres and subtracted from the actual surface (figure 4.2). It was lowered by 7.5 metres because it is based on a subsidence rate of approximately 0.75 millimetres pr. year at the fault (Sofia Pechlivanidou and Patience Cowie, pers. com.), which gives about 7.5 metres of subsidence through the Holocene (10kyr). It should be noted that the subsidence rate I am basing my modelling results on is slightly higher at 0.85 millimetres pr. year because this fits my model better, but this will not cause large deviations in the volume estimate. The lowered surface was subtracted from the actual surface, and the volume was then calculated using the same "cut fill" tool as in the previous calculation. The results gave 2.2×10^8 m^3 for Inahos and 1.8×10^8 m^3 for Xerias.

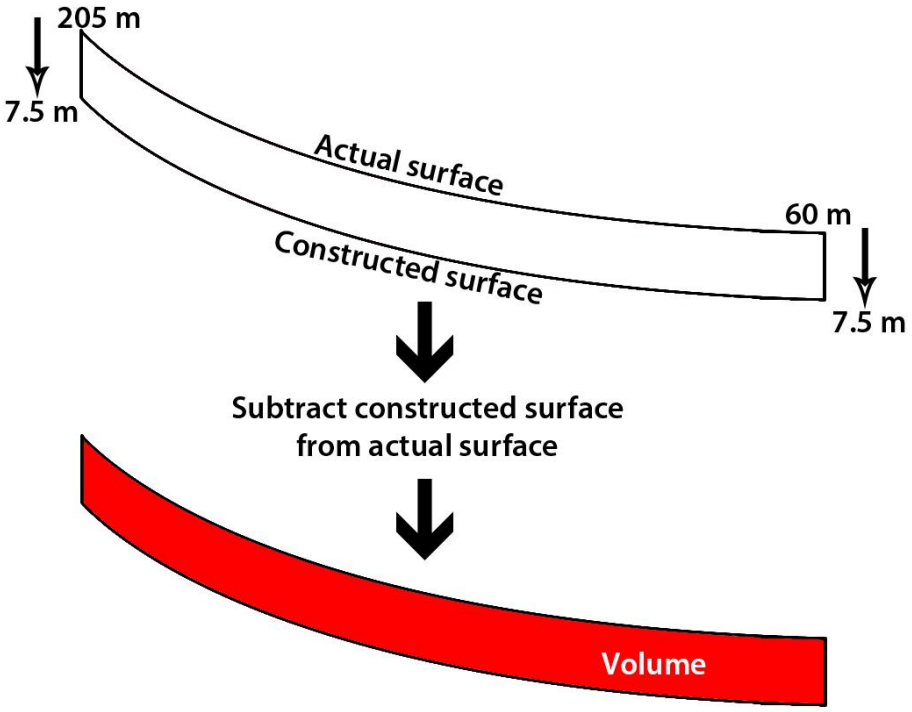

Figure 4.2: This figure illustrates how the volumes for the Holocene were estimated, in this case for the Inahos fan.

These volume calculations are of course very simplistic, but that was also the goal here – to do it as simple as possible, to get an approximate volume.

4.2 Validity of the modelling results

4.2.1 Inahos

Are the volumes of sediment input for Inahos calculated from the modelling reasonable, if we look at the volumes of the fan? By calculating the volume of the fans and taking into account the period of time over which the fan has been built, we should be able to see if the sediment volumes derived from the modelling are sufficient to produce the fans within the right timescale.

According to my modelling (chapter 3.3), the amount of gravel supplied to the Inahos fan, from the catchment, is approximately 1.0×10^4 m^3 per year (table 10, p. 60), or 1.0×10^8 m^3 per 10kyr. This is less than one would expect from the volumes derived from the DEM (chapter 4.1) by an order of 2. It is still considered to be able to build the fan, although a bit on the low side. As previously mentioned, the minimum estimate for the Holocene is 2.2×10^8 m^3. However, if we assume that this estimate should be based on a longer period of time, from the last glacial maximum, the time needed to deposit this amount of sediment approximately doubles, so that the fan needs a sediment input of 1.1×10^8 m^3 pr. 10 000 years. That is very close to the 1.0×10^8 m^3 of sediment pr. 10 000 years that is supplied according to my modelling.

If we look at the amount of sediment deposited vs. bypassed, the model estimates that as much as 60% of the sediment fed into the fan is bypassing (figure 3.25, p. 60) into the axial system. This means that the amount of sediment bypassing the fan is high, but it is still reasonable and can be explained by looking at the fan in the DEM slope measurements (figure 3.1, p. 30) and hillshade maps (figure 1.5, p. 11). As is visible, the fan has a very low gradient, it seems to be very thin and sheet-like, which can explain why it has displaced the Sperchios River to such an extent. Instead of aggradation and vertical stacking of sediment, the fan spreads the sediment more laterally, it progrades rather than aggrading, forcing the axial river to find another path around the fan. The reason for this lateral spread of sediments can possibly be explained by what I have previously described concerning subsidence and infill from the Sperchios River catchment; the axial system is already filling the valley with sediment, so that sediment coming from the transverse catchments is forced to spread laterally and create large, thin fans, and to a large extent also bypass the fans themselves. Also, the large volumes

of sediment coupled with the lower rate of subsidence at 0.85 mm/yr means that the accommodation creation is too low to accommodate aggradation.

Even though the tectonic tilting of the hanging wall block might be expected to cause the axial system to migrate towards the fault (Eliet and Gawthorpe, 1995), the effect of sediment discharge is stronger than the opposing effect of tectonic tilting, consequently displacing the axial system away from the fault. This correlates well with the findings in Miller et al. (2014), where competing effects of sediment discharge and tectonic forces on axial drainage systems in subsiding basins have been explored.

4.2.2 Xerias

As for the Inahos fan, the same questions can be posed regarding the Xerias fan – are the numbers making sense? From the modelling (chapter 3.3) the amount of gravel supplied to the Xerias fan is estimated to be approximately 4.0×10^3 m^3 per year (table 8, p. 57). This amount of sediment is five times lower than the volumes necessary to build the fan during the Holocene, which is estimated to be 1.8×10^8 m^3 as a minimum. However, the case of this fan is a bit more complex, and one of the reasons for this can be seen by looking at the fan in the hillshade map (figure 1.5, p. 11). Here it is evident that the fan is less clearly delimited, so that the volume calculation might in fact be based on more than one fan, or that the extent of the fan might be misinterpreted. Another more important factor that contributes to uncertainty is the fact that the catchment building the fan has likely been much larger before the capturing described earlier (chapter 3.1.5), which might also be a reason for the complexity of the fan. Also, field observations show that in the lower reaches of the fan, the active channel is incising the fan itself, by as much as 2-3 metres, which indicates that this bit of the fan is no longer active and deposition is very limited here (figure 4.3).

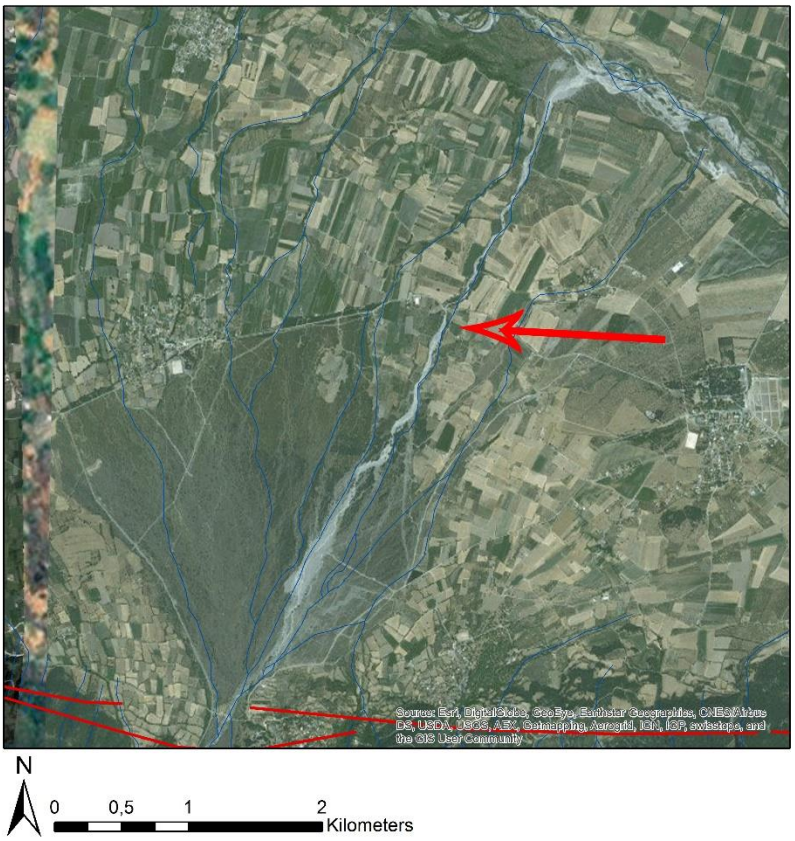

Figure 4.3: The red arrow marks the transition between deposition and incision along the Xerias fan.

Since my data is based on the modern deposits in the active, modern channels, it means that the data is based on the present extent of the catchment which likely produces a fan that is smaller in extent than what is assumed in the volume calculation based on the DEM (chapter 4.1). However, a larger catchment would likely produce a larger volume of sediment that could possibly fit better with the fan volume calculated from the DEM. On the other hand, if the DEM based volume calculations were based on the present extent of the active part of the Xerias fan, the resulting fan volume might fit better with the volumes calculated from the modelling in chapter 3.3.

When it comes to bypassing vs. deposition, we see that 53% of the sediment entering the Xerias fan is deposited in the fan whereas 47% of the sediment is bypassing and entering the axial system. This might be due to slightly higher subsidence amplitude which gives increased accommodation creation, together with lower sediment volumes. Even though the subsidence wavelength is shorter, the combination of higher amplitude subsidence close to the fault and smaller volumes cause the accommodation space to be sufficient close to the fault so that less sediment is bypassing – 47% vs. 60% for Inahos –

and this then creates a shorter and relatively steep fan (figure 1.5, p.11 and 3.1, p. 30) that aggrades rather than prograding as Inahos does.

4.2.3 Age of the fans and related volumes

As discussed in the previous chapters, the modelling results underestimate the volume if we assume that the most recent fan development happened during the Holocene. However, if we impose a timescale that is twice as long, since the last glacial maximum (18kyr-20kyr), the numbers seem to fit quite well. This may suggest that the most recent fan development was initiated already at the last glacial maximum. But as stated in chapter 4.1, the Holocene volumes are based on a subsidence rate of 7.5 metres pr. 10kyr. One could therefore argue that this volume calculation is faulty if one takes into account the assumption that these volumes might have accumulated over a period of time that is longer than the Holocene. We are fairly confident on the subsidence rate, but if we were to impose a time scale of approximately 18-20kyr, the subsidence would be twice as high, at 14 metres. That would also give a volume that is twice as high, and the problem of mismatch in the volumes would remain. However, in these calculations, we are assuming that the catchments themselves are the *only* input of sediment into the accommodation space created by the subsidence related to the faulting. But, as mentioned earlier, it is believed that the axial system is filling up the rift, including some of this accommodation space close to the faults. This means that over a time scale of 18-20kyr and a subsidence rate of approximately 0.75 or 0.85 millimetres pr. year, a fan with the same volume (2.2×10^8 m^3 for Inahos and 1.8×10^8 m^3 for Xerias) can still be produced if at least half of the accommodation created by the subsidence is already being filled up by the axial system.

I have now established that the volumes for Xerias and Inahos derived from my modelling (table 8 and 10, p. 57, 60) match the estimated minimum volumes of the fans (chapter 4.1) if we assume that the time scale is not based on the Holocene (10kyr) but since the last glacial maximum (18kyr-20kyr), and if we assume that the extent of the Xerias fan and catchment has changed over the time since formation. However, there is a problem because the model also shows that a large amount of sediment is bypassing the fans – 47% of Xerias and 60% of Inahos – and this will again reduce the volume of sediment that actually remains in the fan approximately by an order of 2. Even though there might be some uncertainties regarding the exact amount of bypassing, the field

observations and modelling clearly show that there is, without question, sediment bypass in both these fans. This means that again, the time scale necessary to build the fans to their present extent needs to be longer by a factor of 2. However, the volume calculation is the weakest link in the model because it is based on a lot of assumptions and has some uncertain constraints. Adding to this is the fact that, for Inahos at least, data has only been collected for parts of the fan, which further contributes to uncertainty.

4.3 Comparison of drainages

4.3.1 Comparison of the transverse drainages

If we compare the two fans and catchments in terms of total volumes, we see that the Inahos catchment produces a smaller relative amount of gravel, only 2.2% of the total volume, but a much larger total amount of gravel (table 10, p. 60), and more of the gravel is bypassing (figure 3.25, p. 60). The Inahos catchment produces a much higher amount of sediment in total because of its much larger extent. The Xerias catchment produces a larger relative amount of gravel, but a smaller total amount (table 8, p. 57), and less is bypassing than for the Inahos fan, only 47% (figure 3.22, p. 57). This is confirmed by looking at the grain sizes at the toe of both fans – even though Xerias produces a larger relative amount of gravel, and has a larger initial grain size, the fact that more of it is being deposited in the fan causes the grain size at the toe of the Xerias fan to be approximately the same as it is at the end of the Inahos fan. The relative amounts of gravel are very low, especially for Inahos, but it should be noted that the total sediment flux numbers that these percentage values are based on comes from a very different model with a different purpose based on catchment volume and erosion rates with no time constraints (Pechlivanidou et al., 2016, manuscript in preparation), so the only aspect that is interesting for me to pay attention to here is the relative difference between the volumes, not how the volumes derived from my modelling compares to these sediment flux numbers.

The reason why Inahos produces a smaller relative amount of gravel can possibly be linked to its lithology. We know that the Inahos catchment is dominated by flysch whereas Xerias is dominated by limestone (figure 1.6, p. 12). The flysch is a soft rock compared to the limestone, which is reflected in the Schmidt hammer measurement results in appendix B. Although both lithologies fall under the “moderate” category, we

see that the intact rock strength for the flysch is generally lower than for the limestone. It is also worth noting that the measurements of flysch were all executed on the sandstone beds as the siltstone beds were so soft that they disintegrated when struck by the hammer, giving false readings. This means that the hardness recorded for the flysch is higher than what one would expect since the soft siltstone layers are not represented. As explained by Whittaker (2007) and Attal and Lavé (2009), softer lithologies are more prone to abrasion than harder lithologies. As such, the flysch-dominant Inahos catchment is more prone to abrasion, and this abrasion can therefore be the cause of the smaller amount of gravel compared to Xerias which is dominated by the harder limestone that is consequently less prone to abrasion. The larger relative amount of gravel in the Xerias fan, 7% vs. 2.2% in Inahos, can possibly also be linked to its position at the centre of an active fault segment. This position causes the catchment to incise steeply into the footwall block, causing a high degree of incision creating steep slopes which can cause land sliding and feeding of coarser sediment directly into the channel (Cowie et al., 2006, Whittaker et al., 2010).

4.3.2 Comparison of transverse drainages and axial drainage

When comparing the transverse drainages to the axial drainage, the volumes are not the most interesting aspect. The key difference relates to spatial distribution of subsidence and how this impacts the distribution of grain sizes and the distribution of deposition. An important difference between the transverse systems and the axial systems is the properties of the grain size fining trends and sediment bypassing trends. When looking at the transverse systems with an exponential subsidence profile (figure 3.21, p. 56 and 3.24, p. 59), we see that the grain size distribution shows a clearly concave profile, i.e. the fining rate is decelerating downstream, abrupt at first and then flattening out at the toe of the fan (figure 3.20, p. 56 and 3.23, p. 59). For sediment deposition and bypassing we see the same concave profile, i.e. sediment deposition is accelerating at first, and then decelerating and flattening out towards the toe of the fan. When playing with increasingly linear subsidence profiles during the model sensitivity analysis, it was apparent that these concave grain size and deposition/bypassing profiles became increasingly convex with increasing linearity of the subsidence (fig. 3.18, p. 54).

The reason for the concave shape of the grain size and bypass/deposition curves can be explained by the spatial distribution of accommodation creation made by exponential

decrease in subsidence. As the subsidence, and thus accommodation creation, is very large close to the fault but rapidly decreasing with increasing distance from the fault, we see a massive deposition of material close to the fault, where the creation of accommodation space is very high. Since this accommodation creation decreases so rapidly, the amount of space available for deposition decreases, and there is simply no room for more sediment to be deposited, causing a large portion of the sediment to bypass the fan. Since the coarser fractions of sediment in a fluvial system are deposited first, the fining trend consequently shows a rapid decrease in grain size as the coarsest gravel is dumped close to the fault and filling up the accommodation space whereas the finer gravel and sand is to a larger extent bypassing.

When looking at the axial system, which has a linear subsidence profile, we see that the curves for both the grain size distribution (figure 3.26, p. 61) and the distribution of sediment bypassing/deposition (figure 3.28, p. 62) has a clear convexity. From figure 3.26 we can see a sudden increase in grain size approximately 13 and 30 kilometres downstream, which can likely be attributed to input of gravel from the transverse systems (Inahos and Xerias, respectively). Also apparent in figure 3.26 is a typical "gravel front" towards the end of the system where the grain size fines quite abruptly as the system runs out of gravel and only the fines are left. Such gravel fronts are absent in the transverse systems, because they never run out of gravel because they are overfilled. The excess gravel that is not deposited in the fan is dumped into the axial system. The axial system is filled, which means there is no excess gravel; everything is being deposited in the system and nothing is bypassing. This is where we see the gravel front. And since the accommodation creation increases linearly in this system, more of the coarser material is being transported further downstream, which causes the grain size curve to show a convex signal. The linear *increase* in accommodation space also causes the bypass/deposition curve to be convex – accommodation creation is low to begin with, which means that deposition is low and bypassing is high. As accommodation creation gradually increases, so does deposition, while bypassing decreases. This gives the curve its convex signal.

4.4 Uncertainties

The results of this modelling is based on a number of variables, and as demonstrated, the model is very sensitive to some of these. This means that there are some sources of uncertainty that should be discussed, and this will be done in the following chapters.

4.4.1 Fault subsidence rates

The exact rate of subsidence along the fault segments in the Sperchios basin has not been measured. This means that the modelling is based on estimates. As the sensitivity analysis shows, even small changes in subsidence will have a significant effect on the amount of sediment fed into the different fans, and subtle increases in subsidence amplitude will increase the sediment volumes in the modelling.

4.4.2 Fan volume calculation

As I have previously demonstrated, there are some problems with the model results when it comes to the modelled volumes (tables 8, p. 57 and 10, p. 60) compared to fan volumes measured from the DEM (chapter 4.1). The DEM calculation of the fan volumes is as mentioned a simplistic approach to determine the volumes, and therefore gives estimates that are very rough. Furthermore, the sediment volumes calculated from the model might be inaccurate, as they are dependent on factors of which the constraints are not precisely known, such as the exact width of the fans and the exact subsidence rates. Even though the impact of small changes in each of these individual variables might not cause dramatic changes in the modelled volumes, the combined effect of the uncertainties in these variables may have a significant effect.

4.4.3 Limitations in the grain size measuring method

The correct measurement of grain sizes will of course depend on a certain amount of measurements with a certain distance between every measurement. The more measurements made, with the shorter distance between them, the more reliable the results of the measurements. In addition, the accuracy depends on how easily identifiable the gravel bars are, and if they are easy to distinguish from the channel bed itself. A third factor of uncertainty is the fact that I only measured grains in the modern, active channels of the fans. As such, I have got a good picture of the present grain size fining trends, but have no indication of how the trend has varied through time in the stratigraphy. Yet another important factor is also the case of human influence; many of the channels/fans I have measured have seen significant alteration through digging,

mass extraction, construction of artificial banks etc. which is likely to impact the spatial distribution of grain size. As it is not known for how long these activities have been going on, it is hard to establish if, and to what extent, it has affected spatial trends in grain size fining.

A fair question to ask is whether the grain size pictures actually show a real trend of downstream fining in the systems, or if it is all just random. As each point was composed of grain size data from three pictures, one could risk not seeing any fining trends if the selection of photos is poor. A faulty trend could be the case if I were to fail in capturing the complete picture of the grain size spread in the different locations along the system. If I were unable to represent, for instance, the finer fractions in a location, it would give a faulty representation of the grain size spread in that location, and if I made the same mistake at several locations, the resulting grain size fining trend would not represent reality, and I might risk not even getting a fining trend at all. To explore if this problem could have been relevant in my data, I decided to analyse a selection of photos from the Xerias fan to see if the fining trend from my data was realistic. To do so, I first checked the cumulative grain size curves for the combined photos from three waypoints along the Xerias fan (figure 4.4), in total nine photos at three different locations – the apex, mid-fan and at the base of the fan, and then compared these results with the results for the uncombined data from these three waypoints, i.e. data for each of the nine individual pictures is plotted (figure 4.5). As is seen from the graphs, even though the uncombined data shows a large spread in grain sizes, the total picture gives a clear trend where the largest grain sizes are not present in the pictures at the base of the fan, and the smallest grain sizes are mostly not present in the pictures at the apex of the fan. This means that I managed to capture the spread of grain sizes at different locations fairly well, and were able to find grain size distribution trends that are likely to be representative of the actual trends.

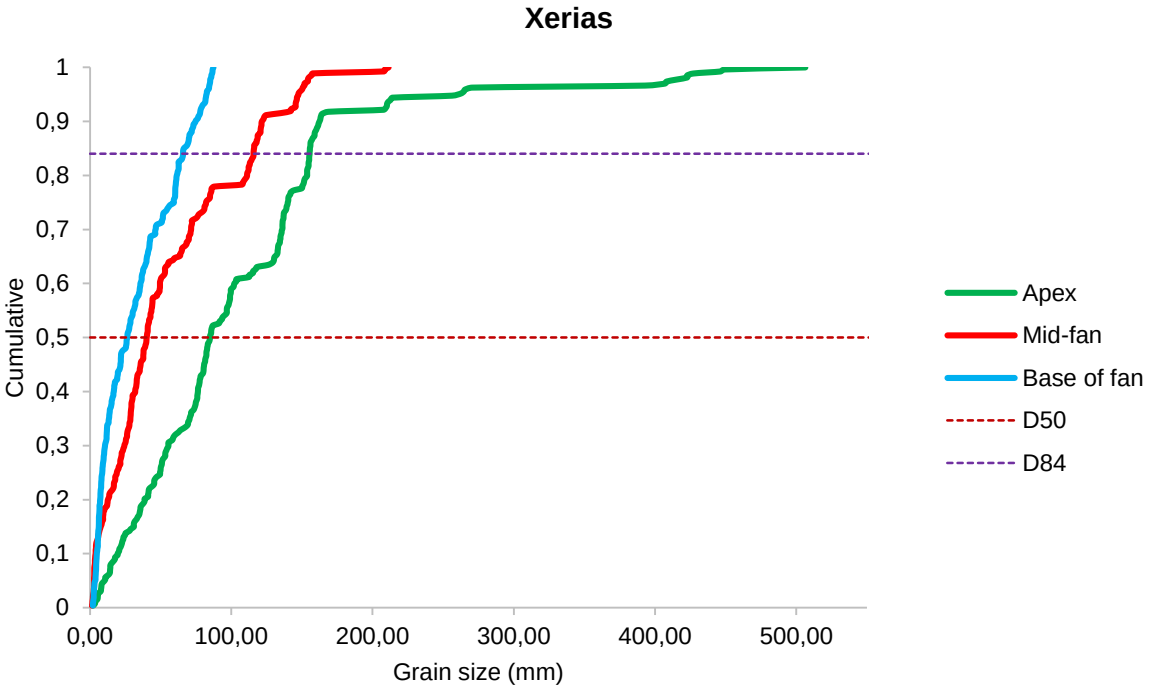

Figure 4.4: This graph shows cumulative grain size data for three locations along the Xerias fan; at the fan apex, a point approximately at the middle of the length of the fan, and a point at the base of the fan. The data for each location is based on a combination of all the data from three pictures taken at each location. Lines marking D_{50} and D_{84} are also shown.

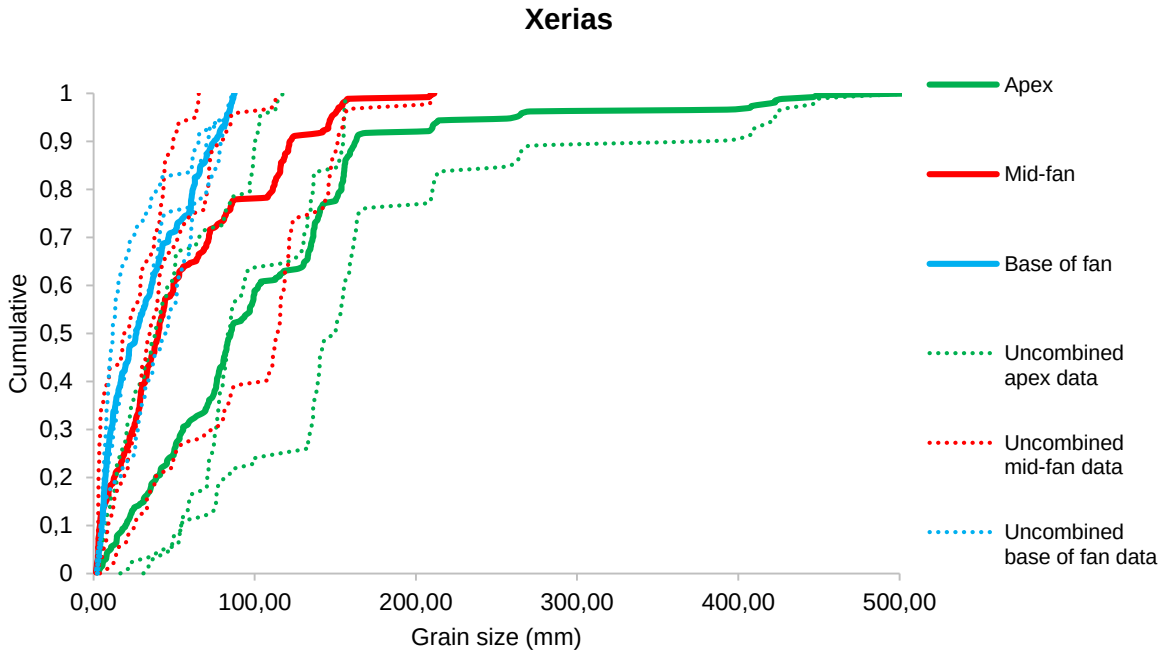

Figure 4.5: This graph shows data for three different points along the Xerias fan, and data for each of the three corresponding photos taken at each of the three points along the fan. Each photo – three from each location – is represented by a dotted line, and the colour corresponds to the location along the fan. The graph is cut at 300 mm in the X-axis for visual simplicity.

Conclusions

In this study, the geomorphology of the Sperchios rift basin, central Greece, was studied by analysing the grain size variations in different fluvial systems in the rift basin, with the goal of quantifying downstream grain size trends along two transverse fluvial systems. Scaled photographs of active gravel bars were used to characterise the grain size distributions. These data were then used to explore the relationship between (1) the spatial distribution of subsidence, (2) sediment supply and (3) spatial distribution of grain sizes in fluvial systems in an active half graben. The main aim was to compare how the transverse systems differ from axial systems in such a setting, and to see if the model itself can yield valid results that are consistent with the geologic development of the basin.

The grain size modelling approach used here has been developed in recent years (Fedele and Paola, 2007, Duller et al., 2010) and has not been widely applied. In this thesis, the model was applied to two transverse fluvial systems, one draining across a normal fault and one draining between two normal fault segments. Parts of my results were compared to results from a similar analysis performed by Pechlivanidou et al. (2016, manuscript in preparation) on the axial river with the combination of her grain size measurements and my own.

The results show that the model does a good job in demonstrating how normal faulting has a very clear impact on grain size fining and sediment deposition. This impact – relating to spatial distribution and wavelength of subsidence – can be quantified based on grain size measurements performed on gravel bars in active modern channels. Furthermore, it demonstrates how normal faulting causes the transverse systems to show a clear and abrupt downstream fining signal which flattens out as the systems approach the axial river. This is because deposition is rapid at first, close to the fault, and decreases with distance from the fault. It also demonstrates that the sediment input is higher than accommodation creation, so that where axial and transverse systems meet a large amount of sediment – 50-60% based on my modelling results – bypasses the fans and flows into the axial system. However, one of the most important discoveries is that the model also explains the mechanisms responsible for the differences between the transverse fans Xerias and Inahos regarding surface slopes, grain size distribution and volumes, by demonstrating that there are differences in tectonic setting for the locations

of the two fans – i.e. amplitude and wavelength of subsidence – and differences in sediment volumes.

Even though the modelling is based on analysis of modern deposits in an active channel, in a system that has undergone both tectonic and climatic changes during the time since initiation, the results show that the model explains the interaction between the controlling variables in a logical way, albeit with some weaknesses in the constrains on sediment volumes. The uncertainty of the modelling results, especially with regards to sediment volumes, can not only be attributed to the model itself, or the measurements done by me, but also to the uncertainties in calculations on fan volumes and time scale uncertainties, and uncertainties in actual slip rate of the active faults in the region which have yet to be directly measured.

References

ALLEN, P. A. 2008. From landscapes into geological history. *Nature,* 451**,** 274-276.

APOSTOLOPOULOS, G. 2005. Geophysical studies relating to the tectonic structure, geothermal fields and geomorphological evolution of the Sperchios River Valley, Central Greece. *Journal of the Balkan Geophysical Society,* 8**,** 99-112.

ATTAL, M. & LAVÉ, J. 2009. Pebble abrasion during fluvial transport: Experimental results and implications for the evolution of the sediment load along rivers. *Journal of Geophysical Research: Earth Surface,* 114**,** n/a-n/a.

COWIE, P. A., ATTAL, M., TUCKER, G. E., WHITTAKER, A. C., NAYLOR, M., GANAS, A. & ROBERTS, G. P. 2006. Investigating the surface process response to fault interaction and linkage using a numerical modelling approach. *Basin Research,* 18**,** 231-266.

COWIE, P. A., WHITTAKER, A. C., ATTAL, M., ROBERTS, G., TUCKER, G. E. & GANAS, A. 2008. New constraints on sediment-flux–dependent river incision: Implications for extracting tectonic signals from river profiles. *Geology,* 36**,** 535-538.

D'ALESSANDRO, W., BRUSCA, L., KYRIAKOPOULOS, K., BELLOMO, S. & CALABRESE, S. 2014. A geochemical traverse along the "Sperchios Basin – Evoikos Gulf" graben (Central Greece): Origin and evolution of the emitted fluids. *Marine and Petroleum Geology,* 55**,** 295-308.

DULLER, R. A., WHITTAKER, A. C., FEDELE, J. J., WHITCHURCH, A. L., SPRINGETT, J., SMITHELLS, R., FORDYCE, S. & ALLEN, P. A. 2010. From grain size to tectonics. *Journal of Geophysical Research: Earth Surface,* 115**,** n/a-n/a.

ELIET, P. P. & GAWTHORPE, R. L. 1995. Drainage development and sediment supply within rifts, examples from the Sperchios basin, central Greece. *Journal of the Geological Society,* 152**,** 883-893.

FEDELE, J. J. & PAOLA, C. 2007. Similarity solutions for fluvial sediment fining by selective deposition. *Journal of Geophysical Research: Earth Surface,* 112**,** n/a-n/a.

GOLDSWORTHY, M. & JACKSON, J. 2000. Active normal fault evolution in Greece revealed by geomorphology and drainage patterns. *Journal of the Geological Society,* 157**,** 967-981.

GOLDSWORTHY, M., JACKSON, J. & HAINES, J. 2002. The continuity of active fault systems in Greece. *Geophysical Journal International,* 148**,** 596-618.

KILIAS, A. A., TRANOS, M. D., PAPADIMITRIOU, E. E. & KARAKOSTAS, V. G. 2008. The recent crustal deformation of the Hellenic orogen in Central Greece; the Kremasta and Sperchios Fault Systems and their relationship with the adjacent large structural features. *Zeitschrift der Deutschen Gesellschaft für Geowissenschaften*.

LEEDER, M. R. & JACKSON, J. A. 1993. The interaction between normal faulting and drainage in active extensional basins, with examples from the western United States and central Greece. *Basin Research,* 5**,** 79-102.

LEEDER, M. R., SEGER, M. J. & STARK, C. P. 1991. Sedimentation and tectonic geomorphology adjacent to major active and inactive normal faults, southern Greece. *Journal of the Geological Society,* 148**,** 331-343.

MILLER, K. L., REITZ, M. D. & JEROLMACK, D. J. 2014. Generalized sorting profile of alluvial fans. *Geophysical Research Letters,* 41**,** 7191-7199.

PARSONS, A. J., MICHAEL, N. A., WHITTAKER, A. C., DULLER, R. A. & ALLEN, P. A. 2012. Grain-size trends reveal the late orogenic tectonic and erosional history of the south-central Pyrenees, Spain. *JOURNAL OF THE GEOLOGICAL SOCIETY,* 169**,** 111-114.

PECHLIVANIDOU, S., COWIE, P. A., HANNISDAL, B., WHITTAKER, A. C., GAWTHORPE, R. L., CHRISTOS, P. & RIISER, O. S. 2016. Source to sink sedimentary systems in active rift settings: the Sperchios River basin, central Greece. *In preparation, for Basin Research*.

SEGER, M. J. & ALEXANDER, J. 1993. Distribution of Plio-Pleistocene to modern fan-deltas along the southern shore of the Gulf of Corinth, Greece. *In:* STEELE, R. J. & FROSTICK, L. E. (eds.) *Tectonic Controls and Signatures in Sedimentary Successions.* Special Publications of the International Association of Sedimentologists.

WHITTAKER, A. C. 2007. *Investigating controls on bedrock river incision using natural and laboratory experiments*, University of Edinburgh.

WHITTAKER, A. C., ATTAL, M. & ALLEN, P. A. 2010. Characterising the origin, nature and fate of sediment exported from catchments perturbed by active tectonics. *Basin Research,* 22**,** 809-828.

WHITTAKER, A. C., DULLER, R. A., SPRINGETT, J., SMITHELLS, R. A., WHITCHURCH, A. L. & ALLEN, P. A. 2011. Decoding downstream trends in stratigraphic grain size as a

function of tectonic subsidence and sediment supply. *GEOLOGICAL SOCIETY OF AMERICA BULLETIN,* 123**,** 1363-1382.

WHITTAKER, A. C. & WALKER, A. S. 2015. Geomorphic constraints on fault throw rates and linkage times: Examples from the Northern Gulf of Evia, Greece. *Journal of Geophysical Research: Earth Surface,* 120**,** 137-158.

WOLMAN, M. G. 1954. A method of sampling coarse river-bed material. *Eos, Transactions American Geophysical Union,* 35**,** 951-956.

APPENDIX A – SLOPE LASER MEASUREMENTS

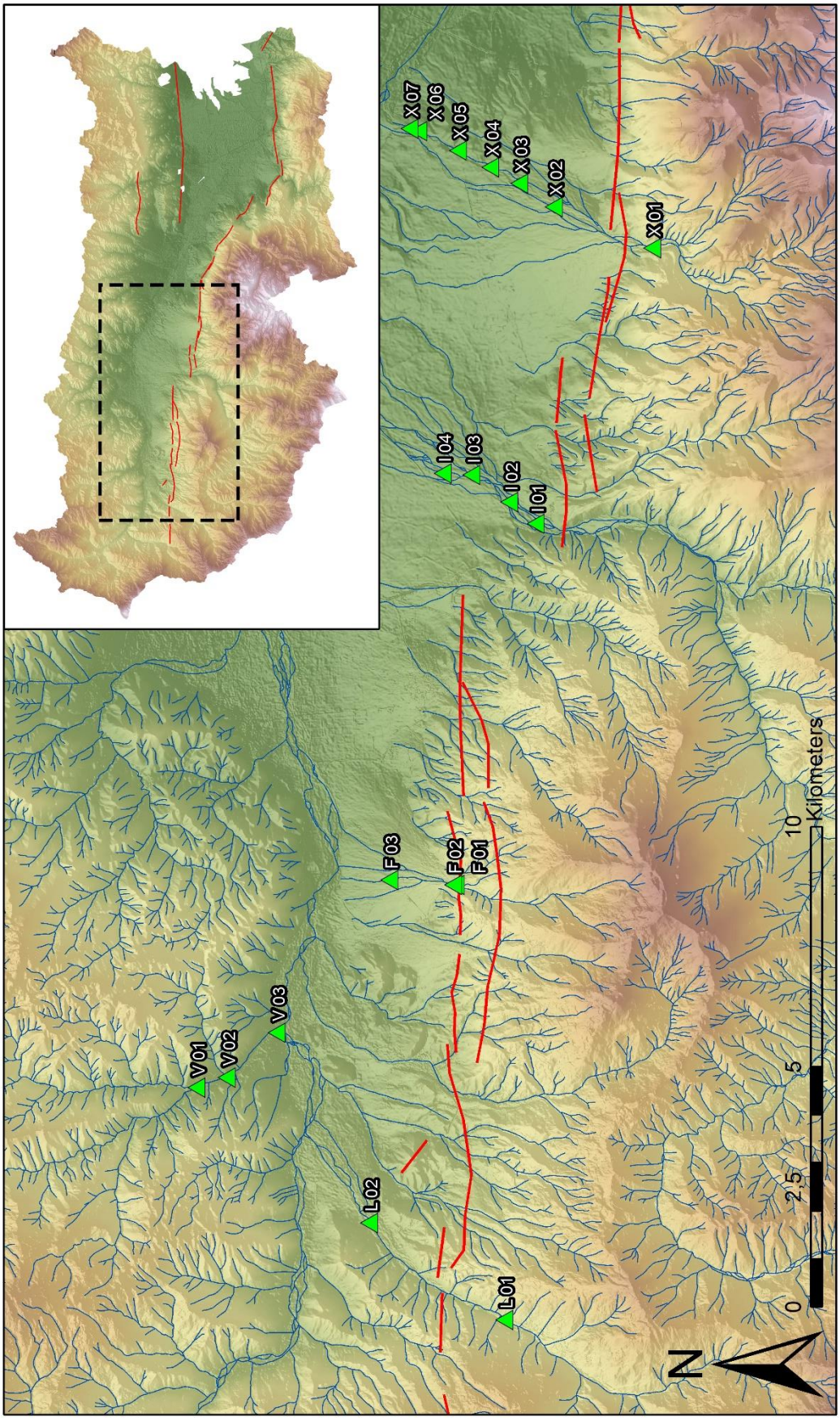

Lefkada	**Slope (degrees)**
L 01	1,8
L 02	1,8
Average:	1,8

Vitoli	**Slope (degrees)**
V 01	1,3
V 02	1,2
V 03	0,8
Average:	1,1

Inahos	**Slope (degrees)**
I 01	0,5
I 02	0,8
I 03	0,4
I 04	0,5
Average:	0,55

Xerias	**Slope (degrees)**
X 01	3,5
X 02	2,4
X 03	1,5
X 04	1,3
X 05	1,1
X 06	1,1
X 07	1,1
Average:	1,71

Fossilized fan	**Slope (degrees)**
F 01	4,7
F 02	5,3
F 03	4,2
Average:	4,73

APPENDIX B – SCHMIDT HAMMER MEASUREMENTS

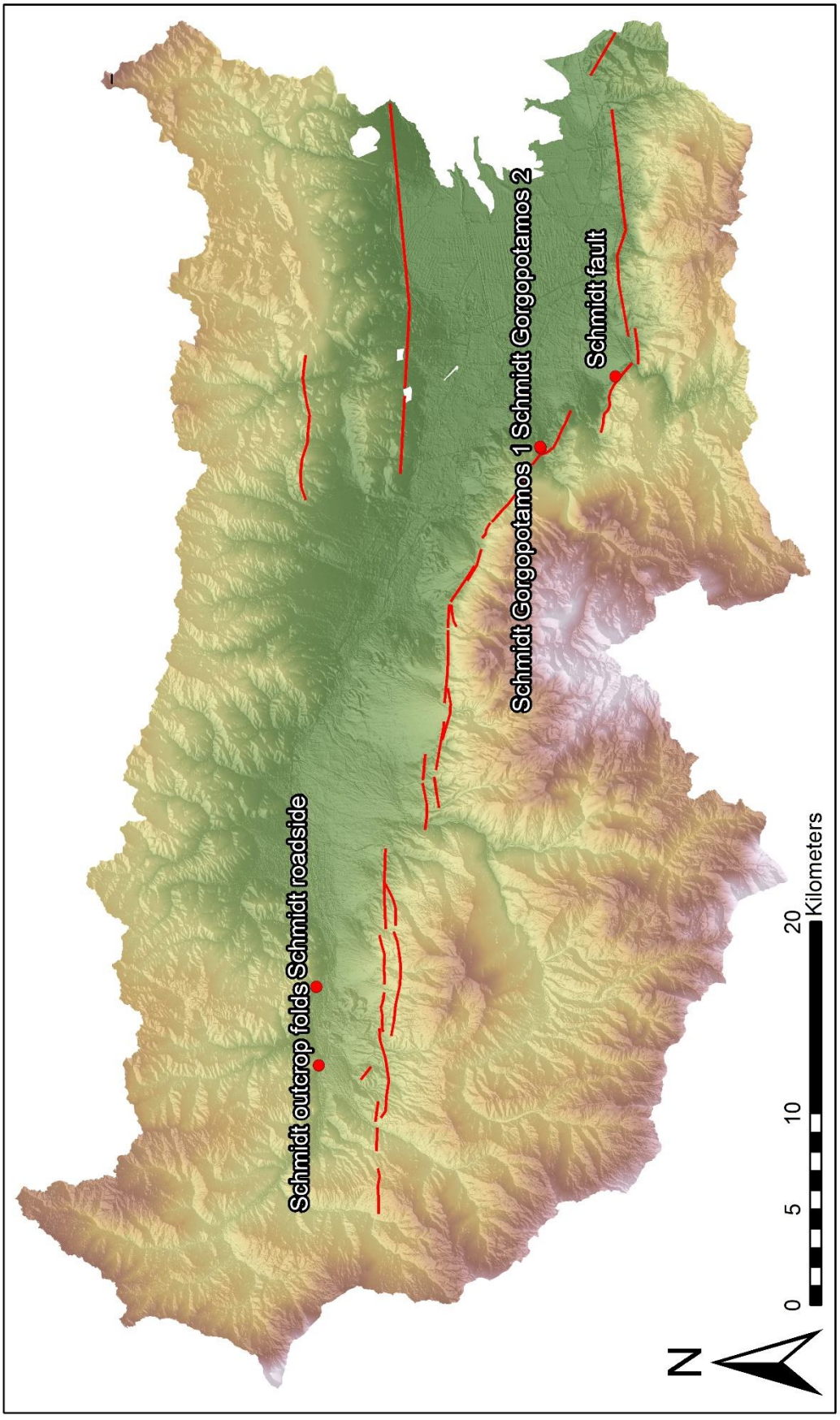

Schmidt Gorgopotamos 1																						
	Rock mass strength classification									**Elevation**				**x**				**y**				
1	**Intact rock strength (Schmidt Hammer)**																					
	1	2	3	4	5	6	7	8	9	10	11	12	13	14	15	16	17	18	19	20		
	39	48	42	25	36	52	39	40	48	38	36	49	41	35	44						40,8	
r	if > 60, r = 20				if 50-60, r = 18				if 40-50, r = 14				if 35-40, r = 10				if 10-35, r = 5				14	14
2	**Weathering**																					
	Unweatherd				Sligthlty				Moderately				Highly				Completely					
r	10				9				7				5				3				7	7
3	**Spacing of joints**																					
	> 3 m				3 -1 m				1 - 0.3 m				300 - 50 mm				< 50 mm					
r	30				28				21				15				8				21	21
4	**Joint orientation**																					
	Steep dips into slope				Moderate dips into slope				Horizontal dips or nearly vertical (hard rocks only)				Moderate dips out of slope				Steep dips out of slope					
r	20				18				14				9				5				14	14
5	**Width of joints**																					
	< 0.1 mm				0.1 - 1 mm				1 - 5 mm				5 - 20 mm				> 20 mm					
r	7				6				5				4				2				4	4
6	**Continuity of joints**																					
	None				Few				Continuous, no infill				Continuous, thin infill				Continuous, thick infill					
r	7				6				5				4				1				5	5
7	**Outflow of ground water**																					
	None				Trace				Slight				Moderate				Great					
r	6				5				4				3				1				5	5
																						70
	Total rating																					
	Very strong	100-91																				
	Strong	90-71																				
	Moderate	70-51																				
	Weak	50-26																				
	Very weak	<26																				

Schmidt Gorgopotamos 2																						
	Rock mass strength classification									**Elevation**				**x**			**y**					
1	**Intact rock strength (Schmidt Hammer)**																					
	1	2	3	4	5	6	7	8	9	10	11	12	13	14	15	16	17	18	19	20		
	36	33	38	52	45	56	55	32	42	40	35	28	38	39	32						40,0667	
r	if > 60, r = 20				if 50-60, r = 18				if 40-50, r = 14				if 35-40, r = 10				if 10-35, r = 5				14	14
2	**Weathering**																					
	Unweatherd				Sligthlty				Moderately				Highly				Completely					
r	10				9				7				5				3				5	5
3	**Spacing of joints**																					
	> 3 m				3 -1 m				1 - 0.3 m				300 - 50 mm				< 50 mm					
r	30				28				21				15				8				15	15
4	**Joint orientation**																					
	Steep dips into slope				Moderate dips into slope				Horizontal dips or nearly vertical (hard rocks only)				Moderate dips out of slope				Steep dips out of slope					
r	20				18				14				9				5				14	14
5	**Width of joints**																					
	< 0.1 mm				0.1 - 1 mm				1 - 5 mm				5 - 20 mm				> 20 mm					
r	7				6				5				4				2				4	4
6	**Continuity of joints**																					
	None				Few				Continuous, no infill				Continuous, thin infill				Continuous, thick infill					
r	7				6				5				4				1				5	5
7	**Outflow of ground water**																					
	None				Trace				Slight				Moderate				Great					
r	6				5				4				3				1				5	5
																						62
	Total rating																					
	Very strong	100-91																				
	Strong	90-71																				
	Moderate	70-51																				
	Weak	50-26																				
	Very weak	<26																				

Schmidt roadside																						
	Rock mass strength classification									**Elevation**				**x**			**y**					
1	**Intact rock strength (Schmidt Hammer)**																					
	1	2	3	4	5	6	7	8	9	10	11	12	13	14	15	16	17	18	19	20		
	33	33	25	12	34	34	31	31	25	34											29,2	
r	if > 60, r = 20				if 50-60, r = 18				if 40-50, r = 14				if 35-40, r = 10				if 10-35, r = 5				5	5
2	**Weathering**																					
	Unweatherd				Sligthlty				Moderately				Highly				Completely					
r	10				9				7				5				3				5	5
3	**Spacing of joints**																					
	> 3 m				3 -1 m				1 - 0.3 m				300 - 50 mm				< 50 mm					
r	30				28				21				15				8				15	15
4	**Joint orientation**																					
	Steep dips into slope				Moderate dips into slope				Horizontal dips or nearly vertical (hard rocks only)				Moderate dips out of slope				Steep dips out of slope					
r	20				18				14				9				5				18	18
5	**Width of joints**																					
	< 0.1 mm				0.1 - 1 mm				1 - 5 mm				5 - 20 mm				> 20 mm					
r	7				6				5				4				2				5	5
6	**Continuity of joints**																					
	None				Few				Continuous, no infill				Continuous, thin infill				Continuous, thick infill					
r	7				6				5				4				1				4	4
7	**Outflow of ground water**																					
	None				Trace				Slight				Moderate				Great					
r	6				5				4				3				1				5	5
																						57
	Total rating																					
	Very strong	100-91																				
	Strong	90-71																				
	Moderate	70-51																				
	Weak	50-26																				
	Very weak	<26																				

Schmidt outcrop folds																						
	Rock mass strength classification									**Elevation**				**x**				**y**				
1	**Intact rock strength (Schmidt Hammer)**																					
	1	2	3	4	5	6	7	8	9	10	11	12	13	14	15	16	17	18	19	20		
	17	18	10	18	12	11	10	16	12	17											14,1	
r	if > 60, r = 20				if 50-60, r = 18				if 40-50, r = 14				if 35-40, r = 10				if 10-35, r = 5				5	5
2	**Weathering**																					
	Unweatherd				Sligthlty				Moderately				Highly				Completely					
r	10				9				7				5				3				5	5
3	**Spacing of joints**																					
	> 3 m				3 -1 m				1 - 0.3 m				300 - 50 mm				< 50 mm					
r	30				28				21				15				8				15	15
4	**Joint orientation**																					
	Steep dips into slope				Moderate dips into slope				Horizontal dips or nearly vertical (hard rocks only)				Moderate dips out of slope				Steep dips out of slope					
r	20				18				14				9				5				18	18
5	**Width of joints**																					
	< 0.1 mm				0.1 - 1 mm				1 - 5 mm				5 - 20 mm				> 20 mm					
r	7				6				5				4				2				6	6
6	**Continuity of joints**																					
	None				Few				Continuous, no infill				Continuous, thin infill				Continuous, thick infill					
r	7				6				5				4				1				6	6
7	**Outflow of ground water**																					
	None				Trace				Slight				Moderate				Great					
r	6				5				4				3				1				5	5
																						60
	Total rating																					
	Very strong	100-91																				
	Strong	90-71																				
	Moderate	70-51																				
	Weak	50-26																				
	Very weak	<26																				

Schmidt fault																						
	Rock mass strength classification									**Elevation**				**x**				**y**				
1	**Intact rock strength (Schmidt Hammer)**																					
	1	2	3	4	5	6	7	8	9	10	11	12	13	14	15	16	17	18	19	20		
	45	57	58	58	51	54	58	60	54	52											54,7	
r	if > 60, r = 20				if 50-60, r = 18				if 40-50, r = 14				if 35-40, r = 10				if 10-35, r = 5				18	18
2	**Weathering**																					
	Unweatherd				Sligthlty				Moderately				Highly				Completely					
r	10				9				7				5				3				9	9
3	**Spacing of joints**																					
	> 3 m				3 -1 m				1 - 0.3 m				300 - 50 mm				< 50 mm					
r	30				28				21				15				8				28	28
4	**Joint orientation**																					
	Steep dips into slope				Moderate dips into slope				Horizontal dips or nearly vertical (hard rocks only)				Moderate dips out of slope				Steep dips out of slope					
r	20				18				14				9				5				14	14
5	**Width of joints**																					
	< 0.1 mm				0.1 - 1 mm				1 - 5 mm				5 - 20 mm				> 20 mm					
r	7				6				5				4				2				4	4
6	**Continuity of joints**																					
	None				Few				Continuous, no infill				Continuous, thin infill				Continuous, thick infill					
r	7				6				5				4				1				4	4
7	**Outflow of ground water**																					
	None				Trace				Slight				Moderate				Great					
r	6				5				4				3				1				5	5
																						82
	Total rating																					
	Very strong	100-91																				
	Strong	90-71																				
	Moderate	70-51																				
	Weak	50-26																				
	Very weak	<26																				